

The Effect of Microstructure on the Abrasion Resistance of Low Alloyed Steels

Proefschrift

ter verkrijging van de graad van doctor

aan de Technische Universiteit Delft,

op gezag van de Rector Magnificus prof.ir.K.C.A.M. Luyben;

voorzitter van het College voor Promoties,

in het openbaar te verdedigen op dinsdag 26 januari 2016 om 10:00 uur

door

Xiaojun XU

Master of Science in Material Science

Southwest Jiaotong University, Chengdu, China

geboren te Jiujiang, China

This dissertation has been approved by the

promotor : Prof. dr. ir. S. van der Zwaag

copromotor: Dr. W. Xu

Composition of the doctoral committee:

Rector Magnificus

voorzitter

Prof. dr. ir. S. van der Zwaag

Technische Universiteit Delft, promotor

Dr. W. Xu

Technische Universiteit Delft, copromotor

Independent members:

Dr. L. Duprez

ArcelorMittal Global R&D Gent, Belgium

Prof. dr. ir. P. De Baets

Universiteit Gent, Belgium

Prof. dr. ir. C. van Rhee

Technische Universiteit Delft

Prof. dr. G.C.A.M. Janssen

Technische Universiteit Delft

Prof. dr. I.M. Richardson

Technische Universiteit Delft

Prof. dr. W.A. Groen

Technische Universiteit Delft, Reservelid



The research carried out in this thesis has been made possible by a grant from the China Scholarship Council with co-financing by OCAS, ArcelorMittal.

Keywords: alloy design, abrasion resistance, scratch test, abrasive wear test, microstructure, work hardening, failure mechanism, dual phase steel, martensitic steel, abrasion resistant steel

Copyright ©2015 by Xiaojun Xu

All rights reserved. No part of the material protected by this copyright notice may be reproduced or utilized in any form or by any means, electronic or mechanical, including photocopying, recording or by any information storage and retrieval system, without the prior permission of the author.

Printed in the Netherlands by Ipskamp Drukkers, Enschede.

ISBN: 978-94-6186-588-5

Author email: x.xu-1@tudelft.nl; x.xu0617@gmail.com; xuxiaojun040121@126.com

To my parents

Contents

1	Introduction	1
1.1	Abrasive wear	1
1.2	State-of-the-art of abrasion resistant steels.....	2
1.2.1	Correlation between the conventional mechanical properties and the abrasive wear resistance	3
1.2.2	Relating microstructural features to abrasion resistance.....	5
1.3	Scope and outline of the thesis	6
	References	7
2	Design of low hardness abrasion resistant steel on the basis of microstructural factors	11
2.1	Introduction	11
2.2	Desirable microstructural features.....	12
2.2.1	The effect of volume fraction of the various phases	13
2.2.2	The effect of grain size.....	14
2.2.3	The effect of Morphology	15
2.2.4	The effect of retained austenite fraction (TRIP effect)	16
2.3	Design strategy	18
	References	20

3	Development of a novel scratch approach: Multi-Pass Dual-Indenter (MPDI) scratch test	23
3.1	Introduction	23
3.2	The concept of multi-pass dual-indenter scratch test	25
3.3	Detailed scratch test procedures	26
3.4	Schematic drawing of scratch tracks and output parameter of scratch tests ...	28
	References	30
4	Application of the MPDI scratch test to unravel abrasion damage formation	33
4.1	Introduction	33
4.2	Experimental procedures	34
4.2.1	Materials and microstructures	34
4.2.2	Sample preparation and hardness test	35
4.2.3	Scratch tests	36
4.2.4	Metallography and worn surface	36
4.3	Results	37
4.3.1	Scratch test	37
4.3.2	Morphology of the groove and observed failure mechanisms	39
4.3.3	Sub scratch surface development	42
4.4	Discussions	44
4.4.1	Effect of work hardening on scratch resistance	44
4.4.2	Comparison of single pass and multiple passes pre-scratching modes	47
4.4.3	Comparison of MPDI scratch tests and conventional scratch tests	49
4.5	Conclusions	56
	References	57

5 Prediction of the abrasion resistance of steels on the basis of the subsurface deformation layer	59
5.1 Introduction	59
5.2 Experimental description	60
5.3 Results	61
5.3.1 Multi-pass dual-indenter (MPDI) scratch tests	61
5.3.2 ASTM G65 abrasive wear test	65
5.4 Discussions	66
5.4.1 The subsurface deformation and work hardening	66
5.4.2 Correlation of MPDI scratch process and ASTM G65 abrasion test ..	69
5.5 Conclusions	76
References	77
6 The effect of martensite volume fraction on the scratch and abrasion resistance of a ferrite-martensite DP construction steel	79
6.1 Introduction	79
6.2 Experiments	81
6.2.1 Test materials and sample preparation	81
6.2.2 Multi-pass dual-indenter scratch test and ASTM G65 abrasion test..	82
6.2.3 Mechanical properties measurement	83
6.2.4 Metallography	83
6.3 Results	83
6.3.1 Microstructures	83
6.3.2 Hardness and tensile properties	85
6.3.3 MPDI scratch test	86
6.3.4 Scratch grooves and failure mechanisms	87
6.4 Discussions	91
6.4.1 The dependence of scratch resistance on the martensitic volume fraction and the loading condition	91

6.4.2	Correlating the MPDI scratch resistance against the strain hardening behavior.....	94
6.4.3	Validation of the MPDI scratch test against the ASTM G65 abrasion test.....	98
6.5	Conclusions.....	100
	References.....	102
7	The effect of ferrite-martensite morphology on the scratch and abrasive wear behaviour of a dual phase construction steel	105
7.1	Introduction.....	105
7.2	Experimental procedures.....	107
7.3	Results.....	110
7.3.1	Microstructures.....	110
7.3.2	Mechanical properties and hardness.....	113
7.3.3	MPDI scratch test.....	116
7.3.4	ASTM G65 tests.....	118
7.4	Discussions.....	119
7.4.1	Effect of ferrite-martensite morphology.....	119
7.4.2	The relation of tensile strain hardening to abrasion resistance.....	123
7.4.3	Relating the scratch and abrasion resistance to the initial hardness.....	126
7.4.4	Correlation of scratch test against the ASTM G65 abrasion test.....	129
7.5	Conclusions.....	130
	References.....	131
8	The scratch and abrasive wear behaviour of a tempered martensitic construction steel and its dual phase variants	135
8.1	Introduction.....	135
8.2	Experimental procedures.....	137
8.3	Results.....	138
8.3.1	Microstructures and mechanical properties.....	138

8.3.2	MPDI scratch test.....	140
8.3.3	Scratch morphology and failure mechanisms	141
8.4	Discussions	144
8.4.1	The dependence of scratch and abrasion resistance on tempering temperature and loading condition	144
8.4.2	Relating the scratch and abrasion resistance to the initial hardness: comparison of martensitic steels and dual phase steels.....	146
8.4.3	The relation of tensile strain hardening to scratch resistance	150
8.4.4	Correlation of the MPDI scratch test with the ASTM G65 abrasion test	152
8.5	Conclusions	153
	References	154
	Summary	159
	Samenvatting	165
	Acknowledgements	169
	Curriculum Vitae	173
	List of Publications	175

Chapter 1

Introduction

1.1 Abrasive wear

Abrasive wear is the most common wear mechanism when the rough surface of a hard object slides over the softer surface of another and is encountered extensively in the automotive, transportation, mining and mineral processing, agricultural and earth moving industries [1, 2]. Abrasion, according to the type of contact, is generally classified into either one of two types: the two-body abrasive wear mode and three-body abrasive wear mode [3]. For the two-body wear mode, there are only two rubbing parts involved, while for the three-body wear mode the abrasive wear is caused by a hard abrasive which is trapped between the rubbing surfaces. Abrasive wear is the dominant wear process in the industrial practice and it is a very costly problem and is responsible for major economic losses [4-6]. The cost of abrasion has been estimated as ranging from 1 to 4% of the gross national product of an industrialized nation [1].

Regardless of the wear mode, abrasive wear is a very complex process involving many variables in the tribo-system. Potential mechanisms explaining how material is removed

during abrasion include ploughing, wedge formation, micro-cutting, micro-fatigue and micro-cracking, and are shown schematically in Fig. 1.1[1].

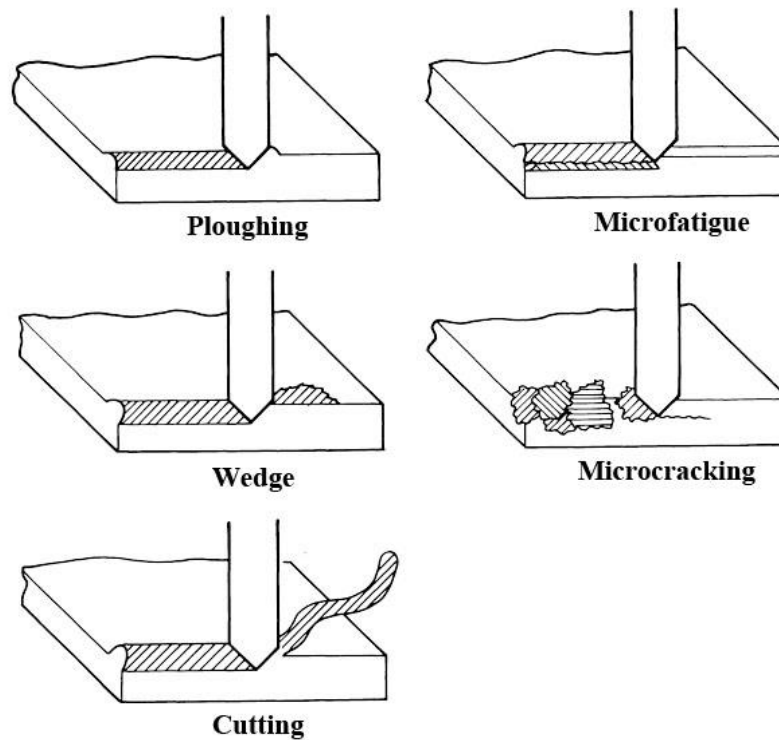


Fig. 1.1 The schematic drawing of abrasive wear mechanism [1].

1.2 State-of-the-art of abrasion resistant steels

To meet the commercial demands for a combination of a high abrasion resistance and a low cost price, the abrasive wear behaviour of a large variety of steels grades has been studied in industry and at academic centres in order to deepen our understanding and to tune the steel grade to the targets set.

1.2.1 Correlation between the conventional mechanical properties and the abrasive wear resistance

Abrasion resistance is not an intrinsic material property, but a tribo-system response depending on the prevailing working/testing conditions. It is a very complex phenomenon and correlates with many parameters. To a first approximation, a monotonous relationship between the abrasion resistance and the hardness of a material has been proposed, i.e., $\varepsilon = k \cdot H$ or $\frac{dV}{dl} = \frac{L \tan \theta}{\pi H}$ [7, 8], where ε is the wear resistance (1/ volume losses per sliding distance), k is a constant, H is the initial hardness of material, V is the wear volume, l is the sliding distance, L is the normal load and θ is base angle. However, many investigations over decades have clearly demonstrated that the simple correlation of abrasion resistance and hardness doesn't always hold true [9-11], especially for advanced low alloyed steels where multiple phases are intentionally present to obtain the balance mechanical properties at low materials cost. Zum Gahr [12] made a large systematic study on the correlation of wear resistance and the initial hardness of the wearing materials, and the results are shown schematically in Fig. 1.2. It must be highlighted that the trends indicated are found only as the abrasives are hard compared with the materials being abraded. As seen, the wear resistance can vary widely for a given hardness of the wearing materials. Alternatively, the steels with different microstructures can have the equivalent abrasion resistance despite their different (initial) hardness. The increase of wear resistance with increasing initial hardness is larger for pure metals than for heat treated steels. In addition to the quasi-linear dependences, 'V' and 'S' shaped correlations between wear rate and initial hardness have been reported [13-15]. The combined results of all investigations suggest that the initial hardness of the wearing materials may only be one indicator for the abrasion resistance, and other mechanical properties of the material have to be taken into account as well.

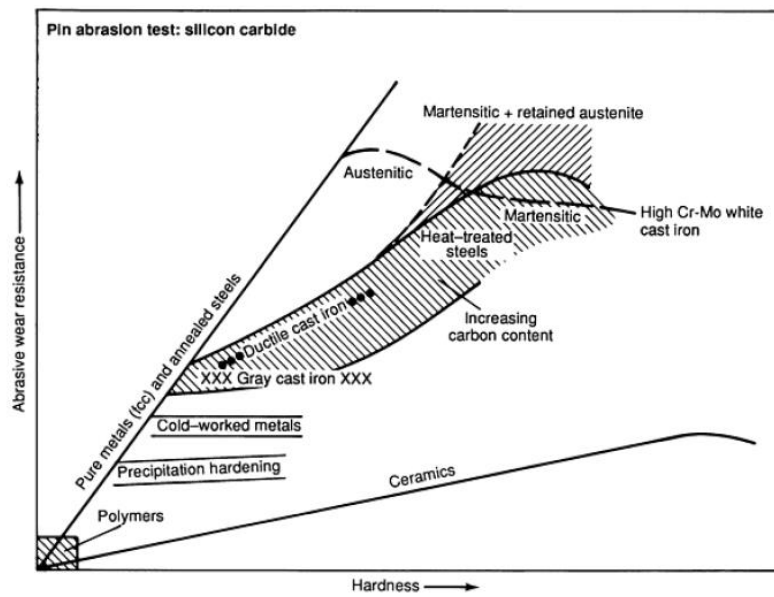


Fig. 1.2 The abrasive wear resistance ($1/\text{volume wear rate}$) of the materials in the pin abrasion test as a function of the initial hardness [12].

More comprehensive models, such as that proposed by Zum Gahr [9, 12, 16], attempted to take into account other mechanical properties, such as fracture toughness and tensile strength, as well as parameters of test conditions, including abrasive type, particle size, shape, attack angle, applied load, etc. Another approach which involves many of the important materials parameters which influence the abrasion resistance is proposed by Atkins and co-workers [17, 18]. It was reported that the abrasive wear resistance correlates with the parameter $EK_{Ic} / \sigma_y^2 h$ (1/m), where E , K_{Ic} , σ_y , and h are the elastic modulus, the materials fracture toughness, the yield strength, and some characteristic length parameter relevant to the crack length or size of cut, respectively. However, considering the complex and very distinctive process of abrasion phenomena compared to other mechanical tests, it is difficult to build a general and quantitative description of the abrasion resistance as a function of other mechanical properties of the as-exposed material, which eventually are all determined by the initial microstructural features and their development during abrasion process. Therefore, an alternative and more attractive approach is to directly link the abrasion resistance to the microstructure of steels.

1.2.2 Relating microstructural features to abrasion resistance

Over the past decades, a large number of investigations have been conducted to study the effects of various microstructural features formed by different heat treatments as well as the addition of alloy elements on the wear behaviour. For single phase ferritic steels, as reported by Kuzucu [19, 20] and Unterwiser [21], the composition is the key tuneable parameter as such alloys cannot be heat treated to give special microstructural features and the grain size is generally rather large. Therefore ferritic steels are relatively softer compared to other steels and are not widely used in applications requiring a high wear resistance. In order to improve the wear resistance of ferritic steels, Aksoy, *et al.*, [20, 22] employed strong carbide-forming elements to improve the wear resistance. In addition, Moore, *et al.* [23, 24] introduced a harder constituent, i.e. pearlite, in the soft ferritic matrix, which indeed resulted in an improved hardness and abrasion resistance. With increasing volume fraction of pearlite up to 100%, the abrasion resistance increases continuously, which implies that the abrasion resistance of pearlite is better than that of ferrite. Works reported by Clayton [25-27] and Chattopadhyay [28] show that bainitic steels with a lower carbon content have an equivalent or higher wear resistance than that of pearlitic steels with a much higher carbon concentration, owing to the good toughness and ductility of bainitic steels. Generally, the martensitic microstructure exhibits a better abrasion resistance compared to ferrite, pearlite, and bainite [29]. Zum Gahr [9] and Tylczak [1] observed that the abrasion resistance increases continuously with material hardness following the order of ferrite, pearlite, bainite and martensite. Moreover, the wear resistance of martensitic [30] and bainitic steels [31, 32] can be further improved by increasing the carbon content. However, if the carbon concentration exceeds a critical level, the wear resistance decreases although the hardness increases with increasing carbon level, which is attributed to the dramatic decrease in the ductility and toughness and hence the resulting microstructure becomes susceptible to crack nucleation and brittle delamination [29, 33]. Therefore, based on analysis of the literature we conclude that an ideal microstructure for a high abrasion resistance should lead to a good combination of strength (resisting the penetration of abrasives) and ductility (resisting the initiation and propagation of cracks). Hence, the abrasion resistance of multi-phase microstructures is of particular interest and in need of a systematic exploration [29].

1.3 Scope and outline of the thesis

This thesis starts in Chapter 2 with a detailed literature study attempted to design low hardness abrasion resistant steels on the basis of a microstructural optimization. The description will help to design the further experimental setup aiming to obtain a more detailed insight into the relation between microstructure and abrasion resistance and most of all to formulate a “translator” function for the translation of abrasion resistance into the most appropriate microstructures. In Chapter 3 the novel multi-pass dual-indenter (MPDI) scratch method developed in this PhD project is given. The MPDI scratch test aims to study the effect of surface hardening on the abrasion resistance of materials under steady state operating conditions and differs significantly from the conventional scratching experiment in which invariably the behaviour of a pristine surface is probed. Details on the origin and preferred execution of each step in the MPDI scratch test procedures are presented. In Chapter 4 the test is applied to five steel grades with different work hardening capabilities. The accumulation of strain due to pre-scratching resulting in either hardening or weakening of the surface layer during the scratch process and the effect of work hardening capability as well as the corresponding abrasion damage formation under different loads conditions are discussed. In order to build the correlation between the MPDI scratch test results with those of the ASTM G65 (multi-body) abrasive wear test, the ASTM G65 tests are performed on the same steel grades in Chapter 5. The response of the subsurface deformation layer during abrasion process on scratch and abrasion resistance is discussed.

After the development of MPDI scratch test and to build the ‘translator’, a systematic experimental investigation of the abrasion resistance for a dual phase steel of fixed chemical composition but widely different microstructures is conducted. Chapter 6 presents an experimental investigation on the scratch/abrasion behaviour of a fixed composition single lean C-Mn steel heat treated to ferrite-martensite dual phase microstructures with different martensite volume fractions using the multi-pass dual-indenter (MPDI) scratch test and the ASTM G65 abrasion test. The effects of martensite volume fractions on scratch and abrasion resistance under different loads are discussed. The effects of ferrite-martensite morphology on the scratch and abrasion resistance are explored in detail in Chapter 7. In order to (semi-) quantitatively interpret the effect of strain hardening on the abrasion/scratch resistance, a two-stage tensile strain hardening

mode was introduced in Chapter 6 and Chapter 7 to relate the scratch resistance under different loads with the tensile strain hardening at different stages following the Hollomon equation ($\sigma = K\varepsilon^n$). In Chapter 8, an experimental investigation into the scratch and abrasion behaviour of tempered martensite produced by quenching and tempering (Q&T) the same single lean C-Mn construction steel is reported. The results for tempered martensite microstructures are compared to those of the DP steels presented in Chapter 6 and 7. A desirable microstructure for low-hardness high-abrasion resistant steel is proposed. Finally, the main findings as reported in this thesis are presented in Summary.

References

- [1] J.H. Tylczak, A. Oregon, in: P.J. Blau (Eds.), ASM Handbook: Friction, Lubrication, and Wear Technology, vol. 18, ASM International, USA, 1992, p.337.
- [2] J. Rendón, M. Olsson, Abrasive wear resistance of some commercial abrasion resistant steels evaluated by laboratory test methods, *Wear* 267 (2009) 2055-2061.
- [3] J.T. Burwell Jr, Survey of possible wear mechanisms, *Wear* 1 (1957) 119-141.
- [4] U. Bryggman, S. Hogmark, O. Vingsbo, Prediction of gouging abrasion resistance of steel by pendulum grooving and other laboratory test methods, *Wear* 115 (1987) 203-213.
- [5] A. Sundström, J. Rendón, M. Olsson, Wear behaviour of some low alloyed steels under combined impact/abrasion contact conditions, *Wear* 250-251 (2001) 744-754.
- [6] X. Xu, W. Xu, F.H. Ederveen, S. van der Zwaag, Design of low hardness abrasion resistant steels, *Wear* 301 (2013) 89-93.
- [7] E. Rabinowicz, *Friction and Wear of Materials*, Wiley-Interscience, New York, 1965.
- [8] A.D. Sarkar, *Wear of Metals*, Pergamon Press, Oxford, 1976.
- [9] K.H.Z. Gahr, *Microstructure and Wear of Materials*, Elsevier Science Ltd., Amsterdam, 1987.
- [10] P. J. Mutton, J.D. Watson, Some effects of microstructure on the abrasion resistance of metals, *Wear* 48 (1978) 385 - 398.

- [11] L.Q. Xu, N.F. Kennon, A study of the abrasive wear of carbon-steels, *Wear* 148 (1991) 101-112.
- [12] K.H.Z. Gahr, Modelling of two-body abrasive wear, *Wear* 124 (1988) 87-103.
- [13] L. Fang, Q.D. Zhou, Y.J. Li, An explanation of the relation between wear and material hardness in three-body abrasion, *Wear* 151 (1991) 313-321.
- [14] K.H.Z. Gahr, D.V. Doane, Optimizing fracture toughness and abrasion resistance in white cast irons, *Metall. Trans. A* 11 (1980) 613-620.
- [15] S. Das, B.K. Prasad, A.K. Jha, O.P. Modi, A.H. Yegneswaran, Three-body abrasive wear of 0.98% carbon steel, *Wear* 162-164 (1993) 802-810.
- [16] K.H.Z. Gahr, Wear by hard particles, *Tribol. Int.* 31 (1998) 587-596.
- [17] A. G. Atkins, Y. W. Mai, *Elastic and plastic fractures*, Wiley, New York, 1985.
- [18] A.G. Atkins, Toughness in wear and grinding, *Wear* 61 (1980) 183-190.
- [19] V. Kuzucu, M. Aksoy, M.H. Korkut, The effect of strong carbide-forming elements such as Mo, Ti, V and Nb on the microstructure of ferritic stainless steel, *J. Mater. Process. Technol.* 82 (1998) 165-171.
- [20] M. Aksoy, V. Kuzucu, M.H. Korkut, The influence of strong carbide-forming elements and homogenization on the wear resistance of ferritic stainless steel, *Wear* 211 (1997) 265-270.
- [21] P.M. Unterwiser, H.E. Boyer, J.J.Kubbs (Eds.), *Heat Treater's Guide: Standard Practices and Procedures for Steel*, ASM international, USA, 1993, p. 418.
- [22] M. Aksoy, V. Kuzucu, M.H. Korkut, M.M. Yildirim, The effect of niobium and homogenization on the wear resistance and some mechanical properties of ferritic stainless steel containing 17-18 wt.% chromium, *J. Mater. Process. Technol.* 91 (1999) 172-177.
- [23] M.A. Moore, The relationship between the abrasive wear resistance, hardness and microstructure of ferritic materials, *Wear* 28 (1974) 59-68.
- [24] J. Larsen-Badse, K.G. Mathew, Influence of structure on the abrasion resistance of a 1040 steel, *Wear* (1969).
- [25] P. Clayton, K.J. Sawley, P.J. Bolton, G.M. Pell, Wear behavior of bainitic steels, *Wear* 120 (1987) 199-220.
- [26] P. Clayton, R. Devanathan, Rolling sliding wear behavior of a chromium molybdenum rail steel in pearlitic and bainitic conditions, *Wear* 156 (1992) 121-131.
- [27] R. Devanathan, P. Clayton, Rolling sliding wear behavior of three bainitic steels, *Wear* 151 (1991) 255-267.
- [28] C. Chattopadhyay, S. Sangal, K. Mondal, A. Garg, Improved wear resistance of medium carbon microalloyed bainitic steels, *Wear* 289 (2012) 168-179.
- [29] W.J. Salesky, G. Thomas, Medium carbon steel alloy design for wear applications, *Wear* 75 (1982) 21-40.

-
- [30] R.C.D. Richardson, The wear of metals by hard abrasives, *Wear* 10 (1967) 291-309.
- [31] N. Jin, P. Clayton, Effect of microstructure on rolling/sliding wear of low carbon bainitic steels, *Wear* 202 (1997) 202-207.
- [32] J.E. Garnham, J.H. Beynon, Dry rolling sliding wear of bainitic and pearlitic steels, *Wear* 157 (1992) 81-109.
- [33] Y.P. Ma, Research on three-body abrasion of martensitic steels with an impact tester, Master Thesis, Xian Jiaotong University, 1990.

Chapter 2

Design of low hardness abrasion resistant steel on the basis of microstructural factors

2.1 Introduction

Notwithstanding the significant progress in understanding of abrasion resistance and influential factors, in the current steel industry the material initial hardness (easy-to-measure) is still taken as the prime indicator for predicting the abrasion resistance and hence engineering steels are classified accordingly. As a consequence, the development of high abrasion resistant steels is oriented towards a high hardness as the first goal. However, as stated in Chapter 1, in many cases a high initial hardness cannot guarantee a high abrasion resistance. Some studies suggested that dual- or multi-phase steels with a relatively lower hardness may possess a significantly improved abrasion resistance due to their good combination of strength and ductility compared to high hardness martensitic grades [1, 2]. To meet such a combination, a dual phase (DP) microstructure composing of a soft ferrite plus a hard constituent such as martensite or bainite may be an attractive alternative to fully bainitic or martensitic steels.

2.2 Desirable microstructural features

DP steels are known to possess a higher ductility, fatigue and impact resistance, at the same tensile strength level, than those of single phase martensitic and bainitic steels [3-5]. The work reported by Jha [2] and Xu [6] showed comparisons of the wear behaviour of ferrite-martensite dual phase steel with fully martensitic steel, and ferrite-bainite dual phase steel with fully bainitic steel, respectively. Their results indicated that dual phase steels (F+M and F+B) show better wear resistance than the martensitic and bainitic steels with the same composition, as shown in Fig. 2.1. However, the hardness of DP steel is clearly lower than that of martensite or bainite. The high abrasion resistance of dual phase microstructure can be attributed to the good combination of stress bearing capability of the hard constituent and a good strain hardening response introduced by the soft and ductile ferrite. Moreover, their results also show that the wear resistance of ferrite plus pearlite is significantly lower than that of F+B/M, but may be comparable to that of single phase bainite. Based on these investigations above, it can be rather qualitatively proposed that an attractive target microstructure of low hardness wear resistant steels is a dual phase mixture of soft phase (F) and hard constituent (M or B). Nonetheless, the specific microstructural factors, such as the exact volume fractions of each phase, the grain size and their morphology, are also of importance. The following intends to investigate their effects on the abrasion resistance.

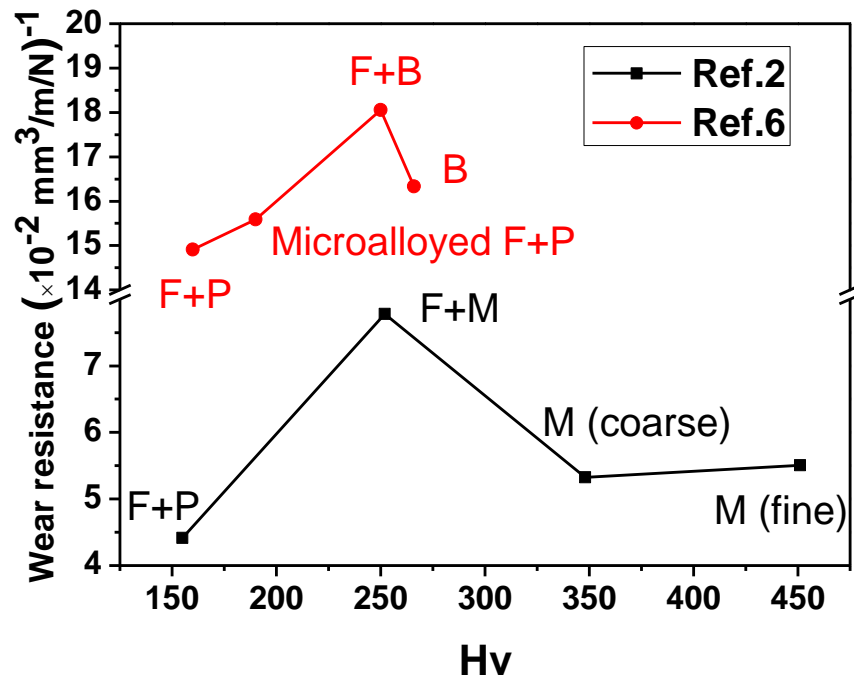


Fig. 2.1 Comparison of abrasive resistance of various microstructures as a function of hardness. Results from Ref.[2] are obtained according to the ASTM G65-81 test, and Ref.[6] is based on MLS-23 wet sand/rubber wheel abrasion test. The different test conditions make direct comparison of the results impossible.

2.2.1 The effect of volume fraction of the various phases

In dual phase microstructures, the volume fractions of two phases are the critical parameter in determining the final mechanical properties, including abrasion resistance. Some investigations [7-12] have studied the effect of volume fraction of martensite on the wear behaviour, yielding results as summarised in Fig. 2.2. It should be noticed that absolute values of the wear rates are not mutually comparable, because the abrasion resistance was determined under different test configurations and conditions. However, in all cases, it can be observed that the wear resistance increases continuously with a volume fraction of the hard martensite phase, up to 60 ~ 80%. As shown in Fig. 2.1, the wear resistance of a fully martensitic steel may be inferior to that of ferrite plus martensite. Therefore, there may exist an optimal volume fraction of martensite in which the abrasion resistance is maximized. The exact optimal volume fractions of each phase may depend on alloy composition, properties of each phase and even the test

condition. Tailored experiments are planned in future to investigate systematically the correlation of martensite volume fraction and abrasion resistance, under an identical test condition and a fixed chemical composition.

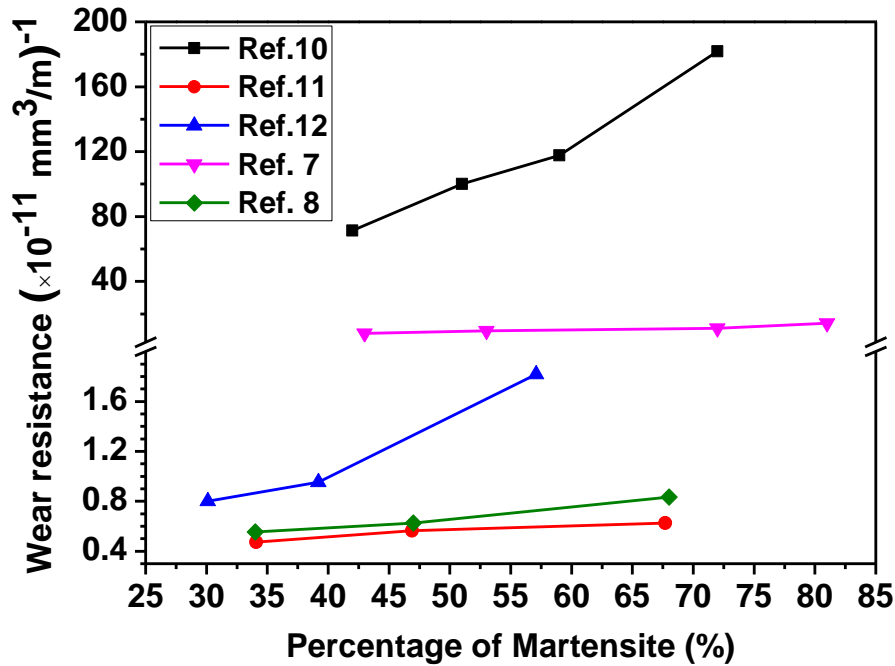


Fig. 2.2 Variation in wear rate as a function of martensite fraction. Note: the test condition in each reference is different.

2.2.2 The effect of grain size

The wear resistance of a material can be correlated to both strength and ductility. Grain refinement is an effective way to increase the yield strength without impairing ductility [13]. Therefore, grain refinement can be expected as an effective way to improve the wear resistance. A number of studies have shown that, by decreasing the grain size, the abrasion resistance increase continuously [13-17], as shown in Fig. 2.3. Again, results should be compared only qualitatively as different test conditions were used. As indicated in the figure, the correlation doesn't follow the Hall-Petch equation describing the yield strength as a function of the grain size, because of the orders of magnitude differences in strain rates and the multiaxial nature of stress during abrasion and those

used in the tensile test for which the Hall Petch correlation is established. Nevertheless, a monotonous increase of abrasion resistance is observed when the grain size decreases, which clearly suggest that the grain refinement is an effective way of enhancing the abrasion resistance.

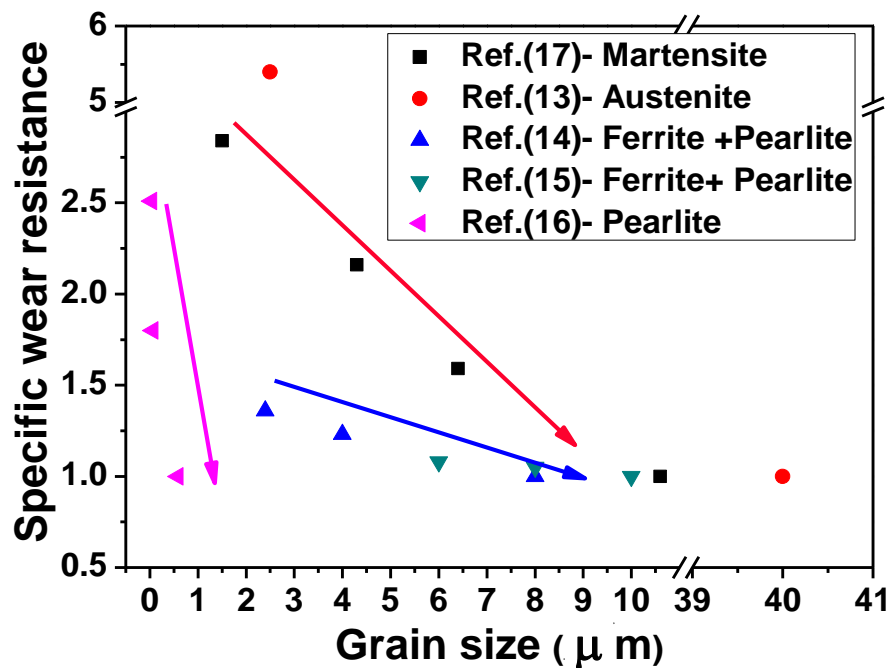


Fig. 2.3 The change of specific wear resistance with grain size. Note the test condition in each reference is different.

2.2.3 The effect of Morphology

Morphology is another important parameter in controlling the wear resistance. For DP steels [18], different ferrite-martensite/bainite morphologies (see Fig. 2.4) can be realized by different heat treatments: e.g., type I: continuous ferrite network encapsulating martensite, which may be achieved by intercritical annealing directly from a fully austenite regime, and type II: continuous martensite network encapsulating ferrite which can be formed by intercritical annealing via revert austenite formation. According to the literature [19-21], morphology of type I displays better wear resistance than type II. However, no explicit explanations were given in the early studies and its

understanding requires further experimental investigations. It could be that, in type II morphology, the hard martensite is continuous network, the hard constituent is susceptible to crack nucleation and it propagates easily along the continuous network, while in type I, in the contrary, the hard constituent is encapsulated by ferrite phase, the crack propagates across the soft phase and the ductile soft phase suppress the crack propagate resulting in enhanced wear resistance.

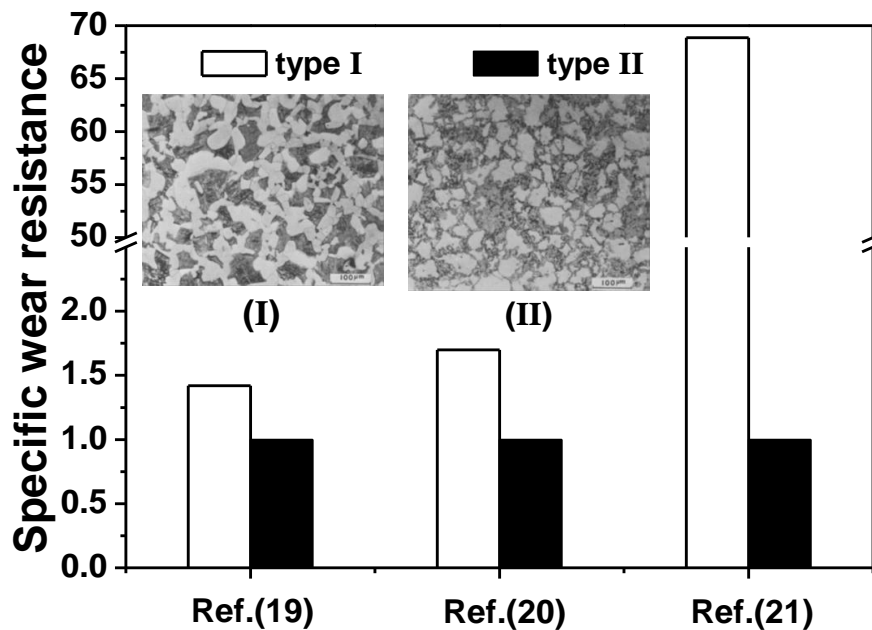


Fig. 2.4 Effect of different morphologies of dual phase on wear resistance. Note that the test condition in each reference is different.

2.2.4 The effect of retained austenite fraction (TRIP effect)

Extensive investigations have reported positive effects of retained austenite on mechanical properties if strain induced martensitic transformation takes place. This also enhances the abrasion resistance [22]. TRIP (Transformation Induced Plasticity) effect is employed in the design of TRIP steels in which a considerable amount of retained austenite with tailored stability is utilized to increase the strain hardening behavior and hence to achieve an improved combination of strength and ductility [23-26]. It is to be expected that a further improvement of wear resistance of DP steels can be achieved by

tuning the amount and distribution of metastable retained austenite. During the abrasion process, the retained austenite at the surface gradually transforms to martensite via TRIP and in doing so introduces compressive residual stress, and hence realize a self-reinforcing abrasion resistant grade. In the literature on the effect of retained austenite on abrasion resistance, some studies [27-30] showed that the presence of retained austenite could indeed further enhance the abrasion resistance. Fig. 2.5 reveals that the wear resistance increases with an increased amount of retained austenite. Chang [31] studied the retained austenite fraction before and after wear tests by X-ray analysis and proved that the amount of retained austenite after abrasion test had decreased considerably. The observation suggests that during the wear process the transformation of austenite to martensite takes place leading to surface hardening. Although a continuous increase of abrasion resistance is found in Fig. 2.5, an optimal amount of retained austenite should exist and is yet to be found by further systematic experiments, especially in the case of DP matrix which will result in different partitioning of strain/stress between two phases.

This section aims to present an investigation on effects of various microstructural features of DP steel on the abrasion resistance, e.g. volume fractions of phases, grain size, morphology, retained austenite, etc. On the basis of these investigations, a qualitative description of the ideal microstructure of a low hardness abrasion resistant steel could be proposed. The qualitative description will give a right direction to design the further experiment setup in order to quantify effects of all relevant microstructure parameters for the given tribosystem in future, and eventually guide the design of high abrasion resistant steels with low hardness.

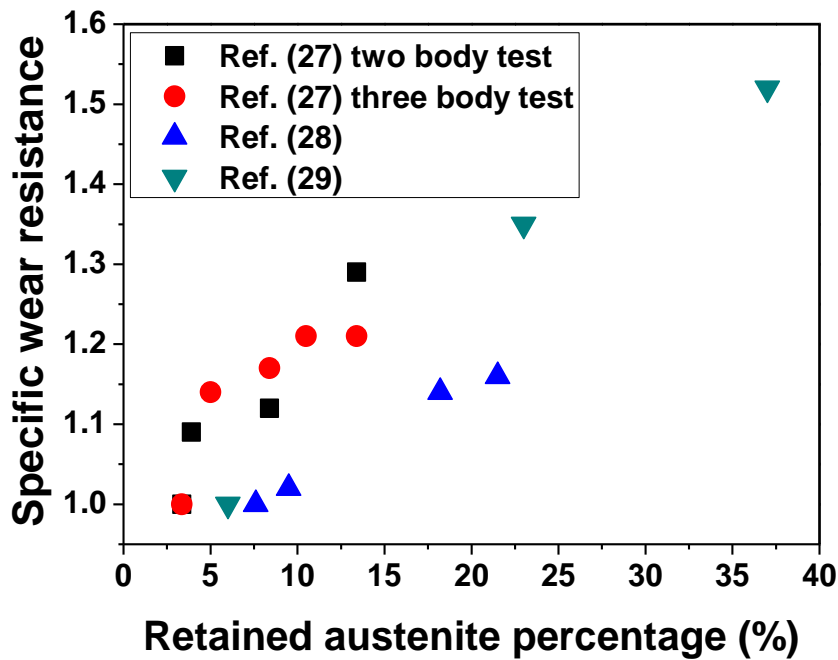


Fig. 2.5 Variation of specific wear resistance as a function of retained austenite fraction. Note: the test condition in each reference is different.

2.3 Design strategy

In the target framework of this thesis, we intend to follow the concept of goal/means oriented alloy design approach [32, 33] to explore the further experimental investigations for the design of low hardness abrasion resistant steel, which involves two key steps: the first is to ‘translate’ the required properties, i.e., abrasion resistance directly to target microstructures other than correlating it first to other mechanical properties, and the second is to ‘create’ the target microstructure by tailoring the heat treatment according to metallurgical principles, as shown in Fig. 2.6. Given the fact that the abrasion process itself is very complex and abrasion resistance is a (tribo-) system response rather than a material’s intrinsic property, it is impossible to derive a simple and general ‘translator’ functions in the design of abrasion resistant steel. Although there are lots of studies and correlations/models between abrasion resistance and other mechanical properties which provide valuable insights, the correlation of abrasion

resistance and microstructure, especially in high strength low alloy (HSLA) engineering steels involving multiple phases remains a challenge. Therefore, the first and most challenging task is to formulate a translator function for the translation of abrasion resistance into the most appropriate microstructures. Based on the investigations above, although a qualitative hypothesis of desirable microstructures could be proposed, but the microstructures cannot yet be well quantified for abrasion resistant steels. Dedicated experiments will be then designed in order to obtain a more detailed insight into the correlation between microstructure and abrasion resistance and to achieve a semi-quantitative description of the desirable microstructure. Once these key microstructural parameters are defined, proper ‘creator’ functions for specific steel grades may be defined by tailoring heat treatments during the steel production.

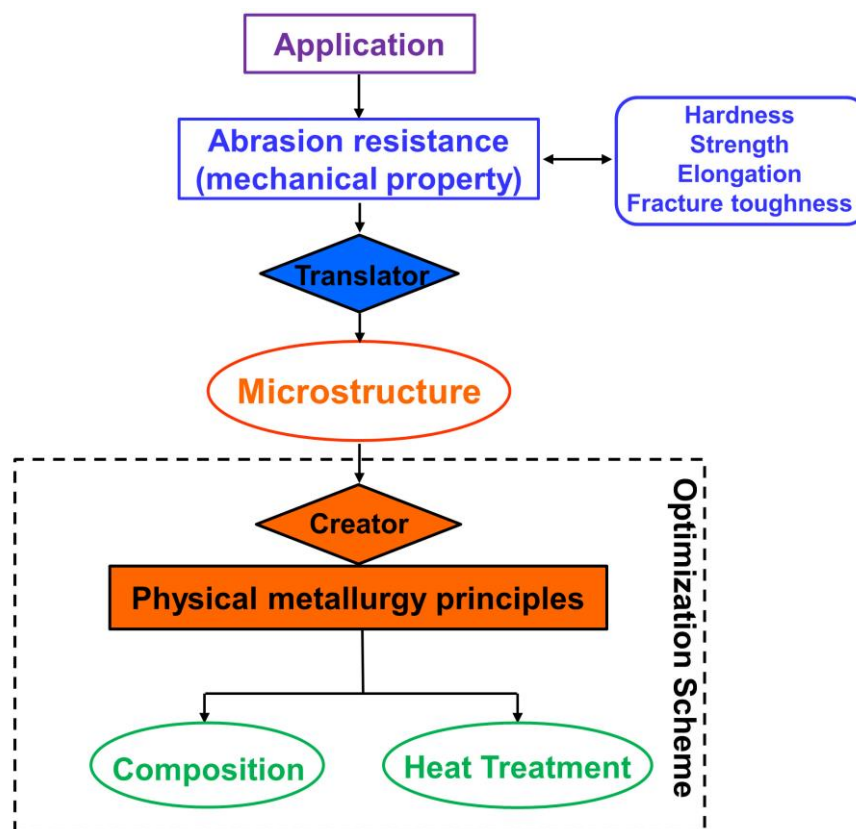


Fig. 2.6 Flow chart of alloy design scheme.

References

- [1] A. Sundström, J. Rendón, M. Olsson, Wear behaviour of some low alloyed steels under combined impact/abrasion contact conditions, *Wear* 250-251 (2001) 744-754.
- [2] A.K. Jha, B.K. Prasad, O.P. Modi, S. Das, A.H. Yegneswaran, Correlating microstructural features and mechanical properties with abrasion resistance of a high strength low alloy steel, *Wear* 254 (2003) 120-128.
- [3] J. Morrow, G. Tither, Molybdenum in intercritically annealed dual-phase steel strip, *J.Met.* 30 (1978) 16-19.
- [4] R.G. Davies, Deformation behaviour of a vanadium strengthened dual phase steel, *Metall. Trans. A* 9 (1978) 41-52.
- [5] A. Kumar, S.B. Singh, K.K. Ray, Influence of bainite/martensite-content on the tensile properties of low carbon dual-phase steels, *Mater. Sci. Eng., A* 474 (2008) 270-282.
- [6] P. Xu, B. Bai, F. Yin, H. Fang, K. Nagai, Microstructure control and wear resistance of grain boundary allotriomorphic ferrite/granular bainite duplex steel, *Mater. Sci. Eng., A* 385 (2004) 65-73.
- [7] H. Saghafian, S. Kheirandish, Correlating microstructural features with wear resistance of dual phase steel, *Mater. Lett.* 61 (2007) 3059-3063.
- [8] O.P. Modi, P. Pandit, D.P. Mondal, B.K. Prasad, A.H. Yegneswaran, A. Chrysanthou, High-stress abrasive wear response of 0.2% carbon dual phase steel: Effects of microstructural features and experimental conditions, *Mater. Sci. Eng., A* 458 (2007) 303-311.
- [9] V. Abouei, H. Saghafian, S. Kheirandish, K. Ranjbar, A study on the wear behaviour of dual phase steels, *J. Mater. Sci. Technol.* 23 (2007) 107-110.
- [10] R. Tyagi, S.K. Nath, S. Ray, Development of wear resistant medium carbon dual phase steels and their mechanical properties, *Mater. Sci. Technol.* 20 (2004) 645-652.
- [11] O.P. Modi, B.K. Prasad, A.K. Jha, R. Dasgupta, A.H. Yegneswaran, Low-stress abrasive wear behaviour of a 0.2% C steel: influence of microstructure and test parameters, *Tribol. Lett.* 15 (2003) 249-255.
- [12] A.P. Modi, Effects of microstructure and experimental parameters on high stress abrasive wear behaviour of a 0.19wt% C dual phase steel, *Tribol. Lett.* 40 (2007) 490-497.
- [13] G. Bregliozzi, A. Di Schino, J.M. Kenny, H. Haefke, The influence of atmospheric humidity and grain size on the friction and wear of AISI 304 austenitic stainless steel, *Mater. Lett.* 57 (2003) 4505-4508.
- [14] D. Bhattacharyya, A. Hajra, A. Basu, S. Jana, The effect of grain size on the wear characteristics of high speed steel tools, *Wear* 42 (1977) 63-69.

- [15] S. Gündüz, R. Kaçar, H.S. Soykan, Wear behaviour of forging steels with different microstructure during dry sliding, *Tribol. Lett.* 41 (2008) 348-355.
- [16] L. Zhou, G. Liu, Z. Han, K. Lu, Grain size effect on wear resistance of a nanostructured AISI52100 steel, *Scripta Mater.* 58 (2008) 445-448.
- [17] A. Sundstrom, J. Rendon, M. Olsson, Wear behaviour of some low alloyed steels under combined impact/abrasion contact conditions, *Wear* 250 (2001) 744-754.
- [18] H. Suzuki, A.J. Mcevely, Microstructural effects on fatigue crack growth in a low-carbon steel, *Metall. Trans. A* 10 (1979) 475-481.
- [19] S.F. Wayne, S.L. Rice, K. Minakawa, H. Nowotny, The role of microstructure in the wear of selected steels, *Wear* 85 (1983) 93-106.
- [20] A. Bayram, A. Uguz, Effect of microstructure on the wear behaviour of a dual phase steel, *Mater. Technol. Test.* 32 (2001) 249-252.
- [21] M. Sawa, D.A. Rigney, Sliding behavior of dual phase steels in vacuum and in air, *Wear* 119 (1987) 369-390.
- [22] H.-J. Kim, Y.-G. Kweon, The effects of retained austenite on dry sliding wear behavior of carburized steels, *Wear* 193 (1996) 8-15.
- [23] J.-Y. Liu, H. Lu, J.-M. Chen, J.F. Jullien, T. Wu, Simulation of mechanical behavior of multiphase TRIP steel taking account of transformation-induced plasticity, *Comp. Mater. Sci.* 43 (2008) 646-654.
- [24] G. Lacroix, T. Pardoën, P.J. Jacques, The fracture toughness of TRIP-assisted multiphase steels, *Acta Mater.* 56 (2008) 3900-3913.
- [25] G.B. Olson, M. Cohen, Stress-assisted isothermal martensitic transformation: Application to TRIP steels, *Metall. Trans. A* 13 (1982) 1907-1914.
- [26] G.B. Olson, M. Azrin, Transformation behavior of TRIP steels, *Metall. Trans. A* 9 (1978) 713-721.
- [27] G.H. Yang, W.M. Garrison Jr, A comparison of microstructural effects on two-body and three-body abrasive wear, *Wear* 129 (1989) 93-103.
- [28] V.F. da Silva, L.F. Canale, D. Spinelli, W.W. Bose, O.R. Crnkovic, Influence of retained austenite on short fatigue crack growth and wear resistance of case carburized steel, *J. Mater. Eng. Perform.* 8 (1999) 543-548.
- [29] L.C. Cheng, T.B. Wu, C.T. Hu, The role of microstructural features in abrasive wear of a D-2 tool steel, *J. Mater. Sci.* 23 (1988) 1610-1614.
- [30] V.S. Popov, Wear of hardfacing alloys by loose abrasive, *Weld. Prod.* 18 (1971) 49-54.
- [31] L.C. Chang, The rolling/sliding wear performance of high silicon carbide-free bainitic steels, *Wear* 258 (2005) 730-743.
- [32] W. Xu, P.E.J. Rivera-Diaz-del-Castillo, S. Van der Zwaag, Genetic alloy design based on thermodynamics and kinetics, *Philos. Mag.* 88 (2008) 1825-1833.

[33] W. Xu, P.E.J. Rivera-Díaz-del-Castillo, W. Yan, K. Yang, D. San Martín, L.A.I. Kestens, S. van der Zwaag, A new ultrahigh-strength stainless steel strengthened by various coexisting nanoprecipitates, *Acta Mater.* 58 (2010) 4067-4075.

Chapter 3

Development of a novel scratch approach: Multi-Pass Dual-Indenter (MPDI) scratch test

3.1 Introduction

As stated in Chapter 1 and 2, often contradictory observations in the correlation of abrasion resistance and mechanical properties as well as various microstructural aspects (e.g. constituents, phase fraction, grain size, and morphology) have been reported. The contradictions are not only attributed to the complexity of the tribosystem and corresponding testing conditions, but also the dynamic nature of the abrasion process, i.e. the development of subsurface layer and its effect on further abrasion. When a material undergoes abrasion, the top surface deforms severely and may result in different local failure modes depending on the working condition, while the subsurface layer also responds to the external strain/stress and can be strain hardened to different extents depending on the microstructure and its strain hardening capability. The severe deformation leads to significant subsurface refinement and the thickness of such layer also varies. As a consequence, the state of abraded (subsurface) microstructures is quite

different from the original state. Many studies [1-5] have revealed that the subsurface work hardening layer plays a very important role in determining the abrasive wear resistance.

Considering the complexity of the abrasion process and the development of the microstructure, a proper understanding of abrasion resistance and associated damage process and truly reflecting the actual deformation and failure mechanisms are of vital importance. The scratch test, sliding a single rigid indenter of controlled shape under a controlled load and speed against a smooth surface, mimics the abrasion process and has been shown to be useful tool to evaluate the abrasion resistance of various microstructures [6-8]. However, the conventional scratch tests are mostly done on the initial surface [9-13], which can be very different to those that form during the abrasion process, e.g. irregularity, continuous development of subsurface deformation and work hardening etc., and hence do not automatically truly reflect the material abrasion resistant response. As mentioned in references [14, 15], the application of scratch test on initial surface to predict the abrasion mechanism in real abrasion process can lead to serious error and mislead the understanding of the abrasive wear resistance. Williams, *et al.* [16] commented that single pass scratching on a pristine surface is an over simplification of the actual situation, wherein the new particles scratch the worn surface which underwent previous processes. To better simulate the real process, methodologies of multiple parallel scratching have been proposed to include the interactions between scratches, e.g. Williams *et al.* [16, 17], Mezlini *et al.* [18] and Khellouki *et al.*[19]. Compared to the single scratch, it was observed that the wear mechanisms change due to the interactions with prior scratches. Moreover, Da Silva *et al.* [20, 21] also employed parallel scratches but introducing a superimposition between scratches, which suggested that the wear mechanisms depend on the degree of superimposition. Furthermore, in addition to parallel scratches, the repetitive scratching in the same track [22] and the interaction of crossing scratches [23] were also employed to investigate the wear mechanisms. Compared to the single pass scratch on a pristine initial surface, all multiple scratching methods provide more insights on wear mechanisms, the interactions of scratches and the effects of work hardening. Nevertheless, in all experimental setups reported to date, only one indenter was utilized and the new scratch was fully or partially superimposed to the previous scratch, which inevitably combined

the effects of surface work hardening and contact geometry. Moreover, even for the work hardening itself, after only one pre-scratch, the surface and subsurface layer may not reach the stable condition with the saturated work hardening, which is most likely the case in real continuous wear process.

In order to mimic the real life abrasion process and exclude the contact geometrical effect, therefore, in this chapter a new multi-pass dual-indenter scratch test methodology is developed to approach the real abrasion condition by carrying out scratch tests using a large indenter to generate a wide pre-scratch (wear track) with stable saturated work hardening representing the subsurface layer formed during the real life abrasion, and a small indenter sliding over the pre-scratched surface to evaluate the wear resistance and record the failure mechanism [24].

3.2 The concept of multi-pass dual-indenter scratch test

In this chapter, the target we pursuit is to develop a new scratch test to approach the real life abrasion process. Inspired by the understanding of the real abrasion process and derived from conventional scratch test, a design concept of scratch methodology is presented which not to use a single indenter but combine a large indenter and small indenter. In this scratch methodology, the large indenter is designed to produce a local pre-deformed surface layer with work hardening equivalent to the surface layer presented during an abrasion test, and the small indenter sliding over the pre-scratched surface is used to mimic the single particle behaviour in a real life steady-state abrasion process involving a work hardened surface state and to reveal the corresponding damage mechanisms. This test method not only probes damage formation during the actual scratching (abrasion) process but also probes its interaction with the damage in the deformed surface layer caused by prior local scratch deformations.

3.3 Detailed scratch test procedures

The multi-pass dual-indenter (MPDI) scratch tests were performed with a CSM micro-scratch tester, schematically illustrated in Fig. 3.1. Two spherical diamond Rockwell indenters with different tip radius and cone angles were employed in the current study, i.e., a small indenter with a tip radius of $5\mu\text{m}$ and a cone angle of 60° , and a large indenter with a tip radius of $100\mu\text{m}$ and a cone angle of 120° . The sliding speed in the tests was $30\text{mm}/\text{min}$. A fixed scratch length of 5mm was produced with the large indenter, and a 4mm scratch was superimposed by the small indenter along the axis of the big pre-scratch track. All tests were conducted at room temperature under a relative humidity ranging from 40% to 80%. A typical MPDI scratch test consists of three steps:

- 1) Pre-scratching of the original surface with the large indenter, employing vertical loads ranging from 1N to 30N in order to create a well-defined deformation hardened layer of variable thickness similar to the layer presented during the real life abrasion.
- 2) Pre-scanning of the profile of the central bottom region of the pre-scratch track formed using the small indenter with a very low load of 0.03N such as not to cause any further damage or deformation.
- 3) Scratching finally at the bottom of the scratch track created by the large indenter using the small indenter with single pass and a fixed vertical load in order to induce local damage in the surface hardened layer, in a manner comparable to that encountered during the steady state of the multi-body abrasion testing.

All sliding tracks made with the small indenter were in the very centre of the pre-scratch tracks made by the large indenter. The schematic setup of the novel multi-pass dual-indenter scratch test was shown in details in Fig. 3.2.

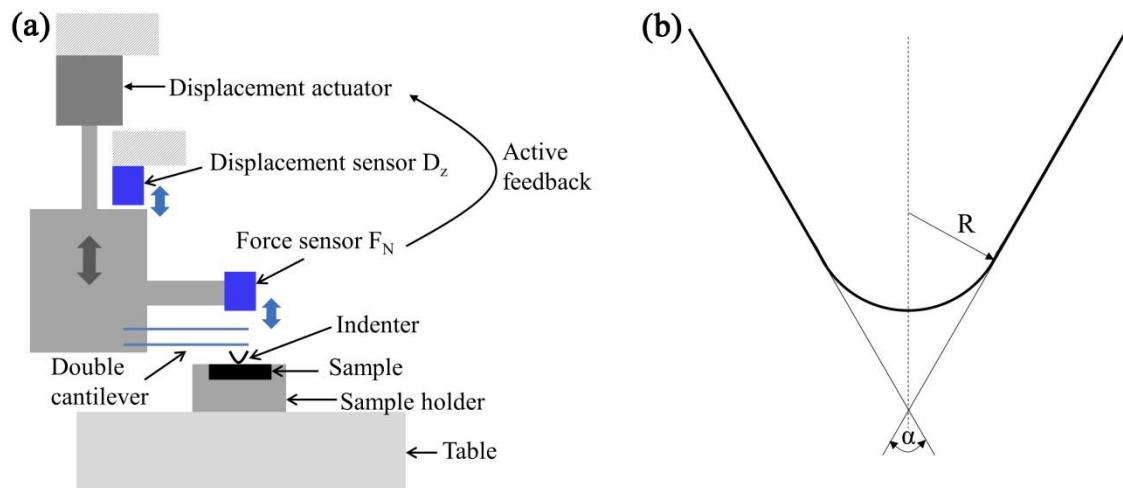


Fig. 3.1 A schematic drawing of the scratch test: (a) the test configuration; (b) the shape of the indenters.

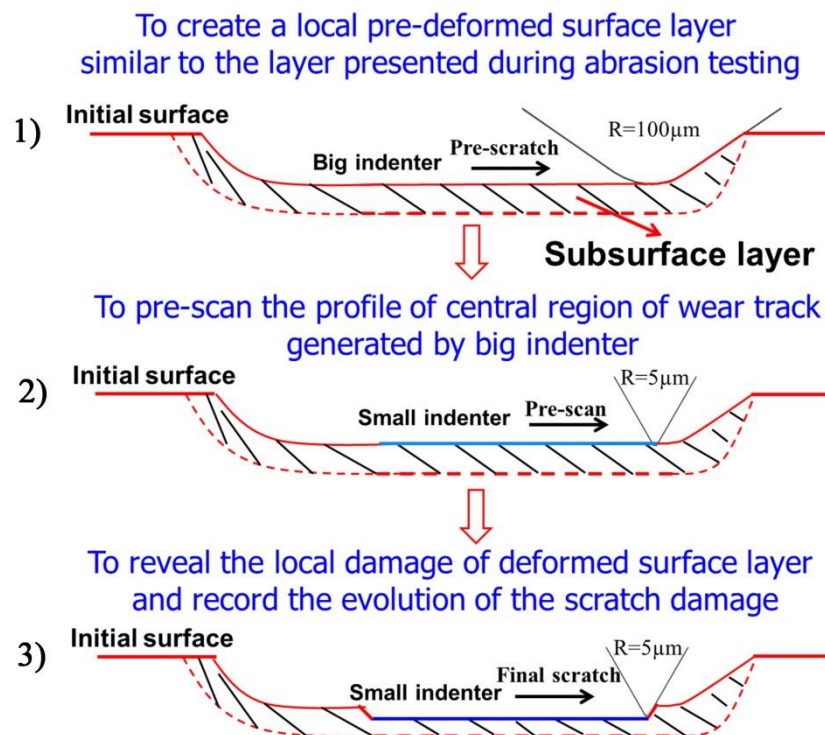


Fig. 3.2 the setup of multi-pass dual-indenter scratch test.

3.4 Schematic drawing of scratch tracks and output parameter of scratch tests

Fig. 3.3 gives the schematic drawing of observations of scratch tracks. The zone enclosed by red dash line refers to the pre-scratch track produced by the large indenter. The scratch track created by the small indenter at the bottom of the big pre-scratch track corresponds to the zone enclosed by the blue dash line. It is worth pointing out that the occurrence of damage appeared right after the small indenter.

Unless stated otherwise, the scratch depth to be reported in this thesis as output parameter refers to the penetration depth by the small indenter scratching with respect to the bottom of the wear track produced by the large indenter. The measurement of scratch depth consists of two steps: firstly, pre-scanning the profile of surface with the small indenter at a very low load of 0.03N and secondly, scratching at the same track with the small indenter using a fixed load. The penetration depth is derived from the difference of the two steps. The scratch profiles as taken according to the description showed a very good reproducibility of the scratch depth of about $\pm 0.1 \mu\text{m}$ in the steady state region of the scratch, which commenced well within 1 mm after the onset of the scratch, as shown in Fig. 3.4. Furthermore, the depth of the profile was nearly constant along the steady state section of the scratch. All sliding tests were run in the same direction. Each test was repeated 3 times to make sure that reproducibility was observed and reported. The final scratch depth was given as average of 3 separate measurements which were taken from the steady state.

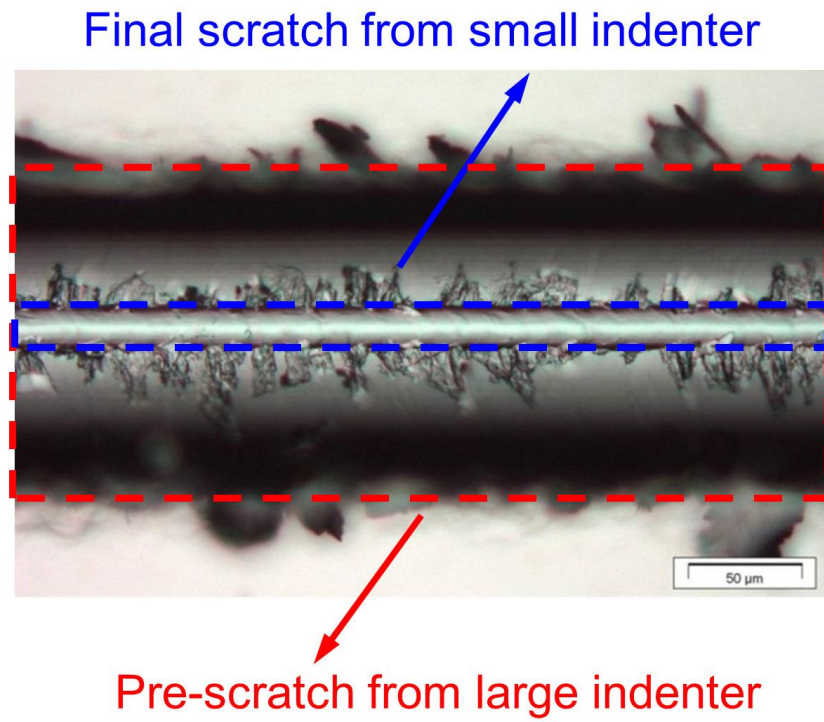


Fig. 3.3 The schematic drawing of morphological observations of scratch tracks.

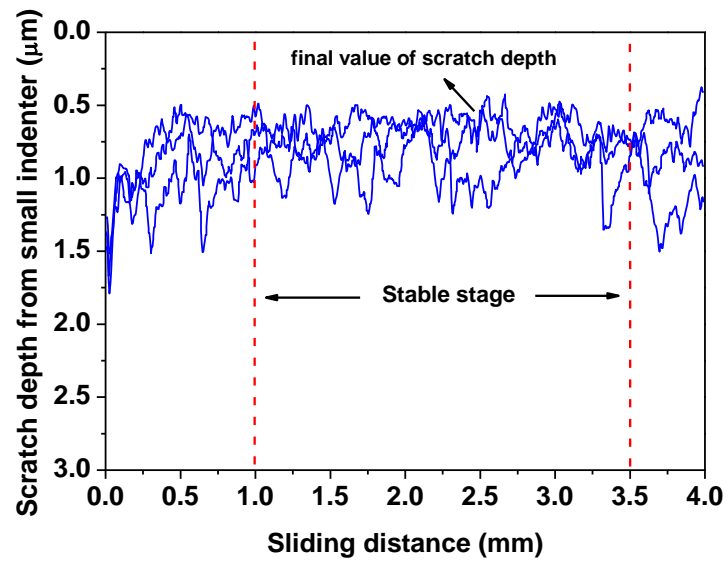


Fig. 3.4 The scratch depths to be reported as output by the small indenter only.

References

- [1] O.P. Modi, B.K. Prasad, S. Das, A.K. Jha, A.H. Yegneswaran, Abrasive wear behavior of an Aisi-5132 steel under low stresses, *Mater. Trans., JIM* 35 (1994) 67-73.
- [2] B.K. Prasad, S.V. Prasad, Abrasion-induced microstructural changes during low stress abrasion of a plain carbon (0.5% C) steel, *Wear* 151 (1991) 1-12.
- [3] L. Fang, Q.D. Zhou, Y.J. Li, An explanation of the relation between wear and material hardness in three-body abrasion, *Wear* 151 (1991) 313-321.
- [4] A. Ball, On the importance of work hardening in the design of wear-resistant materials, *Wear* 91 (1983) 201-207.
- [5] P. J. Mutton, J.D. Watson, Some effects of microstructure on the abrasion resistance of metals, *Wear* 48 (1978) 385 - 398.
- [6] V. Jardret, H. Zahouani, J.L. Loubet, T.G. Mathia, Understanding and quantification of elastic and plastic deformation during a scratch test, *Wear* 218 (1998) 8-14.
- [7] G. Subhash, W. Zhang, Investigation of the overall friction coefficient in single-pass scratch test, *Wear* 252 (2002) 123-134.
- [8] A. Vencel, N. Manić, V. Popovic, M. Mrdak, Possibility of the abrasive wear resistance determination with scratch tester, *Tribol. Lett.* 37 (2010) 591-604.
- [9] T. Kayaba, K. Hokkirigawa, K. Kato, Analysis of the abrasive wear mechanism by successive observations of wear processes in a scanning electron microscope, *Wear* 110 (1986) 419-430.
- [10] K. Hokkirigawa, K. Kato, Z.Z. Li, The effect of hardness on the transition of the abrasive wear mechanism of steels, *Wear* 123 (1988) 241-251.
- [11] T.A. Adler, R.P. Walters, Wear and scratch hardness of 304 stainless steel investigated with a single scratch test, *Wear* 162-164, Part B (1993) 713-720.
- [12] J.C.P. Zuñega, M.G. Gee, R.J.K. Wood, J. Walker, Scratch testing of WC/Co hardmetals, *Tribol. Lett.* 54 (2012) 77-86.
- [13] M.J. Murray, P.J. Mutton, J.D. Watson, Abrasive wear mechanisms in steels, *J. Lubr. Technol.* 104 (1982) 9-16.
- [14] H.R. Shetty, T.H. Kosel, N.F. Fiore, A study of abrasive wear mechanisms in cobalt-base alloys, *Wear* 84 (1983) 327-343.
- [15] H.R. Shetty, T.H. Kosel, N.F. Fiore, A study of abrasive wear mechanisms using diamond and alumina scratch tests, *Wear* 80 (1982) 347-376.
- [16] J.A. Williams, Y. Xie, The generation of wear surfaces by the interaction of parallel grooves, *Wear* 155 (1992) 363-379.
- [17] Y. Xie, J.A. Williams, The generation of worn surfaces by the repeated interaction of parallel grooves, *Wear* 162-164 (1993) 864-872.

- [18] S. Mezlini, P. Kapsa, C. Henon, J. Guillemenet, Abrasion of aluminium alloy: effect of subsurface hardness and scratch interaction simulation, *Wear* 257 (2004) 892-900.
- [19] A. Khellouki, J. Rech, H. Zahouani, Micro-scale investigation on belt finishing cutting mechanisms by scratch tests, *Wear* 308 (2013) 17-28.
- [20] W.M. da Silva, J.D.B. de Mello, Using parallel scratches to simulate abrasive wear, *Wear* 267 (2009) 1987-1997.
- [21] W.M. Da Silva, H.L. Costa, J.D.B. De Mello, Transitions in abrasive wear mechanisms: Effect of the superimposition of interactions, *Wear* 271 (2011) 977-986.
- [22] S. Mezlini, P. Kapsa, J.C. Abry, C. Henon, J. Guillemenet, Effect of indenter geometry and relationship between abrasive wear and hardness in early stage of repetitive sliding, *Wear* 260 (2006) 412-421.
- [23] M.J. Adams, A. Allan, B.J. Briscoe, P.J. Doyle, D.M. Gorman, S.A. Johnson, An experimental study of the nano-scratch behaviour of poly (methyl methacrylate), *Wear* 250-251 (2001) 1579-1583.
- [24] X. Xu, S. van der Zwaag, W. Xu, A novel multi-pass dual-indenter scratch test to unravel abrasion damage formation in construction steels, *Wear* 322-323 (2015) 51-60.

Chapter 4

Application of the MPDI scratch test to unravel abrasion damage formation

4.1 Introduction

After developing the novel multi-pass dual-indenter scratch (MPDI) test methodology in Chapter 3, five steel grades with different work hardening capabilities, i.e. Interstitial-Free ferritic steel (IF steel), Fully Martensitic steel (FM steel), Dual Phase steel (DP steel), Quench Partitioning steel (Q&P steel) and TWining Induced Plasticity steel (TWIP steel) were selected for this study. Systematic scratch experiments were performed by carrying out the new scratch test with different pre-scratched conditions. The abrasion resistance of various microstructures and the work hardening behavior are studied. The worn scar and the development of subsurface deformation layers are investigated. The damage mechanisms upon different test conditions are analyzed.

4.2 Experimental procedures

4.2.1 Materials and microstructures

In the current study, five different types of construction steels with different work hardening capabilities are chosen. Their compositions and corresponding microstructures are summarized in Table 4.1. Their microstructures in the form of SEM micrographs are shown in Fig. 4.1. The IF steel is a single phase ferritic steel with very low interstitial elements. As shown in Fig. 4.1a, the average grain size is about 45 μ m. The FM steel possesses a single phase martensite obtained by full austenitization and water quenching the DP steel. As shown in Fig. 4.1b, no retained austenite is visible in the as-quenched condition. The DP steel is a commercial dual phase steel grade, consisting of approximately 30% ferrite and 70% martensite (Fig. 4.1c), produced by intercritical annealing and subsequent water quenching. The Q&P steel possesses complex microstructure of ferrite, martensite and retained austenite in which the quenching and partitioning (Q&P) process [1] was employed to partition the carbon from oversaturated martensite to retained austenite and hence to increase the stability of the later. The microstructure is shown in Fig. 4.1d in which the retained austenite (~12%) can be clearly identified. It is embedded in a matrix mixture of ferrite (~28%) and martensite (~60%). The TWIP steel is a specific high Mn austenitic steel, which displays very high work hardening capability by forming twins upon deformation. Some twin structures are already observed on the polished surface (Fig. 4.1e).

Table 4.1 Chemical composition, microstructures and Vickers hardness of steel grades investigated.

Material	Chemical composition	Microstructures	Hardness (HV _{0.2})
IF steel	0.0009C-0.1Mn-0.11Ti-0.02Cr	Ferrite	100 \pm 3
FM steel	0.15C-1.9Mn-0.2Si-0.15Cr	Martensite	482 \pm 9
DP steel	0.15C-1.9Mn-0.2Si-0.15Cr	ferrite + martensite	316 \pm 8
Q&P steel	0.22C-1.8Mn-1.4Si	ferrite + martensite + retained austenite	308 \pm 6
TWIP steel	0.60C-18.0Mn-1.5Al	austenite (twin)	241 \pm 2

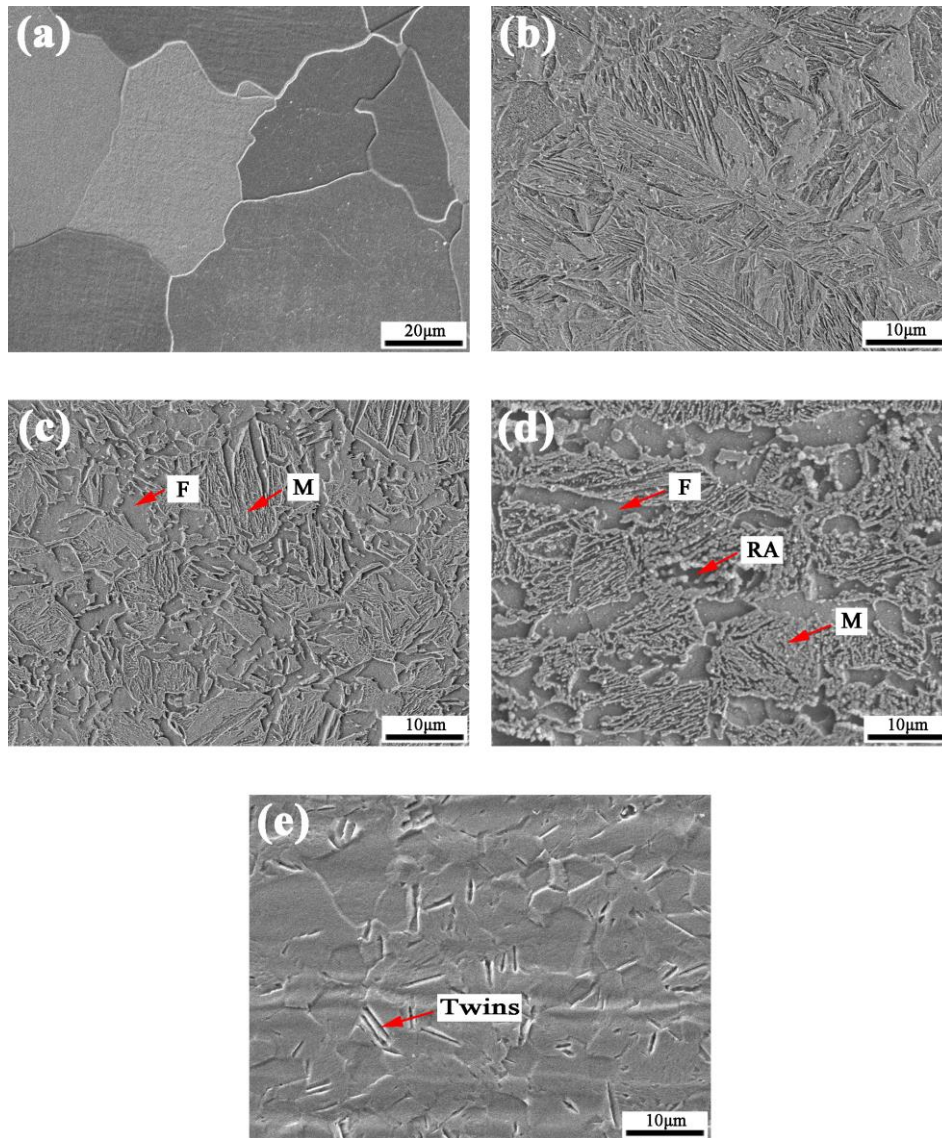


Fig. 4.1 Microstructures of various steels: (a) IF steel; (b) FM steel; (c) DP steel; (d) Q&P steel and (e) TWIP steel.

4.2.2 Sample preparation and hardness test

Prior to the hardness measurements and scratch testing, samples were mounted inside the cold-setting resin and polished following the standard metallographic preparation. Micro-hardness measurements were carried out using Vickers indenter under 2N load and making 10 independent measurements. Hardness values are listed in Table 4.1. The IF steel possesses the lowest hardness owing to the soft nature of the ferrite, while the fully martensitic steel displays the highest hardness of 482Hv because of its

composition and the intrinsic structure of martensite. Hardness of DP and Q&P steel are at an intermediate level due to the mixture of ferrite and martensite phases (in Q&P steel with the presence of retained austenite). The hardness of TWIP steel is quite low, ~240 Hv, corresponding to a fully austenite matrix with limited twinning upon indentation. The size of specimens for scratch testing is 15mm×9mm.

4.2.3 Scratch tests

In this chapter, the MPDI scratch tests were carried out in which three testing modes were employed with conditions as specified in Table 4.2.

- Mode I, the small indenter scratching directly on the initial (polished) surface
- Mode II, the small indenter scratching on a pre-scratch produced by the large indenter with a single pass under different loads
- Mode III, the small indenter scratching on a pre-scratch produced by the large indenter with multiple passes (10 passes) under different loads

Table 4.2 Test conditions of different scratch modes:

Scratch modes	Test conditions of small indenter	Test conditions of large indenter
Mode I	Single pass with constant load of 0.3N	NA
Mode II	Single pass with constant load of 0.3N	Single pass with 1N, 3N, 5N, 10N, 15N, 20N, 25N, 30N
Mode III	Single pass with constant load of 0.3N	Multi-pass (10 passes) with 1N, 3N, 5N, 10N, 15N, 20N, 25N, 30N

4.2.4 Metallography and worn surface

After the scratch test, the worn surface was directly observed by SEM without etching. To this aim, a high-resolution JEOL scanning electron microscope (HR-SEM) operating at 5 kV was employed. Samples of the cross-section perpendicular to the scratching

direction were prepared in order to observe the microstructure development under the worn surface and were investigated by SEM, after etching with a conventional 2% Nital solution, and sputtering with gold.

4.3 Results

4.3.1 Scratch test

Figures 4.2a and 4.2b show the scratch depth as a function of the applied load on the large indenter for single pass (Mode II) and a 10-pass pre-deformation (Mode III) respectively. In both figures the scratch depth at normal load of 0 N corresponds to the scratch depth after scratching the original polished surface (Mode I). In Fig. 4.2a the hardness values for each steel as obtained by indentation are also indicated. A good correspondence between the (static) hardness value and the scratch depth for 0 N data point (i.e. the as-polished surface) is obtained.

While the curves for the various steel grades plotted in figures 4.2a and 4.2b may seem rather different, in essence they follow the same behavior. A relatively high scratch depth is observed for the 0 N load case (the pristine sample). Upon increasing load on the large indenter the (additional) scratch depth of the small indenter decreases first for both testing modes and for all steel grades. The decrease in scratch depth is largest for the softer steel grades and is smallest for the hardest steel grade. The decrease in scratch depth reflects the effect of (sub) surface hardening due to the pre-scratching. The trend of decreasing scratch depth with increasing load on the large indenter continues up to a critical load beyond which the scratch depth of the small indenter starts to increase again. This increase in scratch depth reflects abrasive material removal/damage. This increase in scratch depth is most noticeable for the IF steel and the FM steel grade, yet becomes noticeable for all other steels in mode III testing at higher load levels. Only for the TWIP steel the maximum applied load that could be applied during scratching was below the (assumed) transition load. The main difference between the results for the mode II and the mode III testing is the sharpening of the transition between the region of decreasing (additional) scratch depth due to surface hardening and the region of

increasing scratch depth due do material removal/damage. Furthermore, for IF and FM steels, the critical load values for mode III testing involving ten pre-scratching actions is lower than that for mode II testing involving only one pre-scratch with the large indenter, but the opposite holds for the other steel grades.

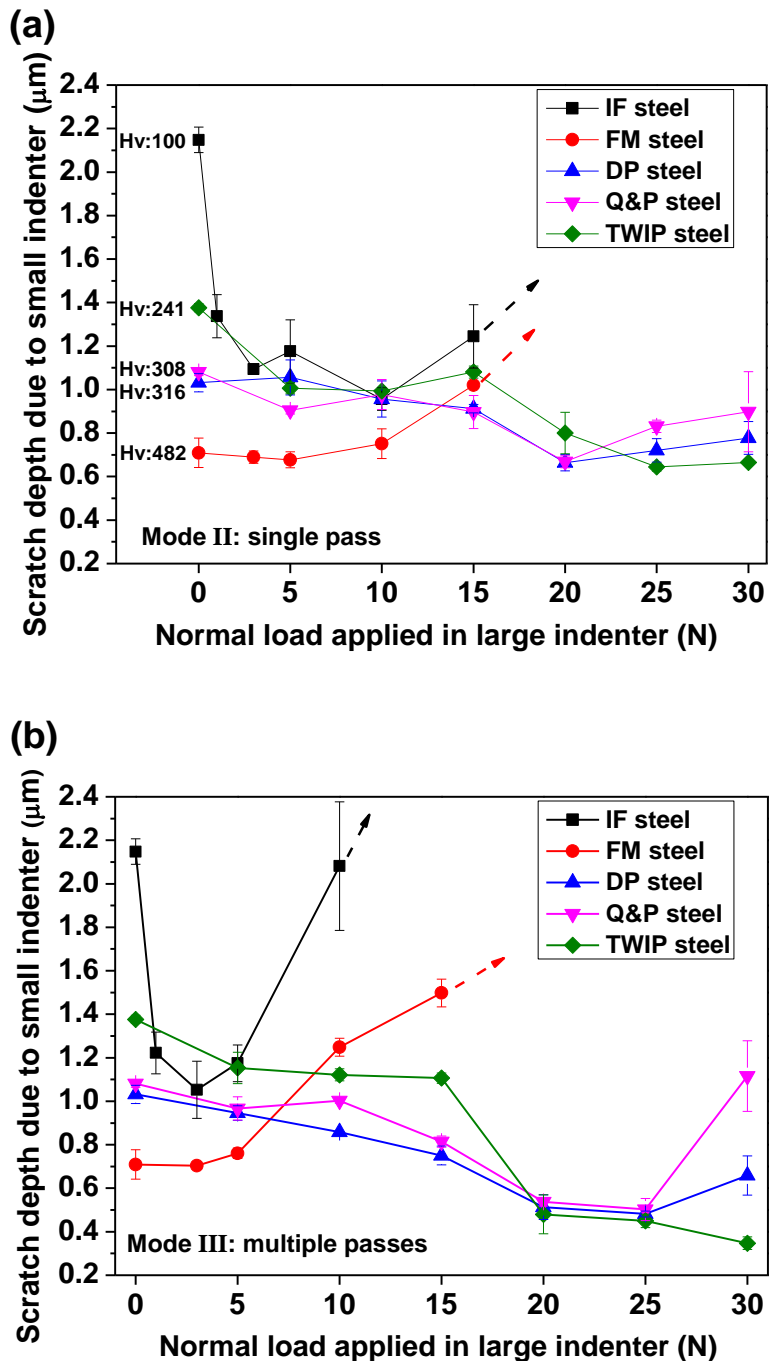


Fig. 4.2 The scratch depth produced on various steels by a single pass with the small indenter as functions of different normal loads applied by the large indenter with (a) single pass scratch-Mode II, (b) multiple passes scratch - Mode III.

4.3.2 Morphology of the groove and observed failure mechanisms

As the behavior of modes II and III were comparable with mode III being more discriminative, samples produced in mode III were selected for further morphological investigation also because they are expected to better represent the failure mechanisms of steady state that occur in the continuous abrasion process. Figures 4.3-4.7 display scratch grooves made by the small indenter on pre-scratch via the large indenter under loads of 0N, 5N and 15N (10N for IF steel) for IF, FM, DP, Q&P and TWIP steels, respectively. The pre-scratch with 0 N refers to that the small indenter scratches on the initial polished surface, which are shown in Figures 4.3a-4.7a. It should be noted that the scratch tracks presented in Figures 4.3(b, c)-4.7(b, c) are grooves produced by the small indenter, while the entire field of view is within the central zone of the big scratches by the large indenter.

Fig. 4.3 illustrates the damage mechanism of the softest IF steel. The scratch track on the initial surface in Fig. 4.3a reveals that the mechanism is mainly ploughing accompanied by some debris formation due to cutting. As the pre-scratch load increases to 5N, delamination starts to appear on the edge and in the center of scratch, as seen in Fig. 4.3b. The failure mechanisms changed from ploughing to micro-cutting. Moreover, a lot of cracks can be observed perpendicular to the small scratch, which suggests that the surface is fully work hardened upon the pre-scratching, and hence explains the lower scratch depth comparing to the initial surface. A further increase of the load on the large indenter to 10N results in severe plastic deformation on the pre-scratched surface, which further leads to the propagation of cracks. Upon subsequent scratching with the small indenter, the cracks connect with each other and lead to significant delamination (as shown in Fig. 4.3c), showing the micro-cracking and cutting mechanism, and resulting in the highest scratch depth.

The FM steel displays a similar damage evolution with increasing pre-scratch load, as shown in Fig. 4.4. Fig. 4.4a reveals the formation of debris in the scratch track, showing ploughing and cutting mechanisms. For the 5N pre-scratching condition a small amount of delamination can be observed on the edge of the scratch as shown in Fig. 4.4b. When the load increases to 15N, severe delamination takes place because of the brittle nature and low work hardening capability of the martensite, as shown in Fig. 4.4c. The failure

mechanism changed to the micro-cracking and cutting mechanism. As a consequence, the (additional) scratch depth significantly increases, which is consistent with the results in Fig. 4.2.

The DP steel possessing a good combination of ductility and strength shows mild damage compared to IF and FM steels as shown in Fig. 4.5. The SEM images on the initial surface and under 5N pre-scratch demonstrate that the main failure mechanisms are ploughing, as shown in Figs. 4.5a-4.5b. Some debris was also found due to cutting in Fig. 4.5a. It is shown in Fig. 4.5c that even when the load increases to 15N only some mild delamination can be observed on the edge of the scratch track but no craters are formed. The width (and hence the depth) of the scratch track under 15N pre-scratch is smaller than those under 0N and 5N, which is in line with results shown in Fig. 4.2.

Similarly, for the Q&P steel scratching at low load produces some craters due to ploughing as shown in Figs. 4.6a and 4.6b, while for the 15N pre-scratch cracks propagate perpendicular to the scratch track and delamination can be found in Fig. 4.6c, showing the micro-cracking and cutting mechanism. It is important to mention that those cracks don't appear right after the pre-scratch with the large indenter but only after the next scratch made by the small indenter within the center of the pre-scratch made with the large indenter. This indicates that the failure mechanisms revealed here is associated to the scratch resistance of the work hardened surface, which may differ from the scratch resistance of the original surface.

Finally, for all pre-loading conditions the scratch groove of TWIP steel always looks smooth and displays very little cracks/delamination, as presented in Fig. 4.7. The systematic analysis of scratch tracks reveals clear the dependence of the failure mechanisms on both the pre-scratch condition, and the microstructures and their associated work hardening capabilities.

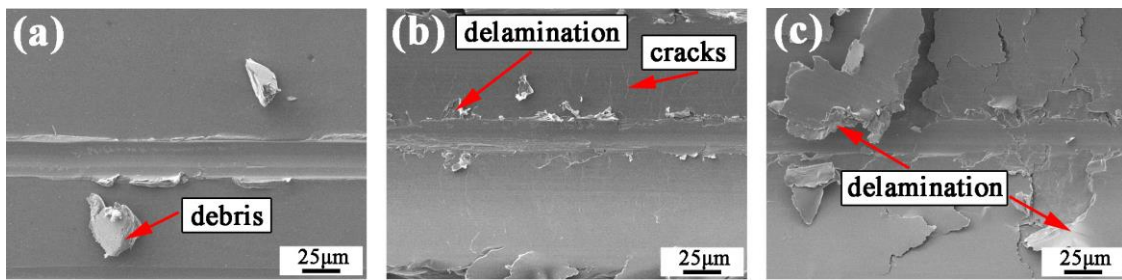


Fig. 4.3 Scratch tracks of IF steel by the small indenter with 0.3N following pre-scratching Mode III under different loads of (a) 0N, (b) 5N and (c) 10N.

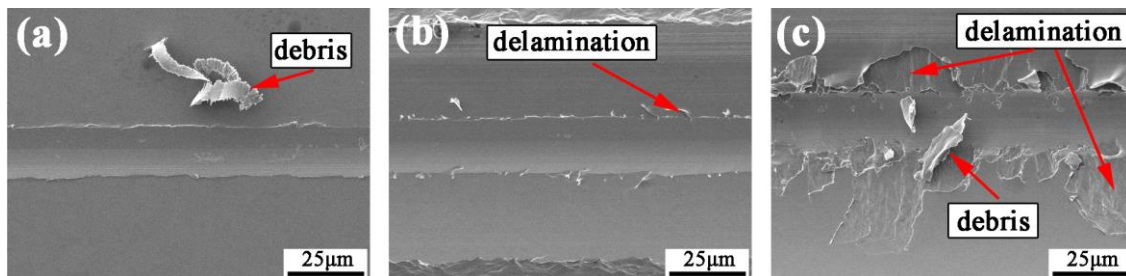


Fig. 4.4 Scratch tracks of FM steel by the small indenter with 0.3N following pre-scratching Mode III under different loads of (a) 0N, (b) 5N and (c) 15N.

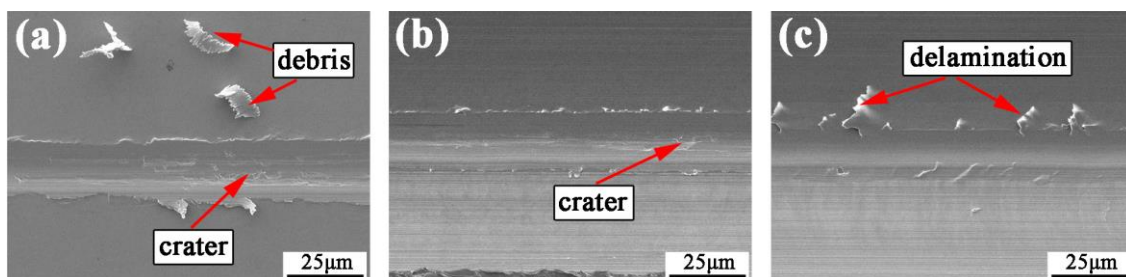


Fig. 4.5 Scratch tracks of DP steel by the small indenter with 0.3N following pre-scratching Mode III under different loads of (a) 0N, (b) 5N and (c) 15N.

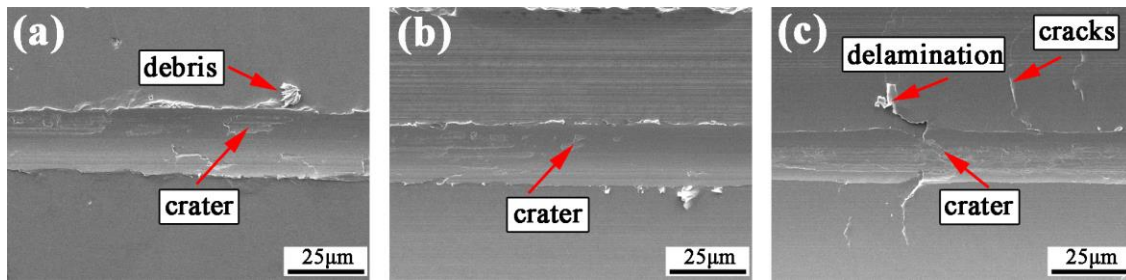


Fig. 4.6 Scratch tracks of Q&P steel by the small indenter with 0.3N following pre-scratching Mode III under different loads of (a) 0N, (b) 5N and (c) 15N.

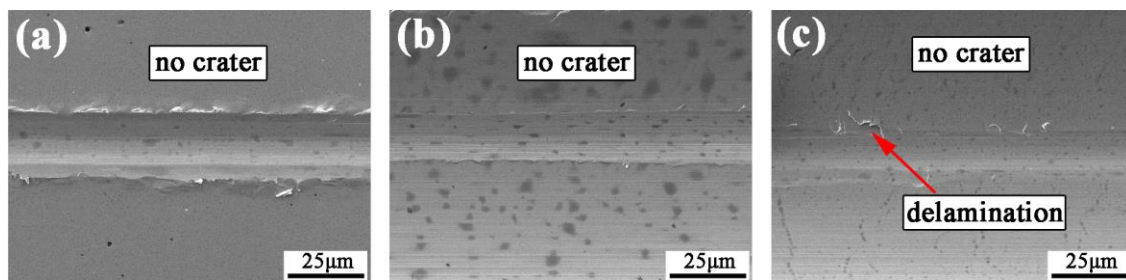


Fig. 4.7 Scratch tracks of TWIP steel by the small indenter with 0.3N following pre-scratching Mode III under different loads of (a) 0N, (b) 5N and (c) 15N.

4.3.3 Sub scratch surface development

To understand the response of material beneath the surface upon (pre)scratch, microstructures of the cross-sections perpendicular to the scratch track were investigated by SEM, and results are shown in Fig. 4.8. In the figures, the scratch tracks produced by the small indenter are highlighted by the dashed red line, while the entire top surface refers to the central zone produced by the pre-scratch with the large indenter. For all micrographs it is clear that the microstructure beneath the surface was severely modified by the pre-scratching. The thicknesses of scratch subsurface are in the range of 11-24 μm depending on the steel microstructures and the preloading conditions. Unless stated otherwise, the load during the pre-scratching with the large indenter was 15N (10N for IF steel). In all cases shear deformation can be clearly observed, as well as the grain refinement. The degree of shear deformation and grain refinement is not uniformly distributed and it shows a decreasing gradient from the surface to the bulk.

This microstructure modification is due to the severe deformation in the normal direction and even more significant in the sliding direction. The plastic deformation and the work hardening response determine the morphology of the subsurface layer. For IF steel, because of the low yield strength, the thickness of subsurface layer is significantly larger than those for steel grades possessing higher yield strength, i.e. FM, DP, Q&P and TWIP steels. Martensite being the strongest materials shows the shallowest layer after deformation. The TWIP steel having a low yield strength but a very high work hardening capability displays a similar subsurface layer thickness as the medium yield strength Q&P steel. It is interesting to point out that in the case of the TWIP steel which employs twin formation for strengthening, clear evidence of twin formation can be observed not only in the subsurface deformation layer, but also further away in the bulk material where no clear signs of shear deformation and grain refinement were observed. All cross sections show that the small indenter only scratches the very surface area of the pre-scratch, which means that the small indenter truly reflects the surface property of the top work hardening layer. The subsurface modification introduced by the small scratch as such cannot be identified because of the low load applied on the small indenter.

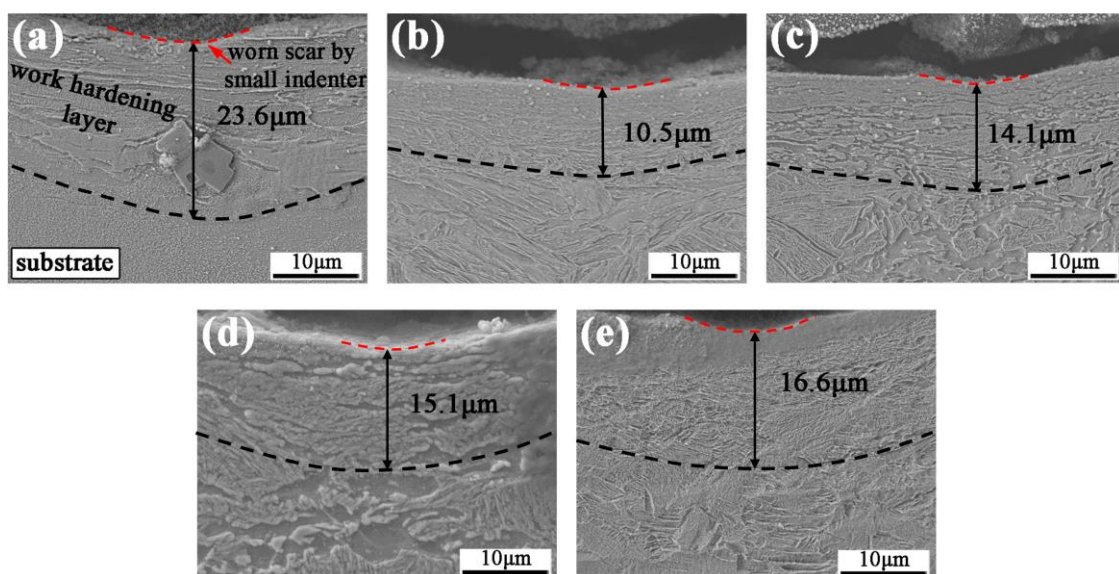


Fig. 4.8 Microstructures in cross-sections perpendicular to scratch track after multiple passes of pre-scratch and the final scratch of (a) IF, (b) FM, (c) DP, (d) Q&P and (e) TWIP steels. Note: for IF steel the pre-scratch load was 10N. For all other steels the pre-scratch load was 15N.

4.4 Discussions

The results on scratch tests, and microstructure developments both on and beneath the surface reveal that the scratch/wear resistance depends on not only the initial microstructure, but also the deformation and work hardening condition of the surface and subsurface layer, which may shift the failure mechanism from one type to another. In the discussion, four major questions are discussed. Firstly, the effect of work hardening layer on scratch resistance in various microstructures is analyzed. Secondly, the comparison of single pass and multiple passes scratch modes in MPDI scratch test is addressed. Thirdly, the MPDI scratch test is compared with conventional scratch tests. Finally, the correlation between the new scratch methodology with the real abrasion process is discussed.

4.4.1 Effect of work hardening on scratch resistance

Commonly scratch tests to study and predict abrasion resistance are performed on the initial surface, while the new scratch methodology presented here involves scratching with a fine indenter on the scratch track made by a larger indenter. Hence the current methodology controls scratching on a work hardened surface layer, which is more similar to the worn surface developed during the continuous abrasion process. Work hardening of a material increases its yield strength but the effect on the wear resistance is more complicated, e.g. cold-worked non-recovered materials may have a lower wear resistance [2], while it is also reported that a material with higher work hardening can display a better abrasion resistance [3, 4]. These contradictories should be attributed to the work hardening capability of materials, the degree of work hardening and the corresponding microstructure development. IF steel is a soft and ductile material and hence it reaches the local yield strength even under a low pre-loading condition and initiates the work hardening process even for mild conditions. Although the work hardening capability of IF steel is not very high, its relative contribution with respect to the initial yield is still considerable and hence work hardening yields a clear improvement of scratch resistance, as shown in Fig. 4.2. However, because of the relative low failure strength, the maximal strengthening is also reached at a low load, i.e.

the transition load shown in Fig. 4.2. Scratching loads beyond the critical load lead to severe delamination as shown in Fig. 4.3 (b, c). As a consequence, the apparent additional penetration depth upon new scratch increases significantly. On the other hand, martensite steel has a very high yield and ultimate tensile strength, and hence displays the shallowest scratch on the initial surface. Because of the low work hardening capability, the improvement in scratch resistance due to strain hardening is very limited. It is interesting to note that, despite of its much higher strength and the difference in initial hardness, the transition load of martensitic steel is similar to that of the IF steel. This may be attributed to the low ductility of martensite. When the pre-loading exceeds the critical value, the corresponding local strains in the scratch track (much smaller than that of IF steel) reaches their limit and the brittle martensite becomes susceptible to crack propagation and brittle delamination [5]. A further increase in pre-scratch load will significantly increase the density of defects/microcracks in the subsurface layer which turn to result in the micro-fracture and severe delamination upon the second scratch pass, as shown in Fig. 4.4(b, c).

As stated in Chapter 2 and the reference [6], a proper dual phase mixture of ductile ferrite and strong martensite could be an attractive alternative to improve the scratch resistance, other than pursuing an even harder full martensite structure. This dual phase mixture enables a high work hardening. The significant amount of hard martensite provides a good starting performance on the initial surface in Fig. 4.5a. In a low pre-scratch condition, ductile ferrite accommodates the strain and simultaneously gets strain hardened and increases the scratch resistance. The combination of the high ductility of ferrite and the significant work hardening of dual phase mixture makes the strengthening regime extend to a high pre-scratch load, up to 25N. The mild damage is in the form of a few craters and mild delamination as shown in Fig. 4.5 (b, c) and cracks in Fig. 4.9a. When the load increases to 30N, the critical load is exceeded and big cracks can form perpendicular to the new scratch as shown in Fig. 4.9b. The much enlarged strengthening domain makes the scratch resistance superior to those of IF and FM steels in a harsh abrasion condition. The observation clearly demonstrates that the combination of ferrite and martensite in a single microstructure leads to synergistic effects on the scratch resistance. In comparison to DP steel, Q&P steel shows two major microstructural differences, i.e. 1) a considerable amount of C enriched retained

austenite and 2) a much lower C concentration in the martensitic phase fraction [1]. Consequently, two effects on wear response can be expected, i.e. 1) retained austenite can increase the work hardening and hence enhances the wear resistance via Transformation Induced Plasticity (TRIP) effect [7, 8] and additional internal stresses due to the volume expansion in the austenite-martensite transformation [3] and 2) The C depletion in martensite decreases the strength of martensite while the recovery of dislocation during partition process increases the work hardening capability of martensite. The multiple mechanisms may also lead to the seemingly double transitions in Fig. 4.2. A possible hypothesis is that at the low load condition up to 5 N, only work hardening of ferrite and martensite are operational. When the load is increased beyond 10N, the TRIP effect is triggered and the material enters the second strengthening regime by effective transformations. It can be observed in Fig. 4.6 that the scratch tracks look similar to that of DP steel in the low preloading condition. However, for the 30 N condition serious delamination as shown in Fig. 4.9d, is observed which may be linked to the newly TRIP formed martensite blocks. Finally, TWIP steel has a fully austenitic microstructure and it is characterized by low yield strength, a very high work hardening capability and hence a high ultimate tensile strength and ductility [9, 10], owing to the formation of mechanical twins upon loading. The current investigations also revealed a very attractive scratch resistance. For the initial surface, the low yield strength leads to a high scratch depth (the second worst) but the scratch depth keeps decreasing when the pre-scratch load is increased because of the very high work hardening capability. Consequently, it can be found in Fig. 4.7(a-c) and Fig. 4.9(e, f) that the scratch tracks under all conditions show smooth morphology and no craters and delamination are observed. During the pre-scratching, a significant amount of mechanical twins form in the subsurface layer, and they even extend into the bulk material where no evident shear deformation could be observed. The twin formation in the bulk which accommodates the strain in a continuous manner contributes to the (assumed) late transition load beyond 30N, as shown in Fig. 4.2.

The results as discussed above clearly point out that the formation of work-hardening layer resulting from plastic deformation on and beneath the scratch surface made by the large indenter plays the vital role in determining scratch resistance and associated damage mechanisms. Depending on the initial yield strength and work hardening

capability, the surface and subsurface layer are modified and strengthened to different degrees upon pre-scratching leading to remarkably different behaviors during the final scratch. The initial hardness value and the scratch test results on the pristine surface may be misleading when evaluating the continuous abrasion resistance as for a large part of the component life time the abrasion process will be on worn/deformation strengthened surfaces, i.e. the steady state.

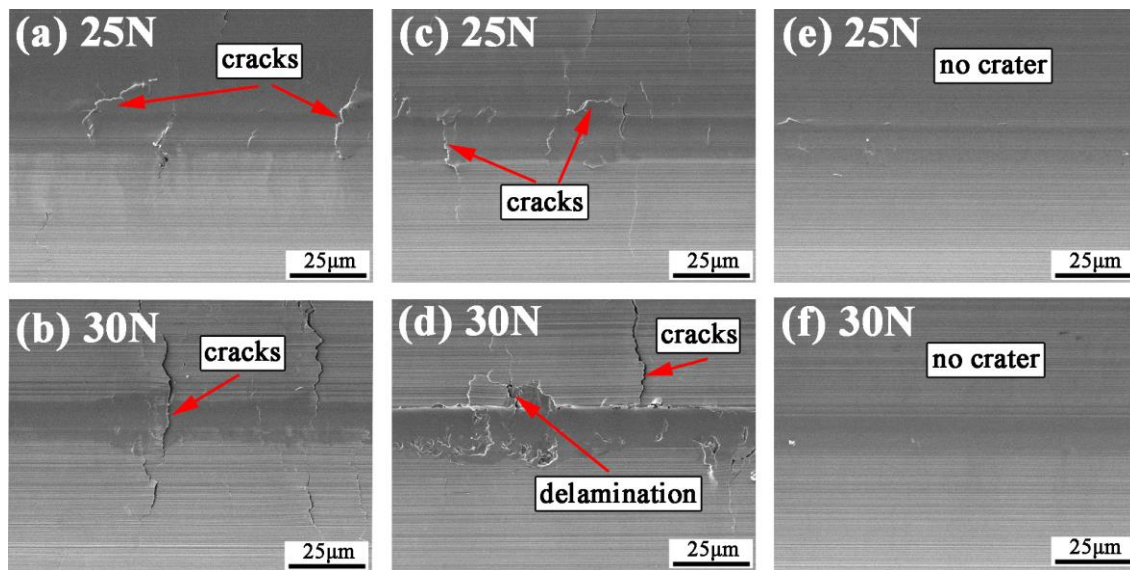


Fig. 4.9 Scratch tracks of DP (a, b), Q&P (c, d) and TWIP (e, f) steels by the small indenter on pre-scratch by the large indenter under 25N and 30N (10 passes).

4.4.2 Comparison of single pass and multiple passes pre-scratching modes

Results of single pass (Mode II) and multiple passes (Mode III) pre-scratching are compared in order to investigate effects of strain accumulation on the subsurface layer development and the scratch resistance. For this purpose, the absolute differences in scratch depth produced by the small indenter, under pre-scratched surface condition of Mode III with respect to Mode II, are plotted as a function of the pre-load as shown in Fig. 4.10. For the IF and FM steels, below the multiple passes transition loads of 3N (see Fig. 4.2b), the results are located in the negative zone indicating an extra

strengthening upon multiple passes, while further increase of pre-load beyond the transition load results in positive values suggesting that multiple passes do not lead to more strengthening but to weakening of the surface layer instead. The transition from negative to positive is in line with the straining hardening discussion before. For a small pre-scratch load below the transition load, the surface predominantly undergoes strain hardening which becomes more significant when subjected to multiple scratch passes. When exceeding the transition load, the strain accumulation reaches the critical fracture strain, and hence cracks can be initiated and delamination can be observed, as shown in Fig. 4.3c and Fig. 4.4c. It should be mentioned that the load for multi-pass surface weakening will be lower than for single pass scratching. For DP, Q&P steel grades the multi-pass transition loads are around 25 N, and in the case of the TWIP steel the transition load is about 30 N. i.e. outside the experimentally accessible load regime. Therefore, curves for DP, Q&P and TWIP steels in Fig. 4.10 are mainly located in the negative zone indicating a strengthening effect of multi-passes due to strain accumulation.

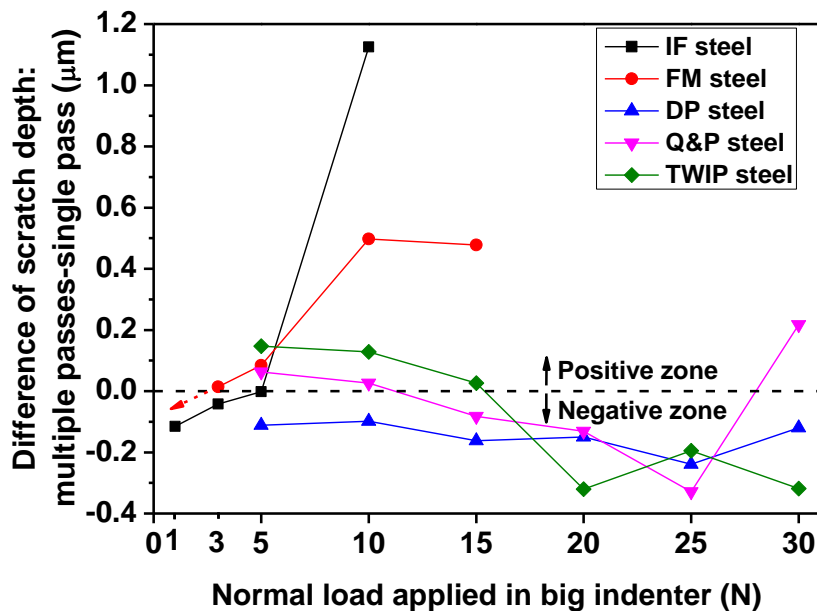


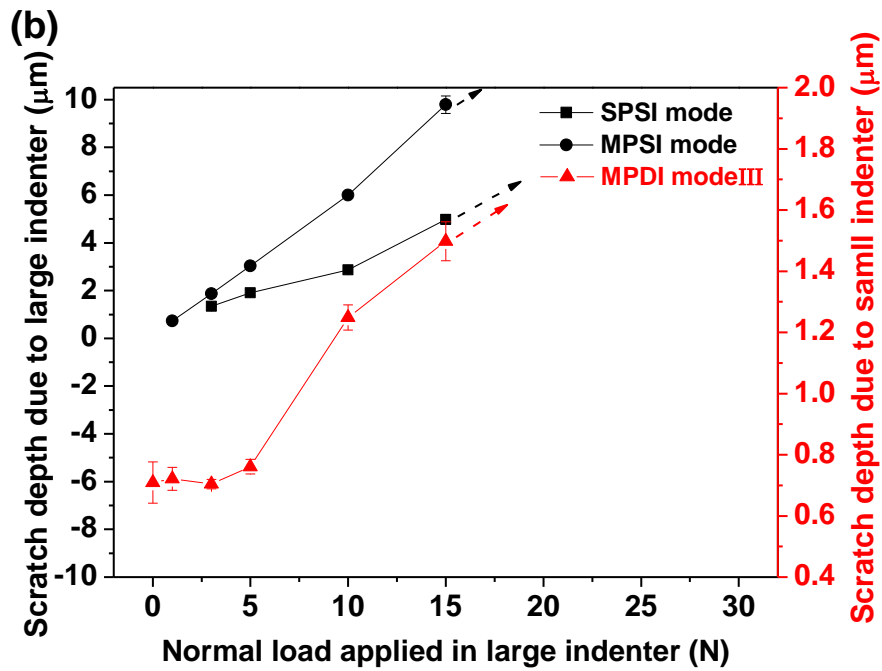
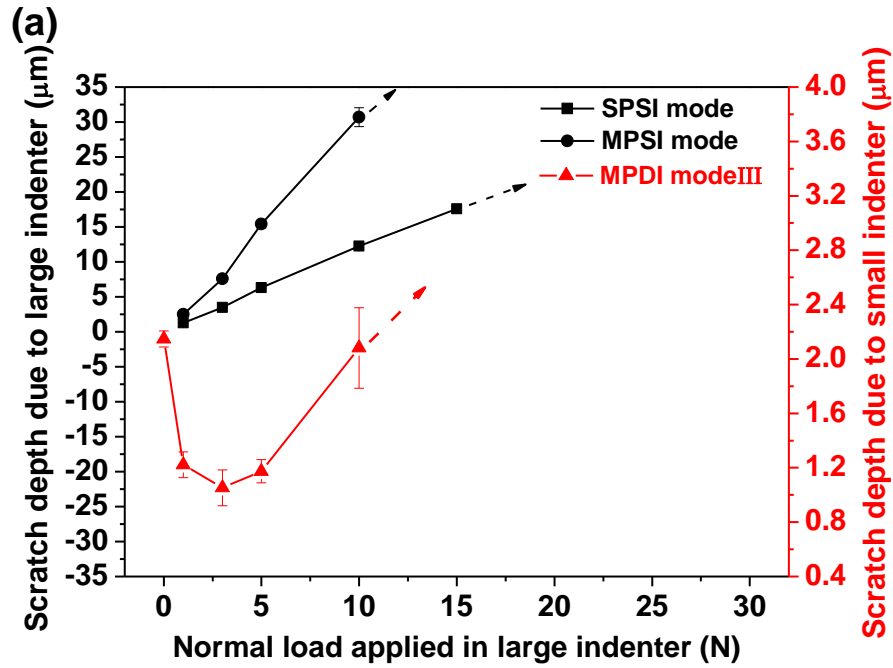
Fig. 4.10 Comparison of scratch depth in single pass mode and multi-pass mode for the five steel grades.

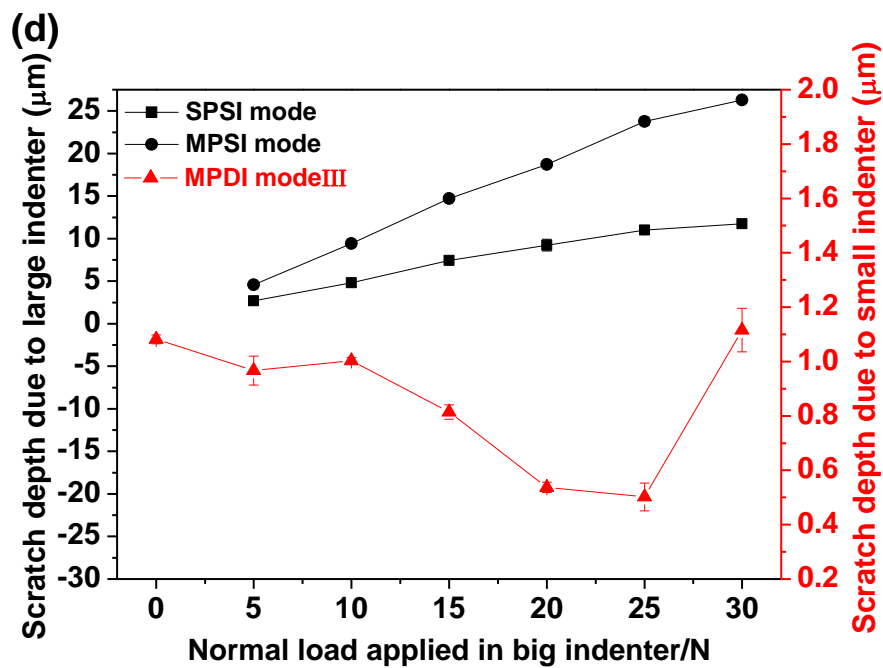
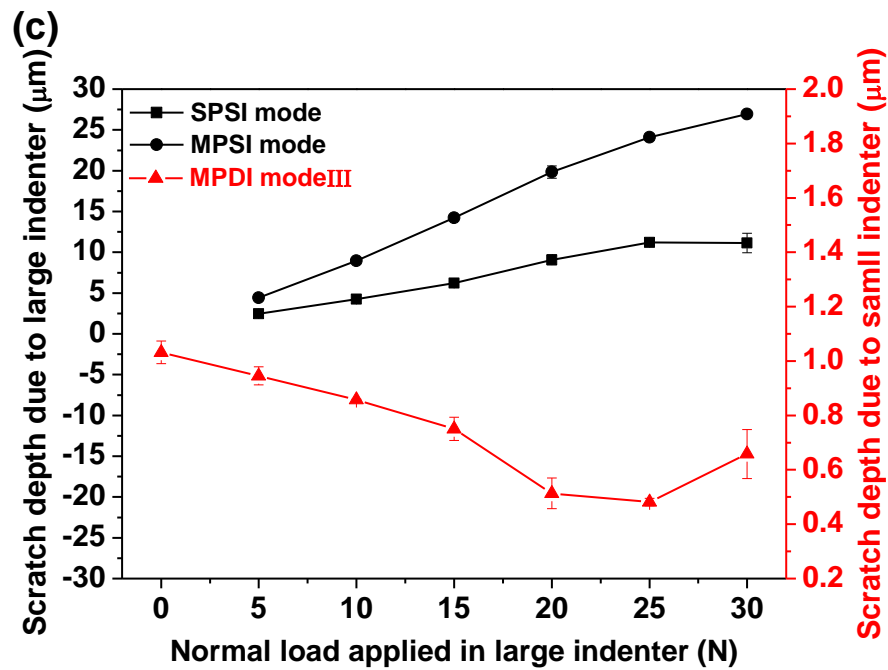
4.4.3 Comparison of MPDI scratch tests and conventional scratch tests

As stated in the chapter 3, the conventional scratch test, i.e. single pass single indenter (SPSI) scratch mode and multi-pass single indenter (MPSI) scratch mode, cannot truly reflect the response of materials on abrasion resistance due to either unsteady state of (sub) surface with non-fully work hardening or the effect of contact geometry. In order to highlight the advantage of the novel MPDI scratch test, it will attempt to compare the scratch results and failure mechanism among SPSI mode, MPSI mode and mode III of MPDI scratch test because of mode III being closer to steady state that occur in the real continuous abrasion process.

The scratch results for all steel grades in the SPSI scratch mode, MPSI scratch mode and MPDI scratch mode (mode III) under different large indenter loads are summarized in Fig. 4.11. It should be noted that the curves in black shown in Fig. 4.11 correspond to the evolutions of scratch depth produced by large indenter only versus the large indenter loads in conventional scratch tests, i.e., single pass (SPSI mode) and multi-pass (MPSI mode), while the scratch curve in red refers to the scratch depth produced by small indenter only on pre-scratched surface. It can be seen that, the evolution of scratch depth versus the large indenter loads in the MPDI scratch mode is quite different from those obtained in conventional scratch modes (i.e. SPSI mode and MPSI mode). For the conventional scratch modes, they follow the similar evolutions of scratch depths for each steel grade in essence, i.e. consistently displaying a nearly linear increase in scratch depth with increasing pre-load, despite of the different slop between SPSI mode and MPSI mode. However, instead of linear relationship, the MPDI scratch mode shows a “V” shaped correlation between the scratch depth and the load applied in large indenter. The evolution of MPDI scratch depth well reflects the metallurgical response of a material on abrasion behaviour under different loading condition, i.e. the decrease in scratch depth corresponds to the effect of strain hardening, and the increase in scratch depth demonstrates the occurrence of the material removal/damage. Moreover, the MPDI scratch test can unravel the different scratch performance for steel grades with different work hardening capabilities. The steel grade with higher work hardening capability possesses a higher critical load. In contrast, the conventional scratch modes give virtually no information on the actual deformation and response of materials on

abrasion processes, but only show a monotonous relationship between scratch depth and applied normal load.





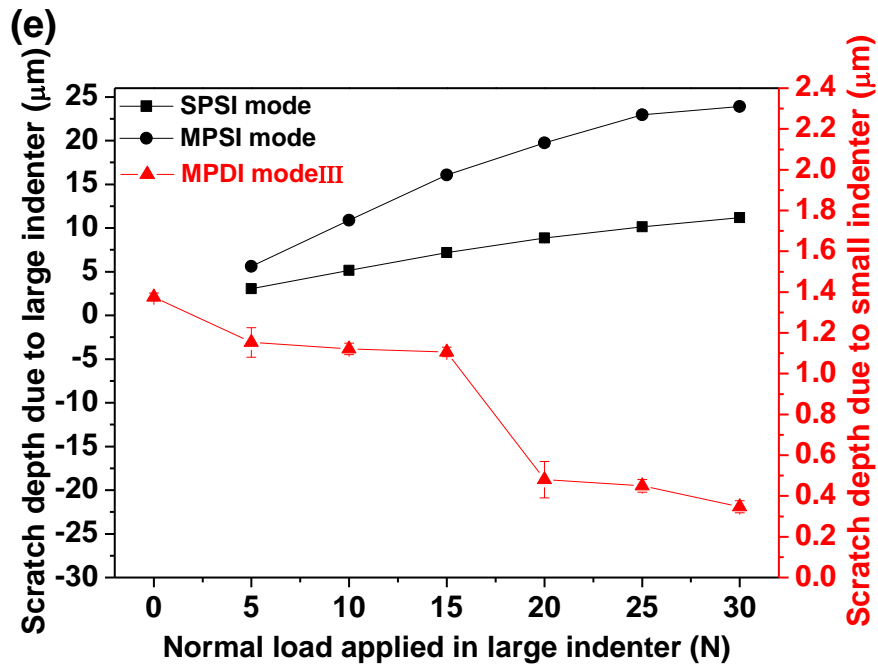
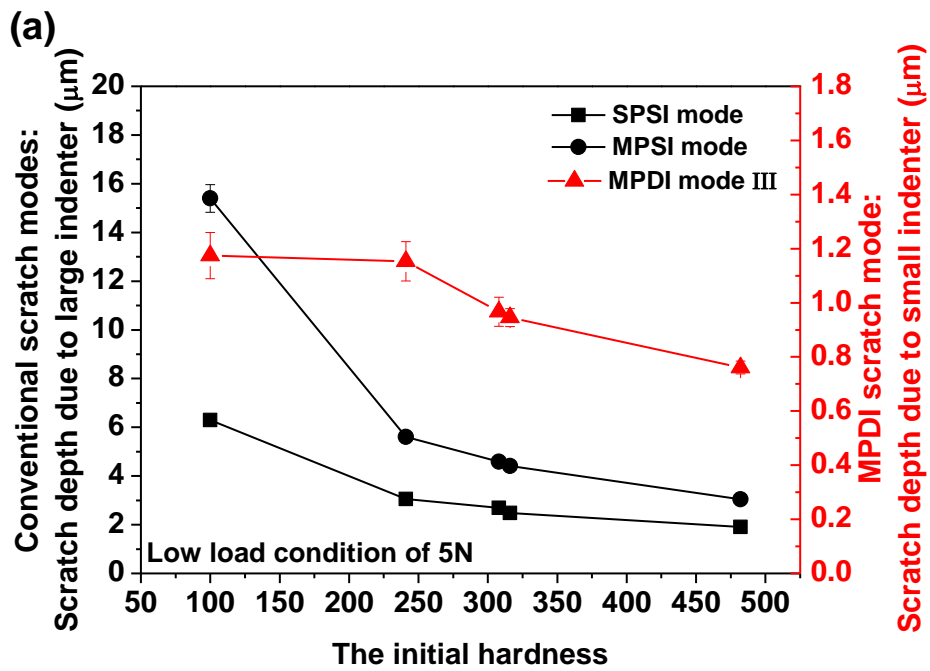


Fig. 4.11 the scratch depths produced by big indenter (black curves) and small indenter (red curves) as functions of different normal load on the big indenter: (a) IF steel, (b) FM steel, (c) DP steel, (d) Q&P steel, and (e) TWIP steel.



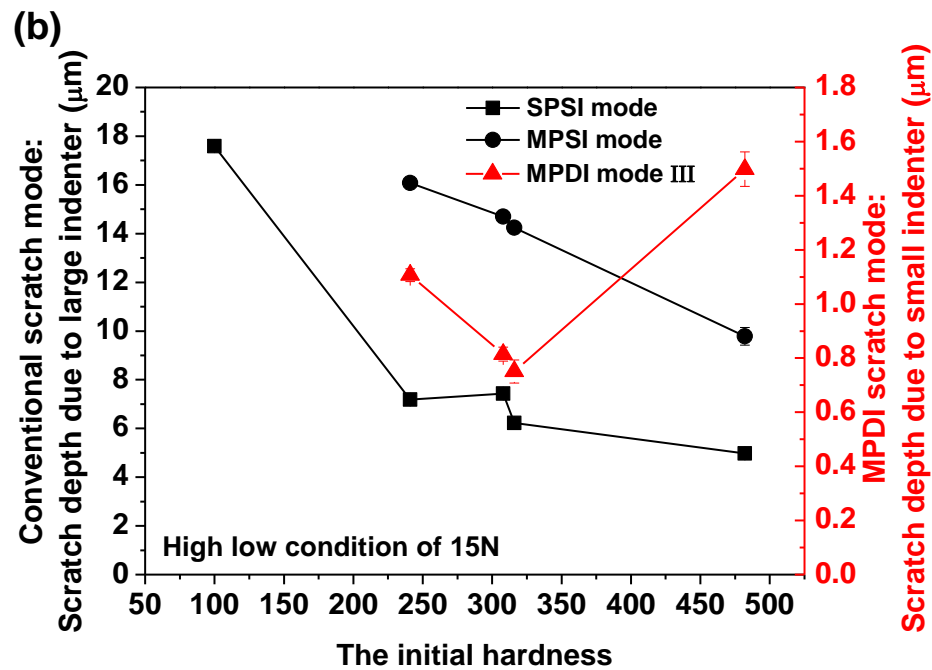


Fig. 4.12 The relationship of scratch depth and the bulk hardness in the conventional scratch modes and in the MPDI scratch mode under (a) the low load condition and (b) the high load condition.

Fig. 4.12 gives the relationship between scratch depth in different scratch modes and the bulk hardness under the low load condition and high load condition, respectively. As can be seen in Fig. 4.12a and Fig. 4.12b, for the conventional scratch modes, the scratch depth corresponds well with the initial hardness regardless of load condition presenting a monotonous correlation between the scratch depth and initial hardness. It agrees well with the general hypothesis [11], i.e. the higher hardness gives a better abrasion resistance. The softest IF steel experiences the maximum scratch depth, and the hardest FM steel shows the lowest scratch depth under each test load. This is very logical for the SPSI scratch mode because the essence of a single scratch on the initial surface is just a continuation, or a horizontal motion of the hardness indenter done on the initial surface, i.e. scratch hardness. For MPSI scratch mode, the process may inherit the nature of SPSI scratch mode and involve the effect of contact geometry, hence shows the similar correlation to the SPSI scratch mode. While for the MPDI scratch mode, although under low load condition it still shows the straightforward correlation of

scratch depth and the initial hardness which is similar to conventional scratch mode, the correlation of the scratch depth under the high load condition and the initial hardness becomes 'V' shape. By comparing the morphology of scratch tracks and the associated failure mechanism, there are quite difference between the conventional scratch mode and MPDI scratch mode as well. As seen in Fig. 4.13, for the conventional scratch modes, with the exception of the IF steel showing some crater/delamination due to the soft nature, the other steel grades all show the pure ploughing regardless of the SPSI mode or MPSI mode. While for the MPDI scratch mode, it shows the different abrasion damage and failure mechanisms for different steel grades depending on the initial microstructure and their work hardening capabilities.

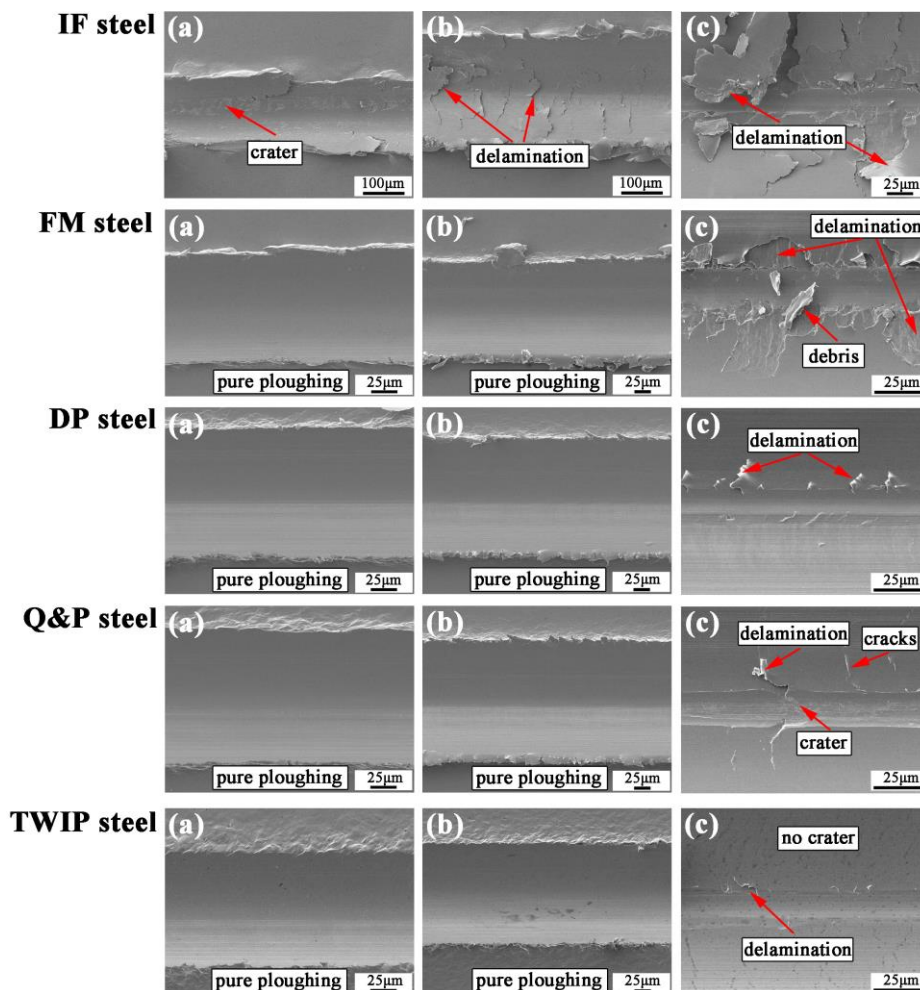


Fig. 4.13 Comparison of scratch tracks of all steel grades under the large indenter 15N (10N for IF steel) in (a) SPSI mode, (b) MPSI mode and (c) MPDI mode III (**Note:** the magnifications of images are different for different scratch modes).

Finally, it should be pointed out that the multi-pass scratching does not linearly increase the accumulated strain with each pass as surface and subsurface hardening as well as widening the scratch track leads to a gradual reduction in additional strain per scratch pass. The final steady state is believed to be closer to the surface condition in a real continuous abrasion process. The state after the single pass is more relevant to the run-in state of a real abrasion test at which higher abrasion rates are observed. Ultimately, the current scratch methodology mode III (pointed sharp indenter after multi-pass pre-scratching with a large indenter) best represents the condition relevant to real life abrasion after the run-in stage. The build-up of the subsurface deformation layer thickness with the scratch depth made by the large indenter for single and multi-pass scratching for the five steels analysed and for different loads shows an interesting almost linear master curve, as seen in Fig. 4.14. The data of this master curve and the thickness of the surface hardened layer for abraded surfaces can be used to derive the optimal loading conditions to be used to turn the multi-pass dual-indenter scratch methodology presented here into a more quantitatively predictive abrasion resistance test. Work to this aim is ongoing and will be reported in next chapter.

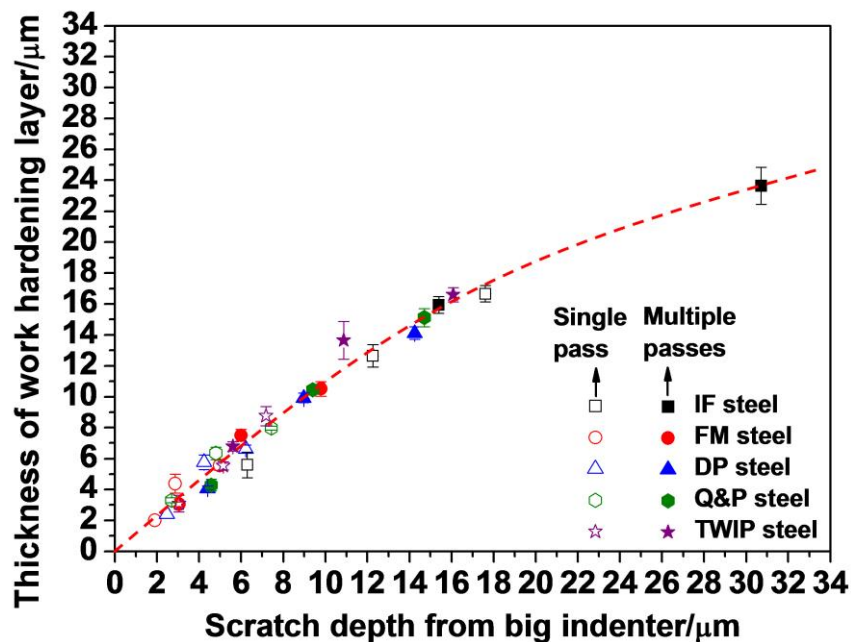


Fig. 4.14 Correlation between the scratch depth after sliding with the large indenter (various loads) and the thickness of the work hardening layer.

4.5 Conclusions

In this chapter, a new multi-pass dual indenter scratch methodology is applied to investigate the scratch behavior of five construction steel grades with different microstructures and work hardening capabilities, which reveals well the various damage mechanisms under different loading conditions. It is shown that the abrasion/scratch resistance of a material is strongly dependent on the strain and damage accumulation in the surface and subsurface layer. The accumulation of strain during the process may result in either hardening or weakening of the surface layer, depending on the pre-scratch load with respect to the work hardenability and failure strain.

Full martensitic steel with a high initial hardness is good for mild abrasion conditions, while DP, Q&P and TWIP steel grades with a significant work hardening capabilities display superior wear resistances under higher loads, notwithstanding their relative low initial hardness.

The conventional scratch modes, i.e. SPSI scratch mode and MPSI scratch mode, seem to act as hardness test behaviour, which will mislead the understanding of abrasion resistance. While the new MPDI scratch mode well reflects the response of material with different strain hardening capability on abrasion behaviour and reveals the various failure mechanisms under different loads.

Once properly calibrated the current MPDI scratch methodology may provide a tool to fast screen the abrasion resistance of construction and other steel grades, and to determine whether the material would sustain the intended abrasive loading conditions.

References

- [1] J. Speer, D.K. Matlock, B.C. De Cooman, J.G. Schroth, Carbon partitioning into austenite after martensite transformation, *Acta Materialia* 51 (2003) 2611-2622.
- [2] K.H.Z. Gahr, Wear by hard particles, *Tribology International* 31 (1998) 587-596.
- [3] T. Jing, F. Zhang, The work-hardening behavior of medium manganese steel under impact abrasive wear condition, *Materials Letters* 31 (1997) 275-279.
- [4] Z.M. He, Q.C. Jiang, S.B. Fu, J.P. Xie, Improved work-hardening ability and wear resistance of austenitic manganese steel under non-severe impact-loading conditions, *Wear* 120 (1987) 305-319.
- [5] A.K. Jha, B.K. Prasad, O.P. Modi, S. Das, A.H. Yegneswaran, Correlating microstructural features and mechanical properties with abrasion resistance of a high strength low alloy steel *Wear* 254 (2003) 120-128.
- [6] X. Xu, W. Xu, F.H. Ederveen, S. van der Zwaag, Design of low hardness abrasion resistant steels, *Wear* 301 (2013) 89-93.
- [7] G.H. Yang, W.M. Garrison Jr, A comparison of microstructural effects on two-body and three-body abrasive wear, *Wear* 129 (1989) 93-103.
- [8] V.F. da Silva, L.F. Canale, D. Spinelli, W.W. Bose, O.R. Crnkovic, Influence of retained austenite on short fatigue crack growth and wear resistance of case carburized steel, *Journal of Materials Engineering and Performance* 8 (1999) 543-548.
- [9] O. Grässel, L. Krüger, G. Frommeyer, L.W. Meyer, High strength Fe-Mn-(Al, Si) TRIP/TWIP steels development-properties-application, *International journal of plasticity* 16 (2000) 1391-1409.
- [10] O. Bouaziz, N. Guelton, Modelling of TWIP effect on work-hardening, *Materials Science and Engineering A* 319-321 (2001) 246-249.
- [11] E. Rabinowicz, *Friction and Wear of Materials*, Wiley, New York, (1965).

Chapter 5

Prediction of the abrasion resistance of steels on the basis of the subsurface deformation layer

5.1 Introduction

As stated in Chapter 3, abrasive wear is a complex process involving not only the complexity of the tribosystem and the prevailing working/testing conditions [1-3], but also the dynamic development of a (sub) surface microstructure due to the plastic deformation of materials during the abrasion process [4-9]. The evolving microstructure of a material at and below the worn surface differs from the initial microstructure because of plastic deformation and local work hardening. During the steady state of the actual abrasion process, it is the work hardened (sub) surface layer that undergoes the abrasive wear [10, 11]. This evolution of local mechanical properties and changes in the damage mechanisms in the zone exposed to abrasive attack is seen as one of the principal obstacles to build a general and quantitative model for the abrasion rate as a function of mechanical properties of the as-exposed material [3].

Usually experiments to study the abrasive wear behaviour of materials are done with a two-body abrasive wear test set-up, such as the pin-on-disc wear test, the paddle wear test, a polished sample against abrasive paper, etc., [2, 12-15] or a three-body abrasive wear test set-up, such as sand/rubber wheel abrasion tester, i.e. materials worn against abrasives [16-20]. Although such experiments provide useful data on the relative wear rate of materials under practical conditions, they give virtually no information on the actual deformation and damage processes. Hence the outcome of such tests does not allow predicting the wear resistance of new (not-yet-tested) materials or new working conditions [21]. In order to study and predict the abrasive wear characteristics of materials under different load conditions relevant to the real work environment, the multi-pass dual-indenter (MPDI) scratch test approach developed in Chapter 3 were employed [22].

The aim of this chapter is to generalize the abrasion resistance and the associated failure mechanism in different preloading condition discussed in Chapter 4 and to establish a relation between the thickness and characteristics of the work hardening layer formed and the abrasion resistance. Of special interests are a comparison of the MPDI scratch test results with those of the ASTM G65 abrasive wear test and the exploration of the notion that the MPDI test may provide insight into the abrasion resistance for working conditions beyond the G65 standard (load and particle size) conditions.

5.2 Experimental description

In this chapter, the five steels grades as used in Chapter 4 were selected. All steels are in the metallurgical state to be expected for their grades. More detailed descriptions of the microstructures of these five steel grades can be found in Chapter 4. Prior to experimental testing, ASTM G65 test samples were mechanically grinded. All samples for MPDI scratch test were mounted in cold-setting resin and mechanically polished following a standard metallographic preparation process. The hardness for all five steel grades can be found in Chapter 4.

Based on the preliminary methodological study reported in Chapter 4 and reference [22], ten sliding passes with the large indenter were selected in the pre-scratching stage in this chapter so as to prepare a well-defined and representative deformed surface in a steady state. In order to benchmark the MPDI scratch responses, a standardized low stress abrasion test was performed on all five materials exactly following the ASTM G65 dry sand rubber wheel abrasion (procedure B). Samples along the rolling direction were prepared and the surface was polished following a standard metallography method. The ASTM G65 test was performed with wheel rotations of total 2000 at a speed of 200 rpm and standard Ottawa silica sand as the abrasive medium. After the test, the weight loss of the sample was measured with a precision of 1mg before and after test. The test for each material in the current investigation was repeated 3 times, and an average weight loss is reported.

After the scratch test and the ASTM G65 abrasive wear test, a scanning electron microscope (SEM) operating at 5 kV was employed to observe the worn surface. After this inspection stage, cross-sections of the wear track perpendicular to the sliding direction were prepared to observe the microstructure development under the worn surface using SEM. After the scratch test on the ASTM G65 worn surface, the surface topography of each steel grade was characterized using the Confocal Laser Scanning Microscopy (CLSM).

5.3 Results

5.3.1 Multi-pass dual-indenter (MPDI) scratch tests

The scratch depths from the small indenter plotted as a function of the normal load applied on the large indenter along with the corresponding failure mechanisms are summarized in Fig. 5.1 for all steel grades. The bulk hardness values obtained for each steel grade are also indicated. In essence, the five steel grades perform similarly as discussed in Chapter 4, i.e., upon increasing the large indenter load, the scratch depth due to the small indenter first decreases and then starts to rise as the large indenter load exceeds a critical value. The decrease in the scratch depth reflects the effect of (sub)

surface strain hardening due to the pre-scratching, which corresponds to the surface hardening regime as indicated in grey in Fig. 5.1. The increase in the scratch depth at higher large indenter loads indicates the occurrence of pre-scratching damages, due to the external applied stress exceeding a critical fracture stress, which refers to the abrasive damage/removal regime highlighted in white in Fig. 5.1. The five steel grades clearly differ in their rates of strain hardening and their critical loads for the onset of damage, which may be attributed to the effect of accumulative strain, the development of the subsurface layer, and the work hardening capability of the steel. Due to their low work hardening capability, IF and FM steels showed similar low transition loads notwithstanding the large differences in their initial hardness, and hence present a narrow surface hardening region. The significant work hardening capability of the DP, Q&P and TWIP steels shifted the transition loads to much higher values, showing a broad region of surface hardening compared to those of the IF and FM steels. It can also be noticed that the transition preload between the surface hardening and damage regimes follows the order IF/FM, DP/Q&P and TWIP steels, which is in line with their work hardening capability.

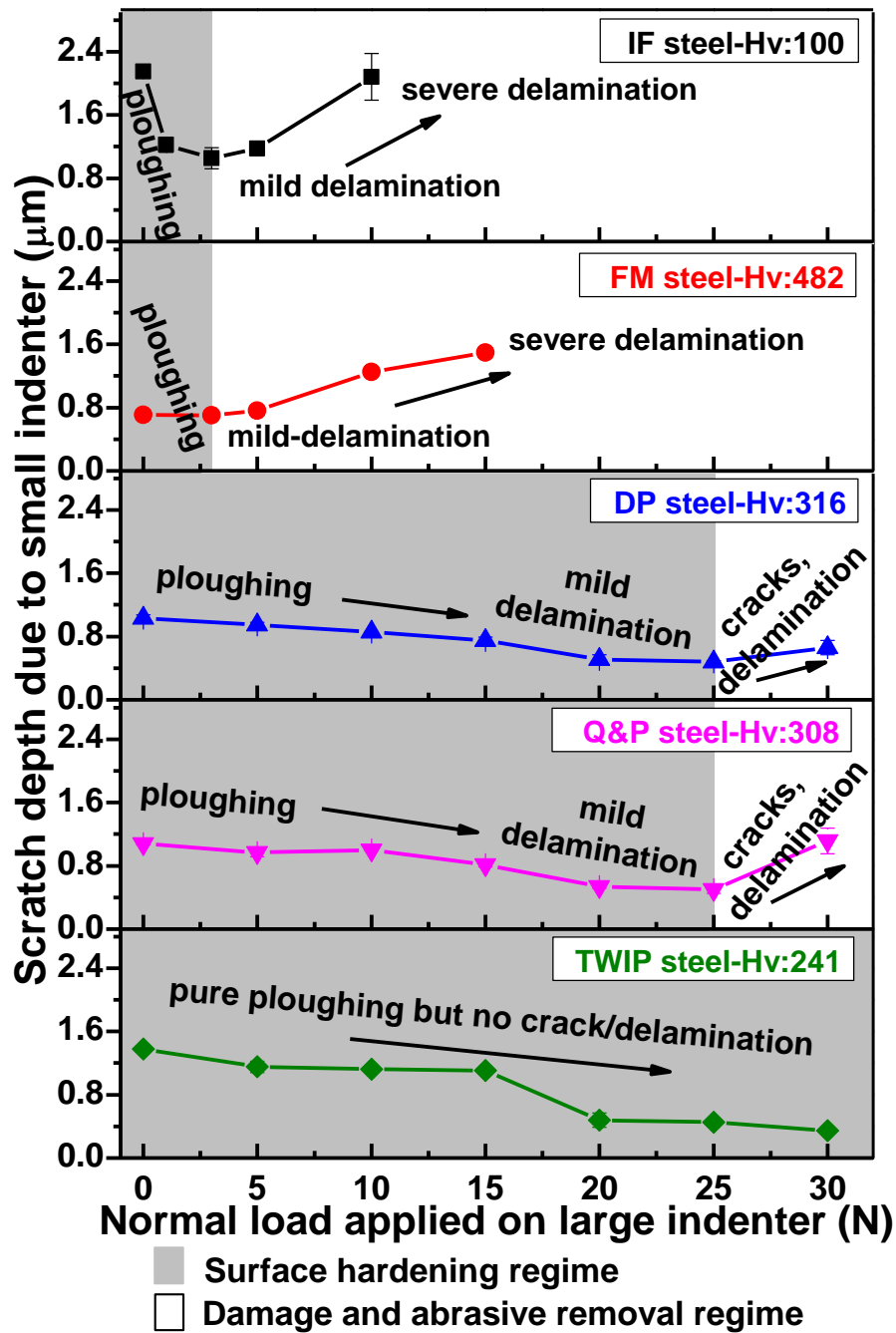


Fig. 5.1 The scratch depth resulting from the single pass small indenter scratch as a function of the normal load applied on the large indenter during pre-scratch of all five steel grades investigated. The evolution of the underlying failure mechanisms is indicated in the plot.

The scratch depth on the initial surface corresponds very well with the indentation hardness, which is to be expected. However, the scratch depth values on the pre-scratch tracks produced at various loads beyond their critical level do not follow the same order as the initial hardness values, thereby reflecting the effect of deformation hardening. For example, the TWIP steel changes from being the second softest in the original state to the intermediate level upon mild pre-scratching, and to the best in the harshest pre-scratching condition.

The corresponding failure mechanisms upon the small indenter single-pass by 0.3N load in the different pre-loading conditions have been reported in Chapter 4. The evolutions of failure mechanisms are generalised in the different preloading conditions and correlated with the corresponding scratch resistance. As indicated in Fig. 5.1 for the five steels explored, the evolutions of failure mechanisms are in good agreement with the resulting scratch depths. For the IF and FM steels, similar failure mechanisms with increasing pre-scratch load were observed. As the pre-load increased to 5N, delamination started to appear even for the lowest load during small indenter scratching. With a further increase of the large indenter load (10N for the IF steel and 15N for the FM steel), severe delamination was seen, which indicates that the worn surface promoted serious damage, resulting in a larger scratch depth and an acceleration of the wear rate. The SEM images of the DP steel only displayed ploughing under a load of 5N. Even when the pre-load was increased to 15N and 25N, only mild delamination and cracks were observed on the edge of the scratch track. However, once the pre-load exceeded the critical load, big cracks were formed perpendicular to the final scratch produced by the small indenter in some cases and delamination appeared, which consequently result in an increase in the scratch depth. The Q&P steel showed a similar evolution of failure mechanisms as the DP steel at pre-loads less than 25N. However, at the pre-load of 30N, serious delamination was observed, which lead to a significant increase in the scratch depth. Finally, for all pre-load conditions the scratch grooves of the TWIP steel looked smooth and displayed very little cracks/delamination, in agreement with the continuous decrease in the scratch depth with increasing pre-load. As stated above, the results showed that the proposed MPDI scratch test approach reflected well the responses of different materials to the scratching process under different work conditions.

5.3.2 ASTM G65 abrasive wear test

The average weight losses of the same samples in the ASTM G65 wear tests plotted against the as-received initial hardness are shown in Fig. 5.2. The IF steel clearly shows the largest wear rate, i.e. the lowest wear resistance, which is in agreement with its low initial hardness. However, regardless of the considerable differences in initial hardness, the other steel grades show a relative smaller variation in the weight loss and there is no monotonous relation between the wear resistance and the initial hardness. It is very interesting to note that the DP, Q&P and TWIP steels, which possess relatively low initial hardness, displayed a wear resistance comparable to the much harder FM steel. The order of abrasion resistance of the five steel grades (with the TWIP steel deviating) agrees with the order produced using the MPDI scratch test under the low pre-load condition.

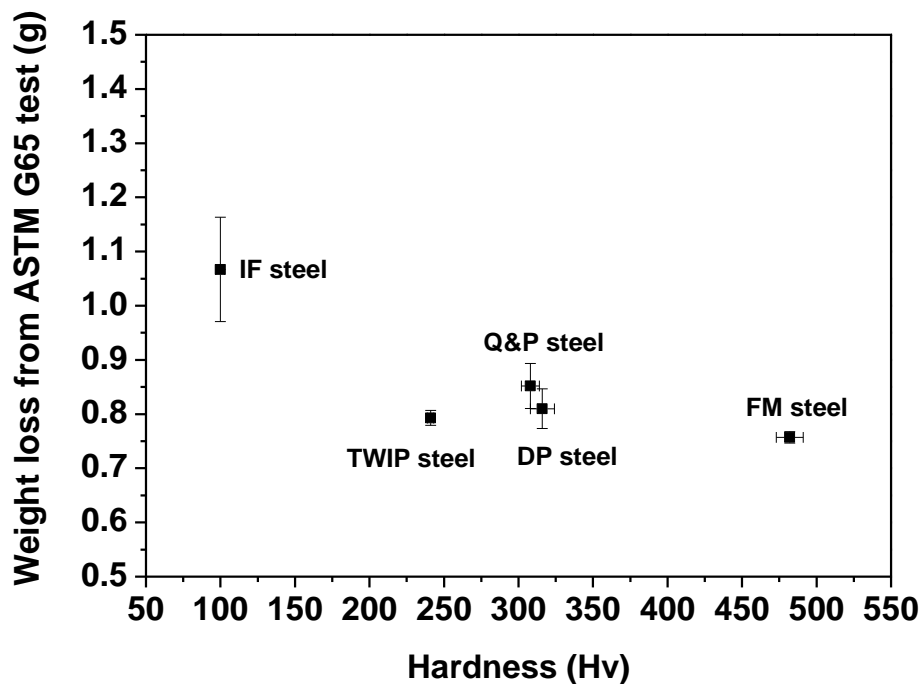


Fig. 5.2 The weight losses of the five steel grades subjected to the ASTM G65 test as a function of the initial hardness.

5.4 Discussions

After showing the different responses of the five steel grades subjected to the MPDI scratch test in different pre-scratching scenarios and the ASTM G65 test in the standardized condition, the discussion will attempt a metallurgical interpretation of the scratch behaviour and correlation of the MPDI scratch test results with those obtained from the ASTM G65 abrasive wear tests.

5.4.1 The subsurface deformation and work hardening

The microstructural observations indicated that there is a substantial deformation layer beneath the surface, as presented in Chapter 4 and the reference [22]. Instead of the initial microstructure, the subsurface layer is the actual component undergoing the continuous abrasion process, eventually determining the abrasion performance of the material. In the MPDI scratch approach, different pre-scratch conditions were applied to produce work hardening layers strengthened to different degrees and expanded to different thicknesses. It should be noted that the strengthening due to work hardening and the development of the subsurface layer thickness are intrinsically coupled, both determined by the work hardening behaviour of a material. Considering that the thickness of the subsurface layer is relatively easy to be quantified metallographically, the thickness of the work hardening layer was selected as the indicating parameter. The variation of the subsurface layer thickness under different pre-load conditions is shown in Fig. 5.3. It consistently displays a nearly linear increase with increasing pre-load for all five grades, regardless of the transitions from the work hardening regime to the damage mode in the high preload condition. However, the slope differs among the different steel grades, e.g., for the IF steel with a low strength and work hardening capability, a thicker subsurface layer is easy to be established, while for the martensite with a high hardness, the deformation for a given applied stress is accommodated primarily elastically leading to only a shallow hardening layer. Given the more or less linear correlations of the subsurface layer thickness and the applied preload, Fig. 5.1 can also be re-plotted using the subsurface layer thickness as the variable, as shown in Fig. 5.4. Therefore, for each steel grade, there is a critical layer thickness at which the

surface hardening reaches a maximum, and a further increase in the thickness causes more damage incubations resulting in a higher scratch depth. The FM steel displayed the lowest critical thickness because of its low transition load and a difficult-to-build hardened layer. Due to the high yield strength and low work hardening capability of the FM steel, the material can only undergo very limited plastic deformation before the failure. Therefore, the subsurface layer (characterized by the plastic deformation) is difficult to generate (requiring a higher load) and will not be built deeply into the bulk other than failure at the near surface. However, although the IF steel possesses a transition load of the same level as the FM steel (as shown in Fig. 5.1), the relatively easy development of the layer leads to a considerably higher critical layer thickness compared to that of the FM steel. Moreover, because of their significant work hardening capability, DP, Q&P and TWIP steels show a good balance of surface strengthening and layer development leading to a robust layer with a significant thickness before the material becomes weakened. Once such a MPDI correlation is established for a specific steel grade, it can be used as a general guideline to classify real life working conditions by determining the subsurface layer thickness after exposure. Materials experiencing mainly surface strengthening can be distinguished from those which have entered the stage of damage/abrasive removal. Such an approach can characterize the abrasive wear behaviour of particular working conditions, and does no longer require a specific lab test setup to simulate the particular working condition. By generalizing the metallurgical response and the surface development, one can determine the essence of the material response in a given application, and can use this knowledge to select the proper material for a specific application or tune the application parameter to allow a best performance of a given material.

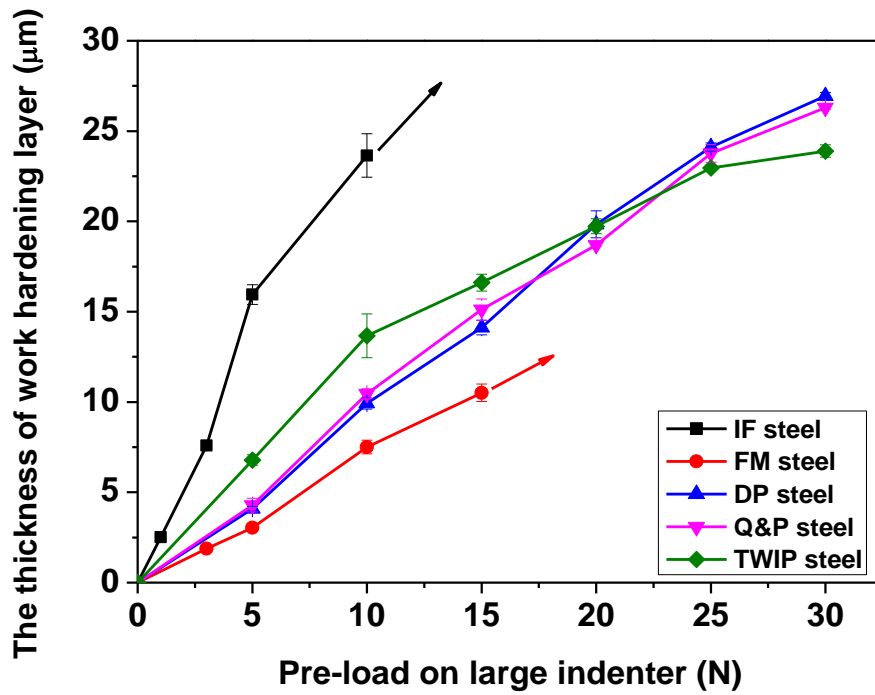


Fig. 5.3 The thickness of work hardening layer for the five steel grades under different pre-load conditions.

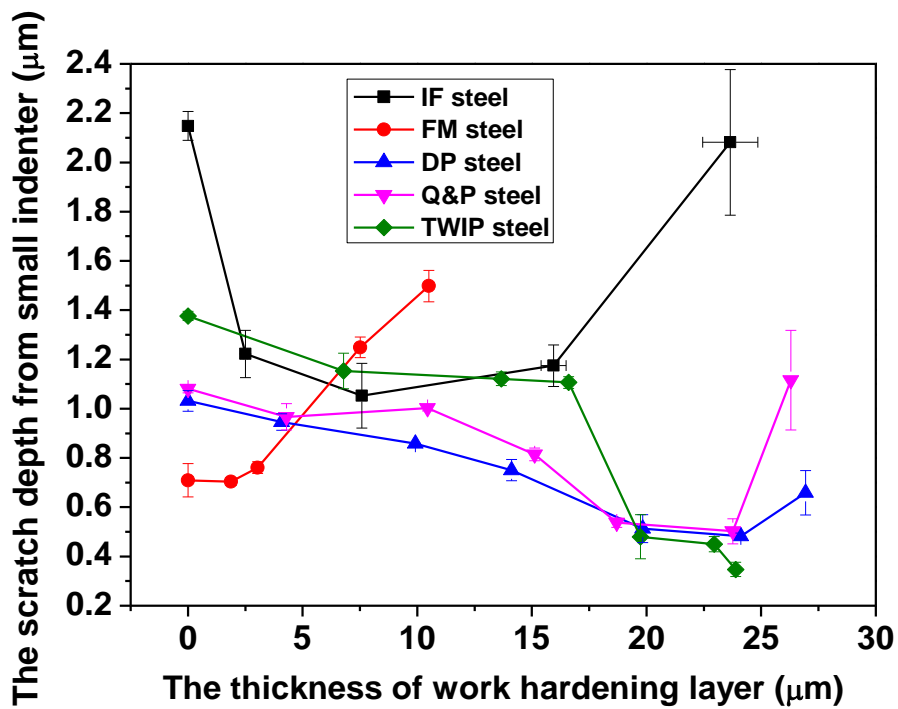


Fig. 5.4 The scratch depth for the five steel grades as a function of the thickness of the work hardening layer.

5.4.2 Correlation of MPDI scratch process and ASTM G65 abrasion test

In a real life abrasion situation, the continuous abrasion process can be divided into two stages: a run-in stage, in which the (sub) surface is not yet fully built, and a steady stage where a dynamic equilibrium of surface development and removal has been established. Both stages can be screened with the MPDI scratch methodology. The run-in stage in a MPDI scratch test starts from the initial surface accompanied by a quite high scratch depth (as demonstrated in Fig. 5.1). Upon further abrasion, the subsurface layer gets progressively developed and then reaches a steady state, which consequently leads to a decrease in the scratch depth up to a steady value. In order to investigate the subsurface development during multiple scratches by the large indenter, different numbers of pre-scratches were applied using a fixed preload of 15N. The resulting subsurface layer thickness was characterized from the cross-section, while the scratch resistance was characterized using the small indenter with a normal load of 0.3N. As shown in Fig. 5.5, in the initial state the subsurface layer is established fast and the resulting scratch depth is high but then decreases rapidly, which refers to the run-in stage. At this stage, the (sub) surface is not yet fully built and has not achieved the maximal work hardening. The main failure mechanism is ploughing due to the relatively low surface strength. After seven passes, the subsurface layer approaches a constant thickness and the resulting scratch depth also decreases towards a stable level, which corresponds to the steady state. While at the steady stage, the (sub) surface is strengthened to a maximal degree and hence the failure mechanisms involve mild ploughing, accompanied by mild delamination in local brittle zone. Further abrasive wear will only result in a dynamic equilibrium of (sub) surface, in which the (sub) surface layer is removed at the same speed as that of the subsurface hardened additionally in depth. The results also clearly suggest that a scratch test performed on a surface that has not reached the steady state will not truly reflect the material's behavior in a continuous abrasion process.

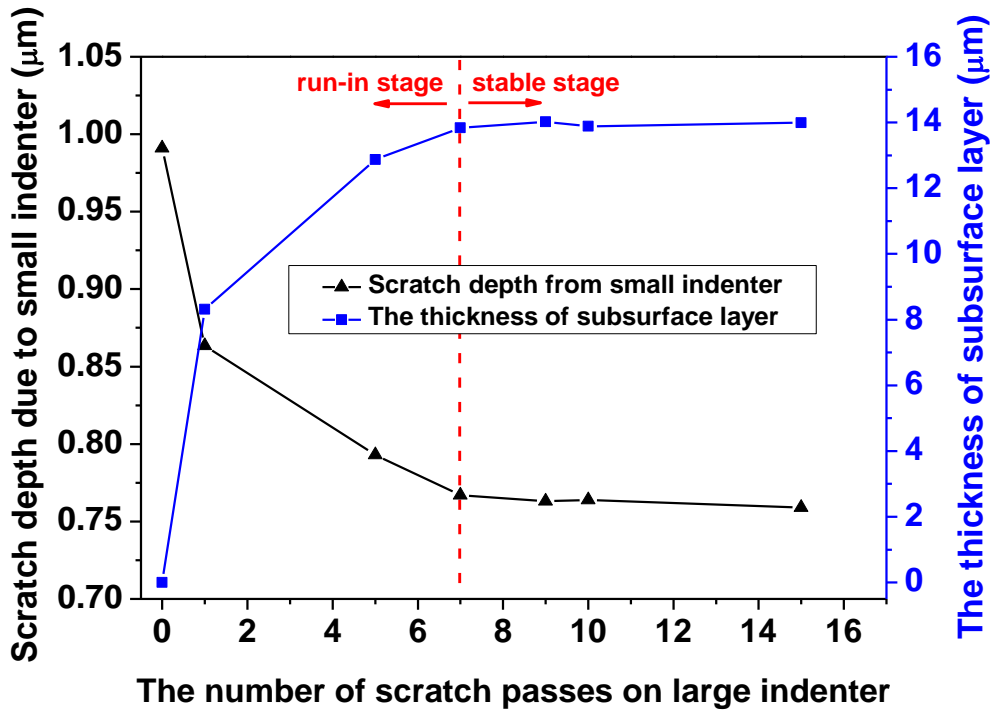


Fig. 5.5 The scratch depth from small indenter and the thickness of the subsurface layer as a function of the number of scratch passes by the large indenter on the DP steel.

The real life abrasion process is that abrasive particles continuously move along the surface being strain hardened and abraded under local contact conditions. This can be well simulated using the MPDI scratch test. In this scratch methodology, the pre-scratching treatment with a large indenter is designed to create a local pre-deformed surface layer equivalent to the surface layer presented during an abrasion test, and the small indenter is used to mimic the single particle behavior of the real life abrasion process and reveal the corresponding damage mechanisms. The two events can be well justified with the following experiments. In order to justify the relevance of the small indenter scratching event (the latter one), a scratching test with the small indenter was performed on the worn surface after the G65 test parallel to the sliding direction. The resulting scratch depth produced by the small indenter is compared to the weight loss in the G65 test in Fig. 5.6. With the exception of the TWIP steel having a different deformation mechanism from the other steel grades, a decent linear correlation can be observed. Furthermore, as seen in Fig. 5.7, the morphologies of the scratch track (marked by the red dashed line) made by the small indenter and the worn surface of the

materials after exposure to the ASTM G65 test show a high degree of similarity and evidence of the same ploughing mechanism. The surface topography after the scratch test on the ASTM G65 worn surface was characterized by the Confocal Laser Scanning Microscopy (CLSM). A line scan perpendicular to the scratch was performed for each steel and results are shown in Fig. 5.7. The scanning profiles clearly reveal the borderline of the scratch produced by the small indenter, although the roughness of the worn surface after ASTM G65 test is relative high and some small grooves produced by G65 test can be visualized.

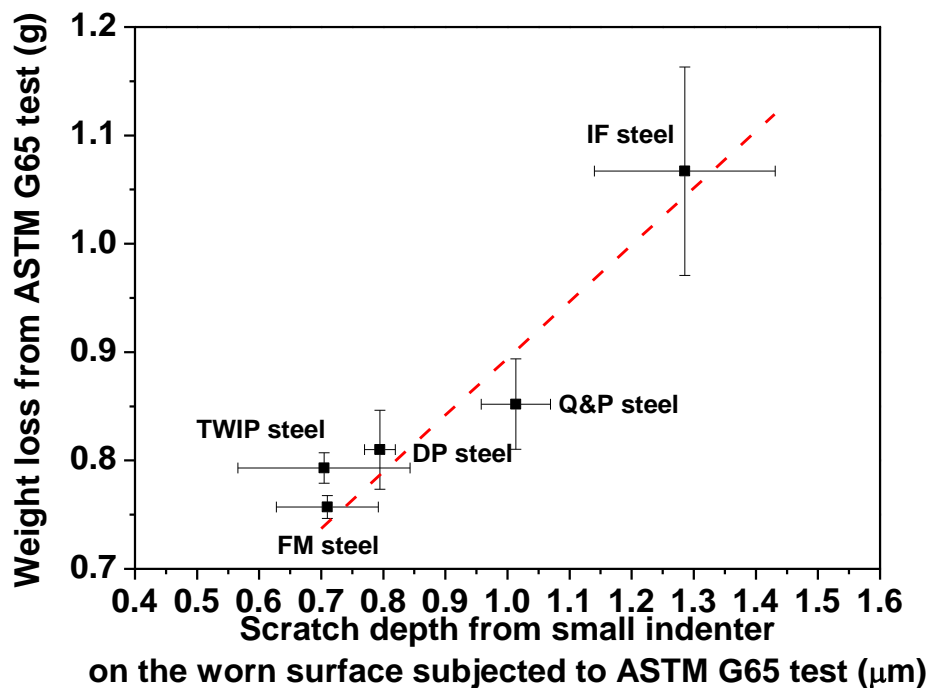


Fig. 5.6 Comparison of scratch depth from the small indenter on the worn surface subjected to the ASTM G65 test and the weight loss.

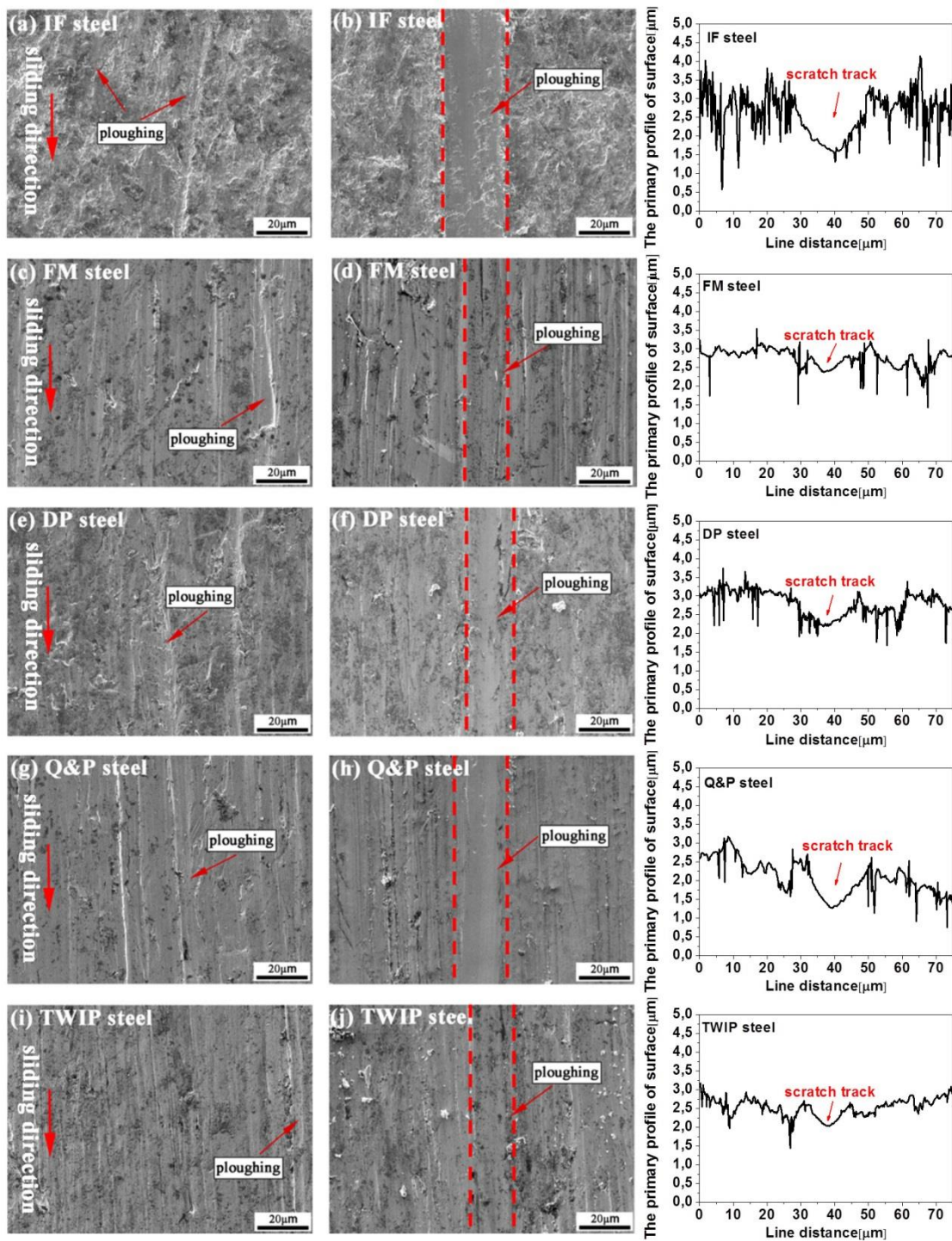


Fig. 5.7 Morphologies of the worn surface of (a) IF, (c) FM, (e) DP, (g) Q&P and (i) TWIP steels from the ASTM G65 test and the scratch track of (b) IF, (d) FM, (f) DP, (h) Q&P and (j) TWIP steels made by the small indenter on the worn surface of the material subjected to the ASTM G65 test, as well as the primary profile of worn surface (including the scratch track) perpendicular to sliding direction.

We now explore the hypothesis that the subsurface layer thickness is the key parameter in the abrasion process a little further. In order to find the pre-loading condition equivalent to the ASTM G65 test for obtaining the same subsurface layer thickness, (ten pass) scratch experiments with the large indenter at different loads were made. It was found that for the IF, FM, DP, Q&P and TWIP steels, the equivalent pre-loads to reach the same hardened surface layer thickness as in the G65 test are 1.7N, 3N, 2.6N, 2.4N and 2N, respectively. After defining the equivalent pre-scratch condition for each steel, the final scratches with the small indenter of 0.3N were performed on the equivalent pre-scratched surface. The resulting scratch depths on the equivalent surfaces are compared to those generated directly by small indenter on the ASTM G65 worn surface. As shown in Fig. 5.8, nearly the same values are obtained, which validates the hypothesis that the (sub) surface generated by pre-scratching can be assumed equivalent to that of the G65 test condition, when the subsurface layer has the same thickness. Finally, the scratch depths under the equivalent pre-scratch conditions and the weight losses in the ASTM G65 test are compared in Fig. 5.9. The results show that the weight losses are in good agreement with the scratch depths. In fact, the correlation is much better than that between the initial hardness and the abrasion rate (Fig. 5.2). This suggests that the MPDI scratch approach can reproduce the ASTM G65 test results assuming that an appropriate preloading condition can be defined. Here, it is important to clarify that, wear debris (wear loss) accompanying the final one-step scratch by the small indenter in the MPDI scratch test cannot always be observed. Especially in the mild pre-scratching conditions, it mainly displays ploughing despite of some material removal piled up at the end of the scratch. Nevertheless, it is necessary to mention the fact that in MPDI scratch test the final scratching by the small indenter is intended to simulate the response of the pre-strengthened surface to one further extra scratch step. In the real process, as a single sharp particle moves along the worn surface, depending on the surface and the contact conditions, it may undergo either ploughing (run-in stage or mild contact) or generate wear debris (fully strengthened surface or severe contact). This is exactly the same as in the MPDI scratch process. The significant wear loss in the real continuous process, e.g. ASTM G65 test, is a result of repeated interactions of multiple-asperity, i.e., the sum of wear loss produced by each particle. Given that the purpose of MPDI scratch test is to reveal the material response and associated failure mechanisms, but not to reproduce the wear loss in a continuous process, the MPDI

scratch methodology only applies one extra scratch but on different preloading conditions. In all correlational figures (in Fig. 5.6, Fig. 5.8 and Fig. 5.9), the data for the TWIP steel deviates from the linear dependence observed for the other steel grades. The non-conformity of the TWIP steel is attributed to its different deformation mechanisms, which involve not only the dislocation glide mechanism, but also the twinning induced deformation mechanism which does not take place for the other steel grades, as well as the fact that in the case of the TWIP steel the exact thickness of the subsurface layer is less easy to determine unambiguously than for the other steels (see Fig. 5.10).

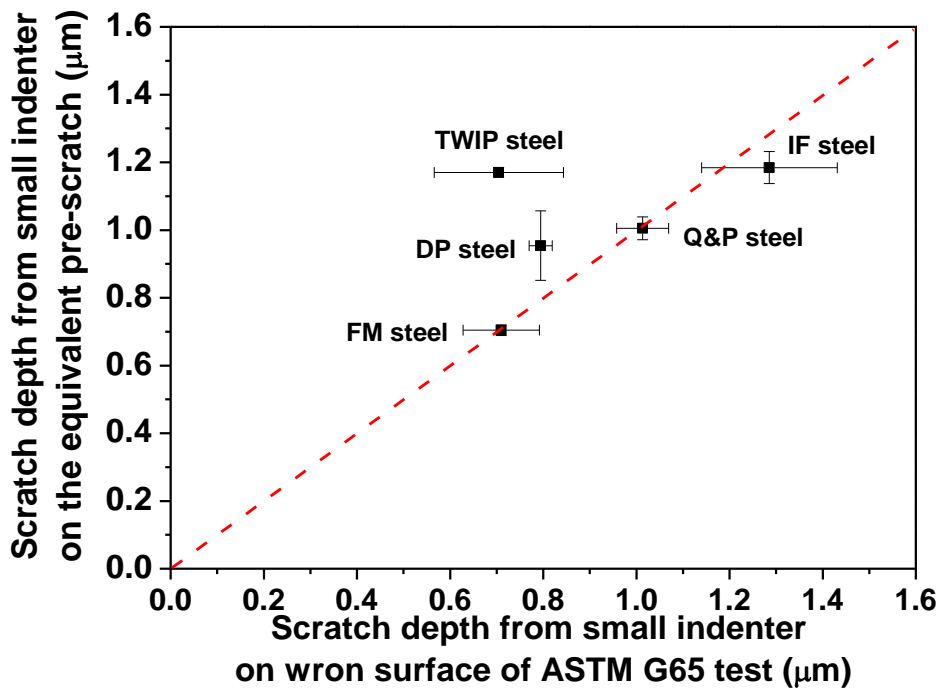


Fig. 5.8 Comparison of the scratch depths produced by the small indenter on the equivalent pre-scratch and on the worn surface of the material subjected to the ASTM G65 test.

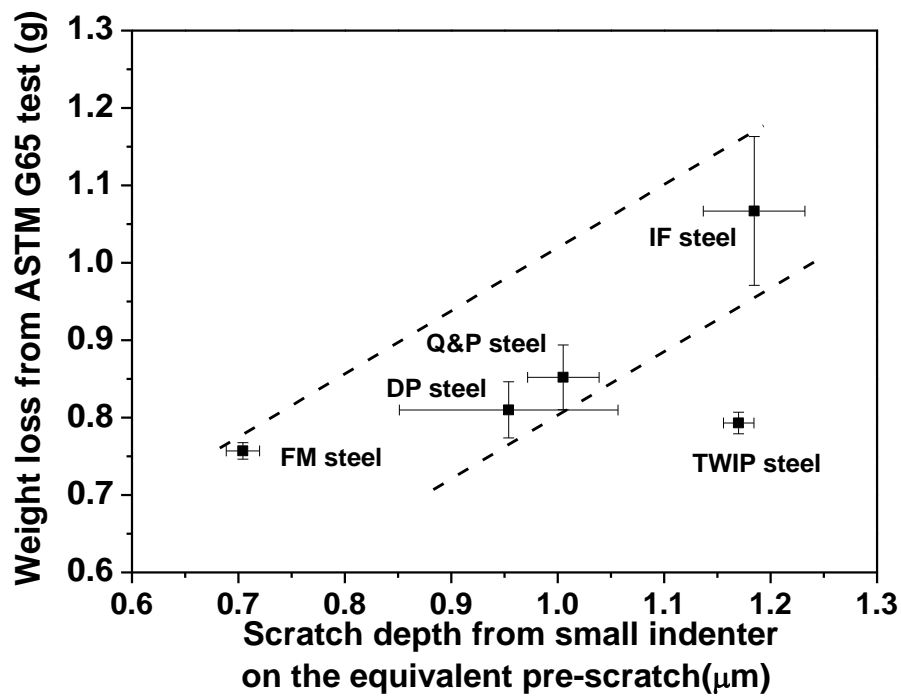


Fig. 5.9 Correlation of the ASTM G65 weight loss and the MPDI scratch depth under the equivalent pre-loading condition.

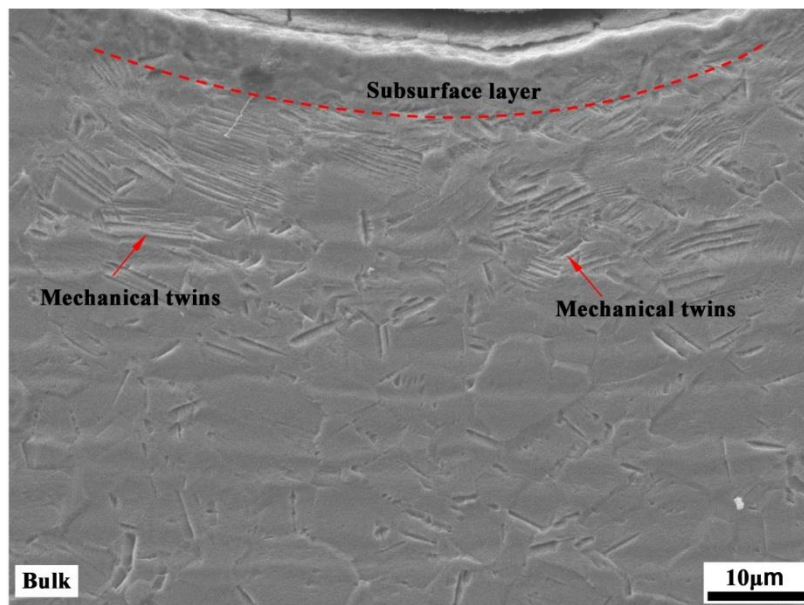


Fig. 5.10 SEM micrograph of the TWIP steel beneath the surface after ten-pass pre-scratches at 5 N.

5.5 Conclusions

The multi-pass dual-indenter (MPDI) test method was applied successfully to reproduce the real abrasive wear process for five construction steel grades with different work hardening capability, and to correlate with the ASTM G65 abrasion test results.

The MPDI test reflects the two stages of the abrasion process and reveals the corresponding damage mechanisms in the materials studied under various loading conditions. The abrasion and scratch resistance were found to be controlled by the development of work hardening subsurface layer, i.e., the balance of the surface hardening and the subsurface layer thickening, which is eventually determined by the work hardening capability.

Given the established correlation of scratch depth and the subsurface layer thickness, the subsurface layer thickness can be considered as a parameter to justify whether the material is applied in its strengthening zone or the damage region. It can also provide the guideline to select the proper material for a given application or tune the application conditions to allow the best performance of a given material. With a proper equivalent preloading condition defined by the thickness of the subsurface layer, the MPDI test well reproduces the ASTM G65 response.

The MPDI approach offers a fast method to quantify the abrasion resistance of material not only for mild loading conditions (ASTM G65 test condition), but also for working conditions beyond those of the standardized G65 test. The MPDI approach is therefore an efficient tool in the development of new steels with a higher abrasion resistance for specific loading conditions.

References

- [1] J.H. Tylczak, A. Oregon, in: P.J. Blau(Ed.), ASM Handbook: Friction, Lubrication, and Wear Technology, vol. 18, ASM International, USA, 1992, p. 337.
- [2] K.H.Z. Gahr, *Microstructure and Wear of Materials*, Elsevier Science Ltd., Amsterdam, 1987.
- [3] X. Xu, W. Xu, F.H. Ederveen, S. van der Zwaag, Design of low hardness abrasion resistant steels, *Wear* 301 (2013) 89-93.
- [4] M.A. Moore, R.M. Douthwaite, Plastic deformation below worn surfaces, *Metall. Trans. A* 7 (1976) 1833-1839.
- [5] A.T. Alpas, H. Hu, J. Zhang, Plastic deformation and damage accumulation below the worn surfaces, *Wear* 162–164, Part A (1993) 188-195.
- [6] S. Das Bakshi, A. Leiro, B. Prakash, H.K.D.H. Bhadeshia, Dry rolling/sliding wear of nanostructured bainite, *Wear* 316 (2014) 70-78.
- [7] V. Rastegar, A. Karimi, Surface and subsurface deformation of wear-resistant steels exposed to impact wear, *J. Mater. Eng. Perform.* 23 (2014) 927-936.
- [8] N. Ojala, K. Valtonen, V. Heino, M. Kallio, J. Aaltonen, P. Siitonen, V.T. Kuokkala, Effects of composition and microstructure on the abrasive wear performance of quenched wear resistant steels, *Wear* 317 (2014) 225-232.
- [9] M. Lindroos, K. Valtonen, A. Kemppainen, A. Laukkanen, K. Holmberg, V.T. Kuokkala, Wear behavior and work hardening of high strength steels in high stress abrasion, *Wear* 322-323 (2015) 32-40.
- [10] D.A. Rigney, W.A. Glaeser, The significance of near surface microstructure in the wear process, *Wear* 46 (1978) 241-250.
- [11] U. Bryggman, S. Hogmark, O. Vingsbo, Prediction of gouging abrasion resistance of steel by pendulum grooving and other laboratory test methods, *Wear* 115 (1987) 203-213.
- [12] A.P. Modi, Effects of microstructure and experimental parameters on high stress abrasive wear behaviour of a 0.19wt% C dual phase steel, *Tribol. Int.* 40 (2007) 490-497.
- [13] J. Rendón, M. Olsson, Abrasive wear resistance of some commercial abrasion resistant steels evaluated by laboratory test methods, *Wear* 267 (2009) 2055-2061.
- [14] S. Gündüz, R. Kaçar, H.Ş. Soykan, Wear behaviour of forging steels with different microstructure during dry sliding, *Tribol. Int.* 41 (2008) 348-355.
- [15] G.H. Yang, W.M. Garrison Jr., A comparison of microstructural effects on two-body and three-body abrasive wear, *Wear* 129 (1989) 93-103.
- [16] L. Fang, Q.D. Zhou, Y.J. Li, An explanation of the relation between wear and material hardness in three-body abrasion, *Wear* 151 (1991) 313-321.

- [17] O.P. Modi, B.K. Prasad, A.K. Jha, R. Dasgupta, A.H. Yegneswaran, Low-stress abrasive wear behaviour of a 0.2% C steel: influence of microstructure and test parameters, *Tribol. Lett.* 15 (2003) 249-255.
- [18] A.K. Jha, B.K. Prasad, O.P. Modi, S. Das, A.H. Yegneswaran, Correlating microstructural features and mechanical properties with abrasion resistance of a high strength low alloy steel, *Wear* 254 (2003) 120-128.
- [19] P. Xu, B. Bai, F. Yin, H. Fang, K. Nagai, Microstructure control and wear resistance of grain boundary allotriomorphic ferrite/granular bainite duplex steel, *Mater. Sci. Eng. A* 385 (2004) 65-73.
- [20] X.T. Deng, Z.D. Wang, Y. Han, H. Zhao, G.D. Wang, Microstructure and abrasive wear behavior of medium carbon low alloy martensitic abrasion resistant steel, *J. Iron Steel Res. Int.* 21 (2014) 98-103.
- [21] J.A. Williams, Y. Xie, The generation of wear surfaces by the interaction of parallel grooves, *Wear* 155 (1992) 363-379.
- [22] X. Xu, S. van der Zwaag, W. Xu, A novel multi-pass dual-indenter scratch test to unravel abrasion damage formation in construction steels, *Wear* 322-323 (2015) 51-60.

Chapter 6

The effect of martensite volume fraction on the scratch and abrasion resistance of a ferrite-martensite DP construction steel

6.1 Introduction

After the development of MPDI scratch test in Chapter 3-5 and to build the ‘translator’ proposed in Chapter 2, a systematic experimental investigation of the abrasion resistance for a dual phase steel of fixed chemical composition but widely different microstructures is conducted in following two chapters.

Dual phase steels combining a low yield to ultimate tensile strength ratio, a good work hardening capability and a good balance of strength and ductility, represent a very successful engineering steel family for automobile and other structural applications [1-3]. The tensile properties, the formability and many other mechanical properties have been extensively studied as a function of microstructural factors such as phase volume fraction [4-6], morphology [7-10] and grain size [11, 12] etc., and the corresponding deformation/strain hardening mechanisms [3, 13-15]. However, the abrasion and scratch resistance of DP steels with different martensite fractions has been studied less. This is because that the development of wear resistant steels mainly focused on fully

martensitic microstructures as a result of the common notion that a higher hardness guarantees a better wear resistance [16, 17], and that there will be complex strain/stress partitioning and different load responses and failure mechanisms may apply at different load conditions given the different properties of both phases for ferritic-martensitic DP steels. As studied in Chapter 2, the volume fractions of both phases in DP steels are the most critical parameter in determining the final mechanical properties, including the abrasion resistance. Some investigations [18-22] have shown that the abrasion resistance continuously increases with increasing martensite volume fraction. However, other reports [23, 24] have suggested that the presence of a small fraction of ferrite may considerably increase the abrasion resistance compared to that of the harder fully martensitic variant, due to a better combination of load bearing by the hard constituent (martensite) and strain accommodation by the soft and ductile phase (ferrite). Moreover, many studies [25-30] have suggested that the strain hardening of the phases plays a key role in determining the abrasion resistance, and it has been concluded qualitatively [31] that the abrasion resistance increases with strain hardening capability. Nevertheless, these studies did not provide any quantitative analysis of the correlation between scratch/abrasion resistance and strain hardening. In contrast, there have been numerous studies [4, 14, 32-36] on the tensile properties of DP steels as a function of the microstructure and the associated strain hardening and strain/stress partitioning. This knowledge could be helpful in analysing the scratch and abrasion resistance of DP steels as a function of the microstructure and the local load conditions.

Given the outstanding issues discussed above, in this chapter, intercritical heat treatments for a single lean C-Mn construction steel (a hot rolled 22MnB5 steel) were designed on the basis of the Local Equilibrium kinetic transformation model to obtain specific martensitic volume fractions [37]. This steel grade is being considered for industrial applications where the abrasion and impact play a key role, e.g., in earthmoving, agricultural and mining equipment. The scratch resistance of resulting microstructures was evaluated using the MPDI scratch test method. The strain hardening analysis was performed to quantitatively understand the effect of martensite fraction on the scratch behavior of DP steels for different point load conditions. Considering the fact that it is difficult to link the real dynamic strain hardening with the scratch/abrasion process, the concept of two-stage tensile strain hardening behavior [4,

5, 34, 36, 38] was employed to correlate the scratch/abrasion behavior. Finally, the standard ASTM G65 test was performed to assess the abrasion resistance of the DP steels, and to establish a correlation between the scratch test and the ASTM G65 standard abrasion test.

6.2 Experiments

6.2.1 Test materials and sample preparation

The composition of a lean C-Mn construction steel (22MnB5 steel) investigated in this chapter was Fe-0.22C-1.2Mn-0.25Si-0.2Cr (in wt. %). The 3mm thick hot-rolled steel sheet was firstly homogenized at 1200°C for 24h in a hydrogen atmosphere followed by air cooling. After homogenization, two types of heat treatment (Fig. 6.1) were performed using a Nabertherm furnace: (a) full austenization followed by intercritical annealing at 625°C, 700°C, 725°C, 750°C and 760°C for 1h and water quenching, and (b) full austenization followed directly by water quenching to generate the full martensite reference state. The heat treatment parameters and resulting microstructures are summarized in Table 6.1. After annealing, specimens for scratch testing (15mm×9mm), ASTM G65 testing (75mm×25mm) and tensile testing (sample geometry A25) were prepared with the longitudinal direction of the sample in the rolling direction.

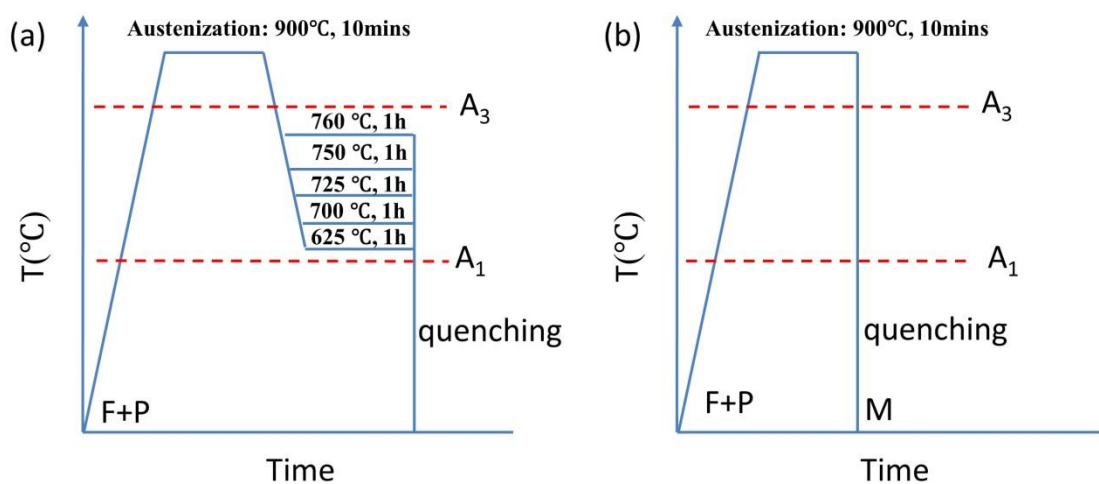


Fig. 6.1 Schematic drawing of the heat treatment procedure.

Table 6.1 Heat treatment conditions and the resulting microstructure.

Heat treatment cycles		Volume fraction of phases (experimental value)
Austenization	Intercritical annealing	
T1: 900°C, 10 mins	625°C, 1h	Ferrite + Martensite (35%)
T2: 900°C, 10 mins	700°C, 1h	Ferrite + Martensite (49%)
T3: 900°C, 10 mins	725°C, 1h	Ferrite + Martensite (68%)
T4: 900°C, 10 mins	750°C, 1h	Ferrite + Martensite (85%)
T5: 900°C, 10 mins	760°C, 1h	Ferrite + Martensite (91%)
T6: 900°C, 10 mins	NA (water quenching)	Full Martensite (100%)

6.2.2 Multi-pass dual-indenter scratch test and ASTM G65 abrasion test

For all samples the multi-pass dual-indenter (MPDI) scratch test [31] was carried out, as described in Chapter 3. For the test conditions, the load on the large indenter with 10 passes was varied between 0N (i.e. maintaining the pristine surface) to 25N (creating an extensively work hardened surface), and the load on the small indenter was fixed with 0.2N with single pass. The test parameters are specified in Table 6.2. The morphology of the scratch track was further investigated using SEM. Further details on the MPDI test and its interpretation can be found in Chapter 3. The ASTM G65 abrasion tests were performed up to total rotations of 2000 at a speed of 200 rpm with standard Ottawa silica sand as the abrasive medium following the procedure B. Samples were tested in the rolling direction. Sample weight upon careful cleaning and removal of unattached abrading particles was measured to 1 mg before and after the test.

Table 6.2 Scratch test parameters

Scratch modes	Test conditions of small indenter	Test conditions of large indenter
Scratching on pristine surface	Single pass with constant load of 0.2N	NA
Scratching on pre-scratched surface	Single pass with constant load of 0.2 N	Multi-pass (10 passes) with 5N, 10N, 15N, 20N, 25N

6.2.3 Mechanical properties measurement

The micro-hardness measurements were carried out using a Vickers indenter under 2N load and the average value of 10 measurements is reported. The tensile test was repeated two times for each heat treatment condition, using A25 specimens with the longitudinal sample direction parallel to the rolling direction. The strain rate was $10^{-3}/s$.

6.2.4 Metallography

Samples for metallurgical characterisation of the six initial microstructures created were polished to a high standard and subsequently etched with a 2% Nital solution. A Leica optical microscope was used for the microstructural examinations. The volume fractions of the various phases were determined by image processing using Photoshop (adjusting the contrast) and MATLAB (calculating the pixels). Scanning electron microscope (SEM) operating at 5 kV was employed to investigate the worn surface.

6.3 Results

6.3.1 Microstructures

The microstructures created by the different heat treatments (Table 6.1) are shown in Fig. 6.2. Samples T1 to T5 subjected to intercritical annealing have dual phase microstructures consisting of ferrite (white regions) and martensite (black regions). No other phases were present. The martensite and ferrite fractions depend on the annealing temperature. The martensite volume fractions (V_m) in Fig. 6.2 were quantified at 35(\pm 5) %, 48(\pm 5) %, 68(\pm 4) %, 85(\pm 3) %, and 91(\pm 2) %, for the annealing temperatures of 625°C, 700°C, 725°C, 750°C and 760°C, respectively. Sample T6, subjected to full austenization and water quenching, displays a fully lath martensitic microstructure without notable fractions of retained austenite. With increasing intercritical annealing temperature, not only the martensite fraction but also the size of martensitic islands increases due to the growth of austenite grains during the intercritical annealing. The

typical morphology of the DP microstructures is that of martensite islands surrounded by ferrite rims, in accordance with the transformation taking place during intercritical annealing.

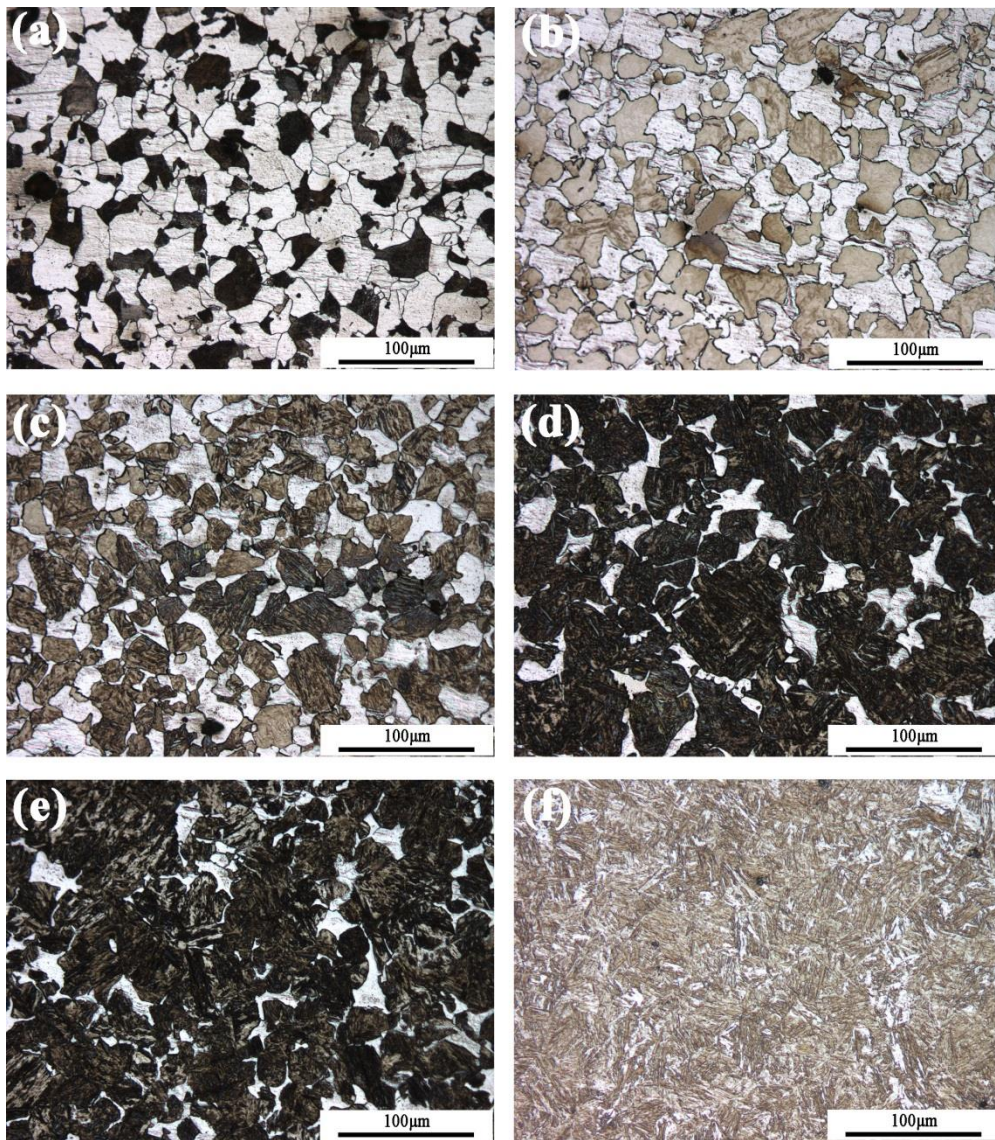


Fig. 6.2 Microstructures after austenization followed by intercritical annealing (a) 625°C, (b) 700°C, (c) 725°C, (d) 750°C, (e) 760°C, and (f) full austenization and direct water quenching.

6.3.2 Hardness and tensile properties

Fig. 6.3 shows the micro-hardness, the yield strength (YS), the ultimate tensile strength (UTS) and the uniform elongation (UE) as a function of the martensite volume fraction for all conditions. It can be observed that the increase in martensite volume fraction leads to an increase in hardness, YS and UTS, while the uniform elongation generally decreases. The full martensite possesses the maximum hardness, YS and UTS, and displays the lowest uniform elongation. It should be noticed that the DP steels have a strong work hardening rate as the YS/UTS ratios are quite low.

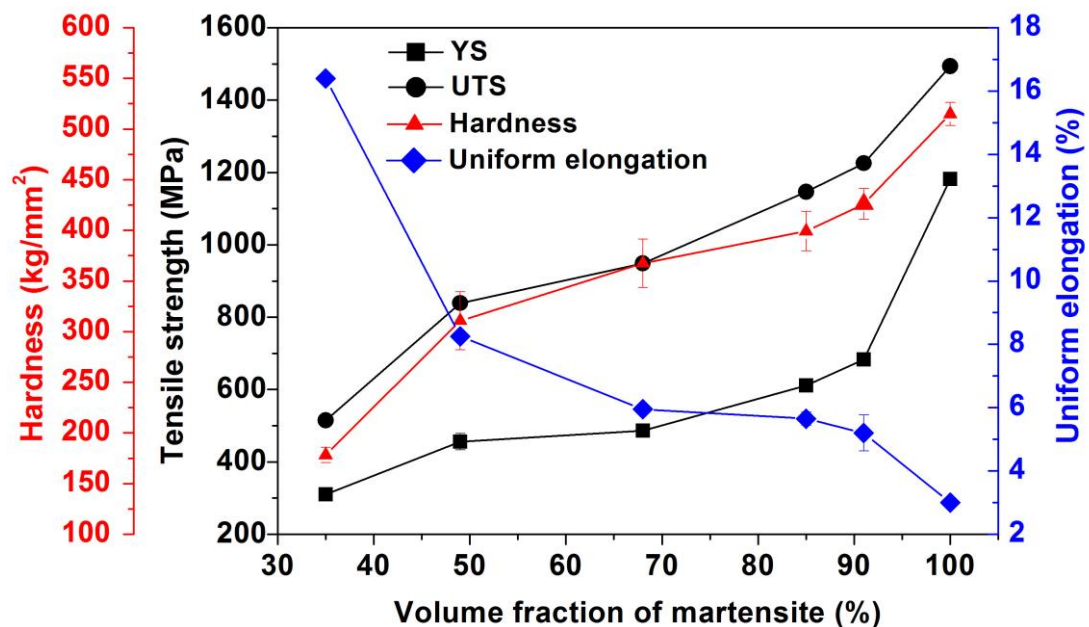


Fig. 6.3 The yield strength, ultimate tensile strength, uniform elongation and Vicker's hardness as a function of the volume fraction of martensite in the microstructures.

6.3.3 MPDI scratch test

In line with the MPDI scratch test methodology, the average depth of the scratch produced by the small indenter in the centre of the wear track produced by the large indenter is plotted in Fig. 6.4 as a function of the pre-load applied on the large indenter. A low scratch depth implies a high scratch resistance. As described and analysed extensively in Chapter 4 involving a wider range of steel grades, the curve of the scratch depth versus the normal pre-load used to create the wear track has a characteristic shape, i.e. it first decreases due to sub surface hardening in the wear track and then increases due to local damage/material abrasive removal around the new scratch in the wear track at higher pre-loads. The transition load varies and depends on the strain hardening capability of the material. In Fig. 6.4, it can be observed that the transition only occurs in the full martensite while no transitions can be found in DP microstructures, i.e. the DP microstructures possess good hardenability and resistance to fracture so that the transition load is greater than the maximum normal load which could be applied on the large indenter in experimental set-up. For all DP steels, the scratch depth decreases with pre-load. The decrease is relatively sharp at the low load region, while upon further increase of the pre-load, the decrease of scratch depth becomes marginal. For the FM steel, the scratch depth and pre-loads show a “V” shaped correlation in which a transition load of 10N can be found.

As is clear from figure 6.4, the volume fraction of martensite plays a key role in determining the scratch resistance depending on the loading condition, due to different material responses to the pre-load conditions used to create the wear track with its work hardened subsurface layer as shown clearly in Chapter 4. At low pre-load condition, a higher martensite fraction generally leads to a better scratch resistance. However, for high pre-loads, if the martensite fraction increases to 100% (FM), the transition occurs at the preload of 10N beyond which it results in an inferior scratch resistance of the full martensite with respect to the DP microstructures. In the case of the 25N pre-load results suggest that the full martensite is considerably less scratch resistant than a DP steel possessing 68% martensite, although the hardness of the latter and its scratch resistance in a low pre-load condition is clearly lower. The results clearly suggest that, the scratch resistance does not only depend on the volume fractions of martensite, but

also closely link with the scratching conditions and in particular the severity of the conditions creating the work hardened subsurface layer.

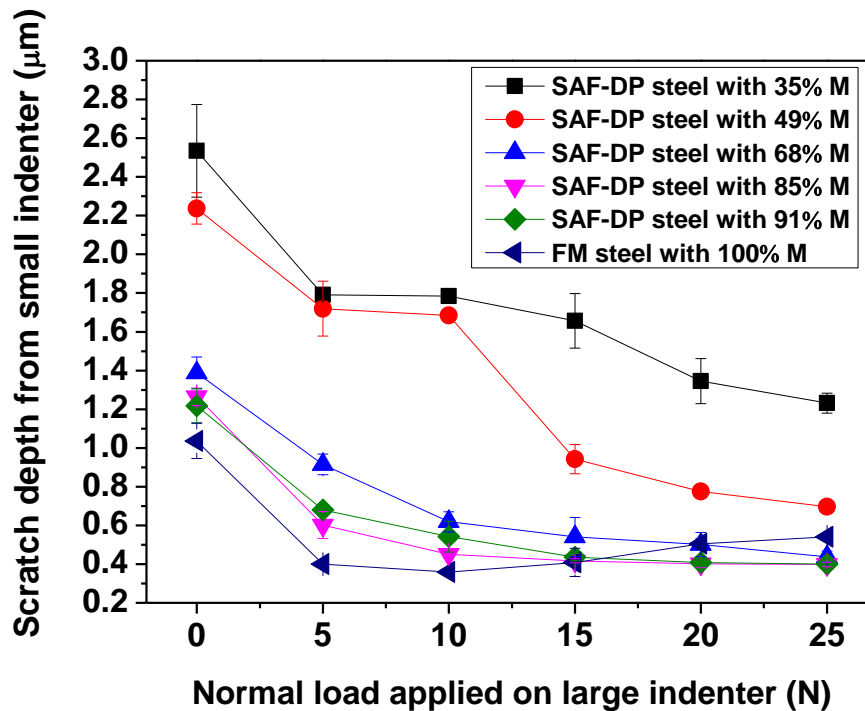


Fig. 6.4 The scratch depth produced on various steels by a single pass with the small indenter as a function of the normal load applied on the large indenter during pre-scratching.

6.3.4 Scratch grooves and failure mechanisms

Fig. 6.5 shows the morphologies of scratch tracks and the resulting failure mechanisms of all steels examined under different pre-loads. It should be noted that the scratch tracks presented in these figures are the grooves produced by the small indenter, while the entire field of view is within the central zone of wear track made with the large indenter, as described in Chapter 4.

In the case of ferrite-rich DP microstructures, i.e. DP steel-35% M and DP steel-49% M, the scratch tracks for the low pre-load of 5N reveal that the failure mechanisms are mainly ploughing and delamination, as shown in Fig. 6.5 (a1 and b1). With an increase

of pre-load to 15N, the delamination becomes milder and the width (and hence the depth) of scratch track is smaller than those under 5N pre-load due to the strain hardening upon pre-scratching, which is in line with results shown in Fig. 6.4. A further increase of the pre-load on the large indenter to 25N results in the production of a more extensively strengthened work hardening subsurface layer, which consequently leads to a lower damage degree and a narrow and shallower scratch as shown in Fig. 6.5 (a3 and b3). The failure mechanisms changes to ploughing, accompanied by occasional formation of chips and cracks as shown in Fig. 6.5 (a3). Here it is worth noting that for the DP steel-35%M with 25N pre-load (Fig. 6.5 (a3)), cracks perpendicular to scratching direction can be observed. These cracks are not initiated by scratching with the small indenter, but are formed during the multi-pass scratching with the large indenter. The formation of the perpendicular cracks is attributed to the fact that the external applied stress exceeds a critical limit beyond which the energy/deformation cannot be accommodated anymore by either the work hardening or the deepening of the subsurface layer. Furthermore, the fact that the martensite in a DP steel with a lower martensite fraction is harder due to a higher carbon concentration makes the material more susceptible to crack formation than a material having higher (yet softer) martensite fraction [39]. Nevertheless, the presence of micro cracks does not reduce the scratch resistance and the depth of the scratch track is still smaller than that at 5 or 15N pre-load. For a volume fraction of martensite to 49% the groove remains smooth and no perpendicular cracks were observed due to a higher strain hardenability and the resulting stronger surface under a higher load condition (see Fig. 6.5 (b3)).

In the case of the martensite-rich DP steels, i.e. DP steel-68%M, DP steel-85%M and DP steel-91%M, the scratch damage is generally milder than for corresponding samples made on ferrite-rich microstructures. SEM images for DP steel-68%M and DP steel-85%M in 5N and 15N pre-scratch conditions (Fig. 6.5(c1 and c2) and Fig. 6.5 (d1 and d2)) reveal that the main failure mechanism is ploughing, while additional delamination may take place in DP steel-68%M. It is interesting to note that the scratch track become very smooth for a pre-load of 25N and no delamination or cracks can be observed, especially for the DP-85%M and the DP - 91%M grades (Fig. 6.5 (d3 and e3)). Clearly, the substrate is very strong owing to the large fraction of ductile martensite. It is also worth noting that, despite of the increase of martensite fraction, the DP -91%M grade

does not show a milder damage but some delamination under relatively low load of 5N and 15N comparing to the DP -85%M grade, as seen in Fig. 6.5 (e1 and e2). Nevertheless, the DP -91%M grade performs very well under the high load of 25N, showing a very light and smooth scratch track similar to the DP steel-85%M in Fig. 6.5 (d3).

For the full M steel, under a low pre-load of 5N, a small amount and degree of delamination can be observed (Fig. 6.5 (f1)). The failure mechanism appears to be ploughing accompanied by a light delamination. When the pre-load increases to 15N and 25N, clearly visible delamination takes place due to the low work hardening capability of the martensite. The failure mechanism changes to micro-cracking as shown in Fig. 6.5 (f2 and f3). As a consequence, the scratch width and depth increase, as was also shown in Fig. 6.4.

The set of observations on the various scratch tracks clearly reveal the dependence of failure mechanisms on the pre-scratching conditions and the volume fractions of martensite. The results are in good agreement with the scratch depth data shown in Fig. 6.4. The analysis of the scratch depth and resulting deformation and damage features allow the selection of a proper material for a specific application or to tune the application parameters to allow the best performance of a given material. In Fig. 6.5, the best combinations of microstructure and pre-load condition are enclosed by a dashed blue line. All combinations within the marked region have in common a low degree of abrasive damage for severe point loading conditions.

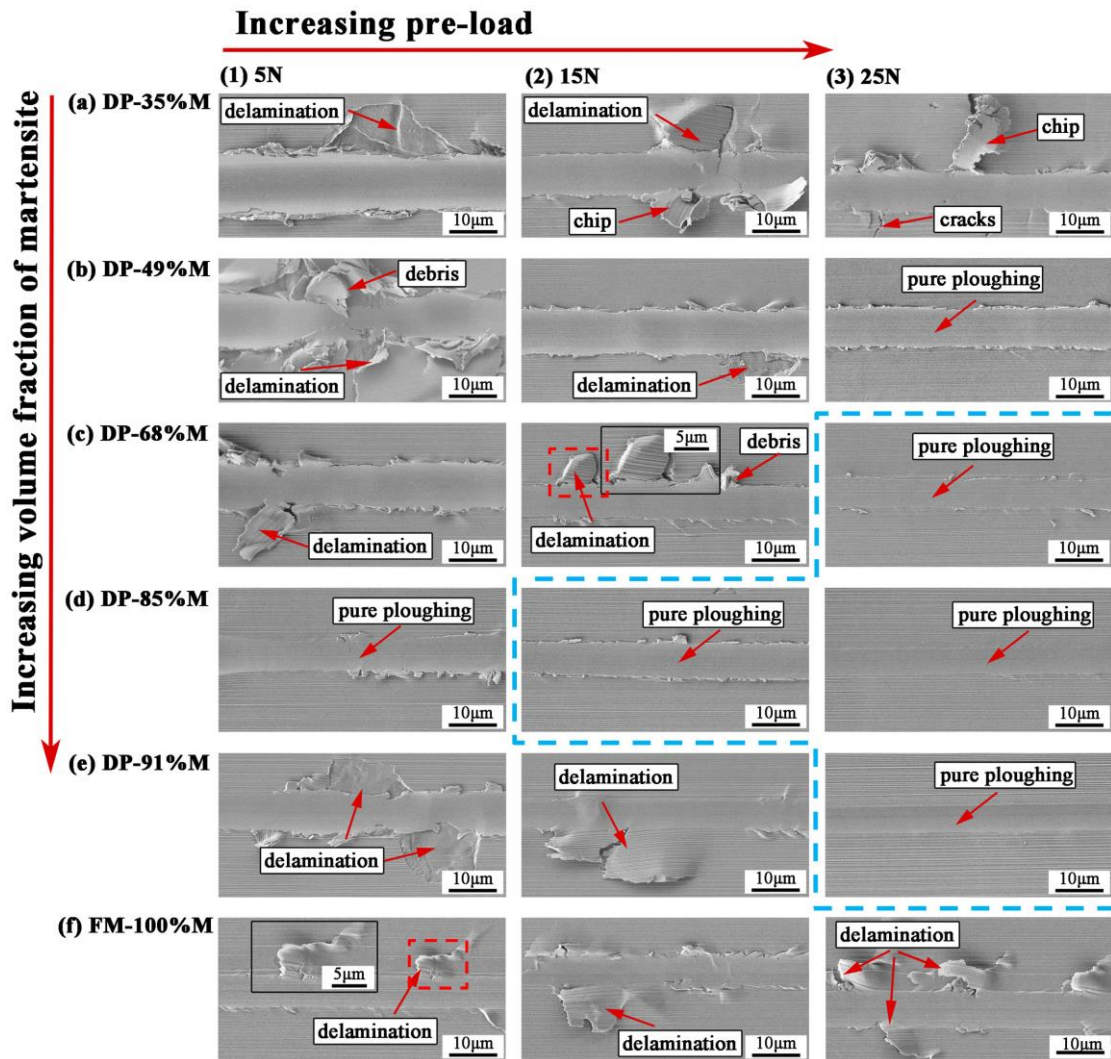


Fig. 6.5 Scratch tracks of all steels subjected to MPDI scratch methodology: single pass scratching with small indenter at 0.2 N, and 10 passes pre-scratching with large indenter at 5N, 15N and 25N load.

6.4 Discussions

6.4.1 The dependence of scratch resistance on the martensitic volume fraction and the loading condition

The well-known increase in yield strength, ultimate tensile strength and hardness with increasing volume fraction of martensite for a given steel composition subjected to different intercritical annealing conditions is confirmed in the present study. The effects can be attributed to the composite effect. The differences in the strain/stress partitioning between different constituents depending on the morphology and texture affect the dependence. However, such a simple and monotonous correlation between the martensite volume fraction and scratch/abrasion resistance does not always exist and the dependence is shown to be strongly dependent on the working conditions, in particular the work hardening of the surface. Fig. 6.6 shows the scratch depths as a function of the martensite volume fraction under different pre-loads. In addition, the hardness evolution is also plotted so as to correlate with the scratch depth. The normal load of 0N corresponds to the scratch directly on the polished surface. As shown in Fig. 6.6, the scratch depth on the initial surface continuously decreases with increasing martensitic volume fraction, in line with the consistent increase of hardness. As discussed in Chapter 5, scratching on initial (undeformed) surface does not truly reflect the real continuous abrasion process and may at best reflect material response during the run-in state. For a wear track created at a load of 5N, the scratch depth generally decreases with increasing martensite fraction up to 100%, a trend of which is similar to that of the initial surface. For this condition the absolute scratch depth is much lower than that for the condition of 0N owing to the surface work hardening. So, the MPDI test indicates that for mild abrasion conditions, the best abrasion resistance is obtained for the hardest, fully martensitic condition, in accordance with the crude engineering guidelines for material selection for abrasive applications.

However, under a high pre-load of 25N which represents very demanding abrasion conditions, it can be observed that the scratch depth firstly decreases with increasing martensite fraction up to a critical value (optimal volume fraction) beyond which the scratch depths clearly start to increase. In such working condition, an optimal martensite

fraction in DP steel exists for which a higher scratch resistance is obtained than for the FM steel despite a lower initial hardness.

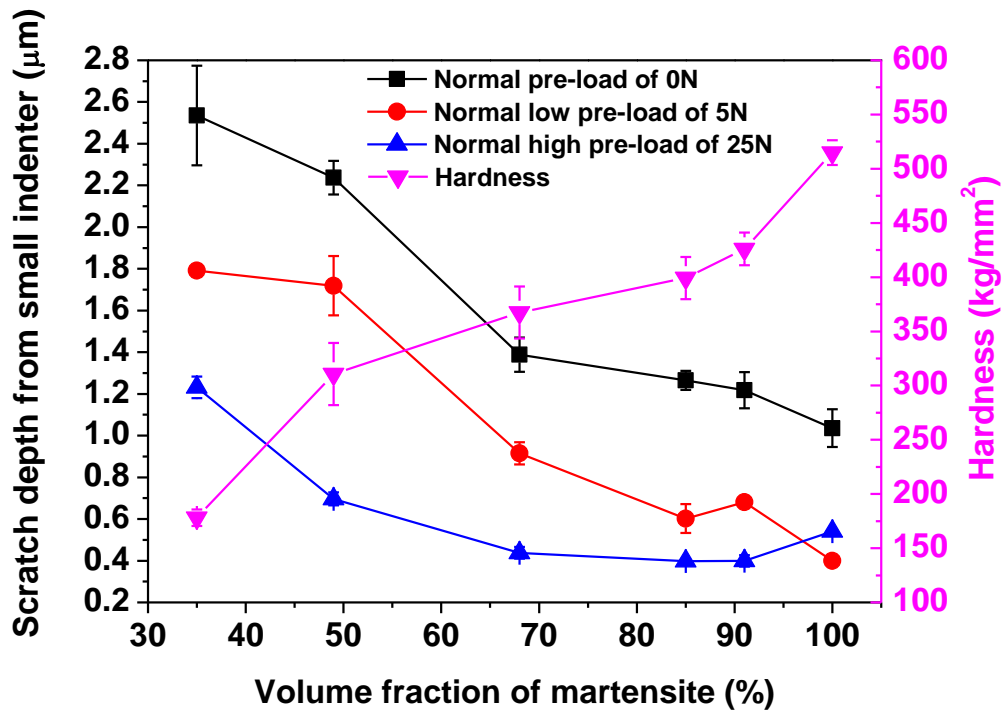


Fig. 6.6 Variations of scratch depths by the small indenter and hardness as a function of the martensite volume fraction for pre-loads of 0N, 5N and 25N.

Fig. 6.7 gives the difference in normalised scratch depth (scratch depth difference divided by difference in martensite fraction) between two neighbouring martensite fraction levels with increasing martensite fraction level and for different pre-loads. For ferrite-rich DP steels, the increase in martensite fraction results in a very marginal decrease in scratch depth under low load conditions, but in a significant decrease in scratch depth under high load conditions. For the martensite-rich DP steels, the opposite results are obtained. Moreover, the degree of decrease in scratch depth due to the increase of martensite fraction becomes lower at higher martensite levels, and even becomes negative at higher martensite fractions suggesting that a further increase in martensite fraction does not lead to an improvement in scratch resistance but instead to an inferior scratch resistance, especially for harsh conditions. Assuming such a qualitative dependence to hold for other steel compositions as well, it suggests that the

design of abrasion resistant steels should focus not only on the high martensite fraction, but to tailor the martensite fraction depending on the work conditions. For ferrite-rich DP steels and low load conditions it is not necessary to increase the volume fraction of hard constituent phase at the expense of ductility in order to improve the scratch resistance, but for high load conditions such an increase would be beneficial. For the martensite-rich DP steels and low load conditions, a higher martensite volume fraction can significantly raise the scratch resistance. For high load conditions DP steels with a somewhat lower martensite fraction may show a better scratch resistance than the hardest FM condition, as is also suggested by the images in Fig 6.5.

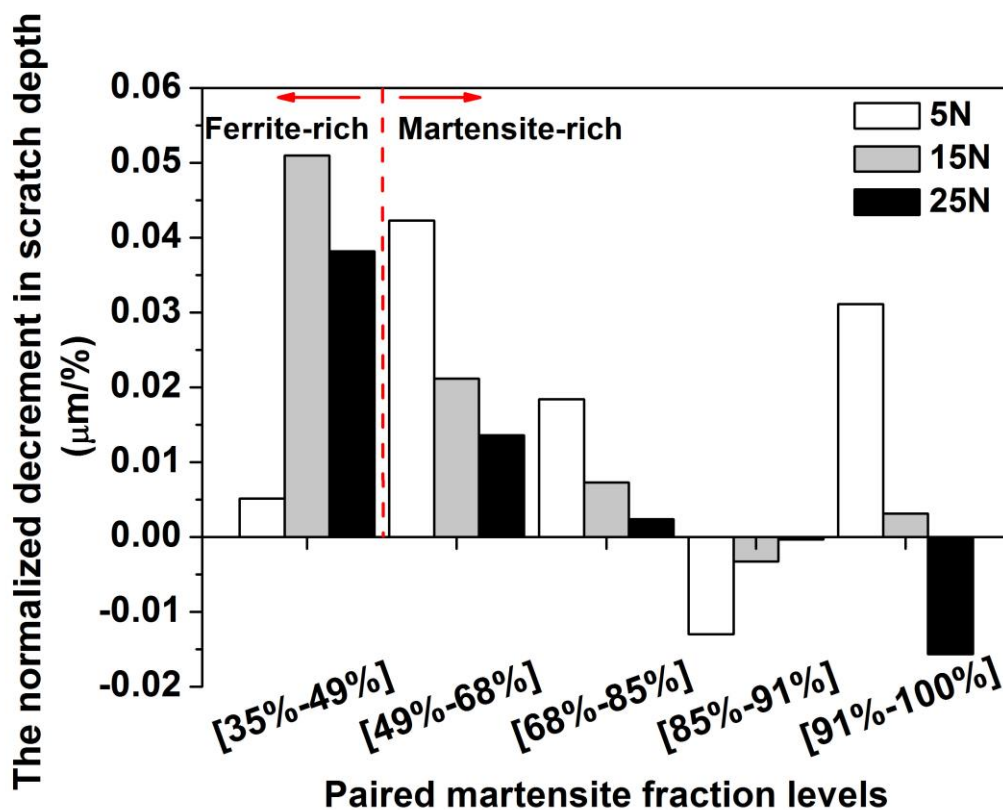


Fig. 6.7 The decrement in scratch depth per martensitic volume percentage for increasing martensite fraction levels for pre-loads of 5N, 15N and 25N (see text).

6.4.2 Correlating the MPDI scratch resistance against the strain hardening behavior

It has been suggested many times that the abrasion resistance is also determined by the property of (sub) surface layer generated during the abrasion process, which itself strongly depends on the strain hardening capability of the substrate [28, 40-42]. However, most investigations only attempted a fully qualitative analysis and hence no (semi-)quantitative interpretations of the effect of work hardening on the abrasion/scratch resistance have been reported. Moreover, the complex and inhomogeneous plastic deformation in the subsurface during the abrasion process makes it impossible to determine the real dynamic strain hardening as a function of the depth below the surface. The situation is a lot less complex in the MPDI test and we may attempt to link the tensile strain hardening behaviour to the scratch resistance data presented above. To this aim, the tensile strain hardening behaviour of the microstructures created was analysed using the Hollomon model [43]:

$$\sigma = K \varepsilon^n \quad (6.1a)$$

or

$$\ln \sigma = \ln K + n \cdot \ln \varepsilon \quad (6.1b)$$

where σ and ε are the true stress and strain, and K and n are strength coefficient and strain hardening exponent, respectively. Fig. 6.8 shows a typical plot of $\ln \sigma$ v.s. $\ln \varepsilon$ of the DP-85% M steel. As reported in the literature for such microstructures [4, 5, 34, 36, 38], it displays a nonlinear relation between $\ln \sigma$ and $\ln \varepsilon$, suggesting a two-stage strain hardening behaviour with different deformation mechanisms at low and at high strain levels. In stage I, the low-strain stage, the strain hardening rate is high; in stage II, the high strain stage, the strain hardening rate is low, as seen in Fig. 6.8. For each of the two stages, the values for K and n can be determined by appropriate linear fitting.

In analogy to the Hollomon plot, we can plot the strengthening of the surface (i.e. the scratch resistance as determined by the reciprocal of (sharp indenter) scratch depth) versus the load applied on the large indenter. Such a curve is shown in figure 6.9 for the DP-85% M steel. As can be seen, it also shows clearly a different surface hardening rate depending on the pre-load: at the low pre-load region, the significant increase in scratch

resistance (i.e. scratch depth) means that the subsurface experiences strengthening at a high surface hardening rate; while under high pre-loads the scratch resistance reaches almost comparable work hardening levels. In the DP grades the critical strain level for crack formation was not yet reached during the 10 passes sliding pre-treatment, even for the highest load of 25 N (as shown in Fig. 6.4 and Fig. 6.5), so one can argue that the pre-scratching experiments were performed below the UTS condition. On the basis of this comparative analysis, we now explore the hypothesis that the low-strain stage I corresponds to the surface hardening behavior at low-preloading conditions in the MPDI scratch test, and that the high-strain stage II is related to high-preloading MPDI conditions.

Fig. 6.10 and Fig. 6.11 present the strain hardening parameters (n_1 , K_1 and n_2 , K_2) and the scratch characteristics versus the martensite volume fraction (in %) for the low load 5N and the high load 25N, respectively. As can be seen in Fig. 6.10, the variation of n_1 and K_1 at the stage I with martensite fraction corresponds well with the change of the scratch depth under the low pre-load condition. With increasing martensite fraction, the increase in both n_1 and K_1 results in a decrease in scratch depth and suggest the best scratch resistance at the highest martensite fraction. The FM steel (100% martensite) with the highest n_1 and K_1 indeed gives the best scratch resistance amongst the microstructures examined, yielding mild scratch damage (Fig. 6.5 (f1)). Fig. 6.11 (the high load results) shows that n_2 gradually decreases with increasing martensite fraction but the strength coefficient K_2 keeps increasing. The opposite behaviour of n_2 and K_2 with martensite fraction should lead to the optimal martensite volume fraction being different from 100%, as is indeed observed. As shown in Fig. 6.10, there is a critical fraction (optimal martensite fraction) in which the scratch resistance is maximal. For the martensite-rich DP grades, the slight change in n_2 (decreasing) and in K_2 (increasing) with increasing martensite fraction matches the observation of relatively small differences in scratch depth compared to the low load condition as shown in Fig. 6.7 and Fig. 6.11. The further increase in martensitic volume fraction up to full martensite does not result in further improvement of scratch resistance but deteriorate the scratch resistance under the high load condition, which may be linked to the low value for the work hardening exponent n_2 and the damage pattern shown in Fig. 6.5 (f3).

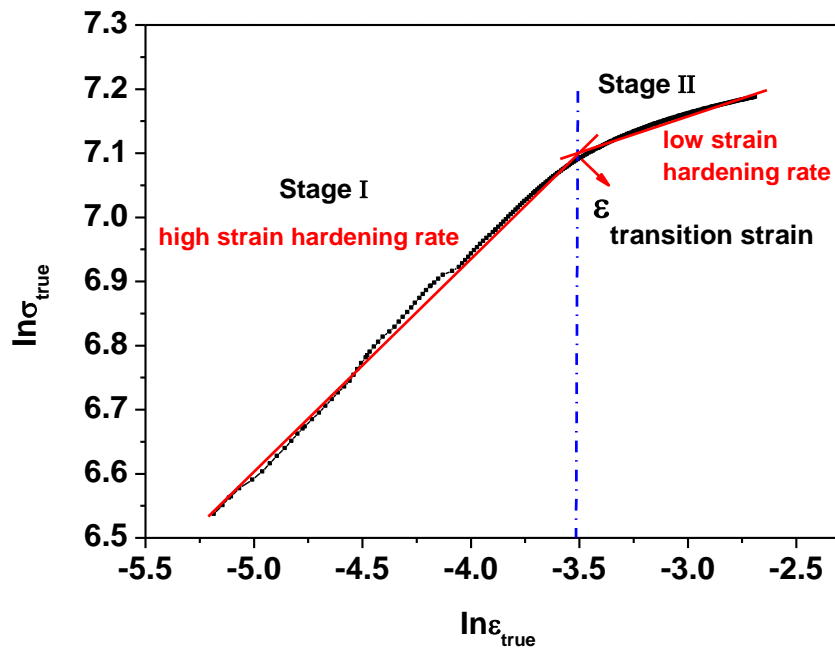


Fig. 6.8 typical plot of $\ln \sigma$ v.s. $\ln \epsilon$ and fit lines to determine the strain hardening exponents (n) and strength coefficients (K) for the DP-85%M grade.

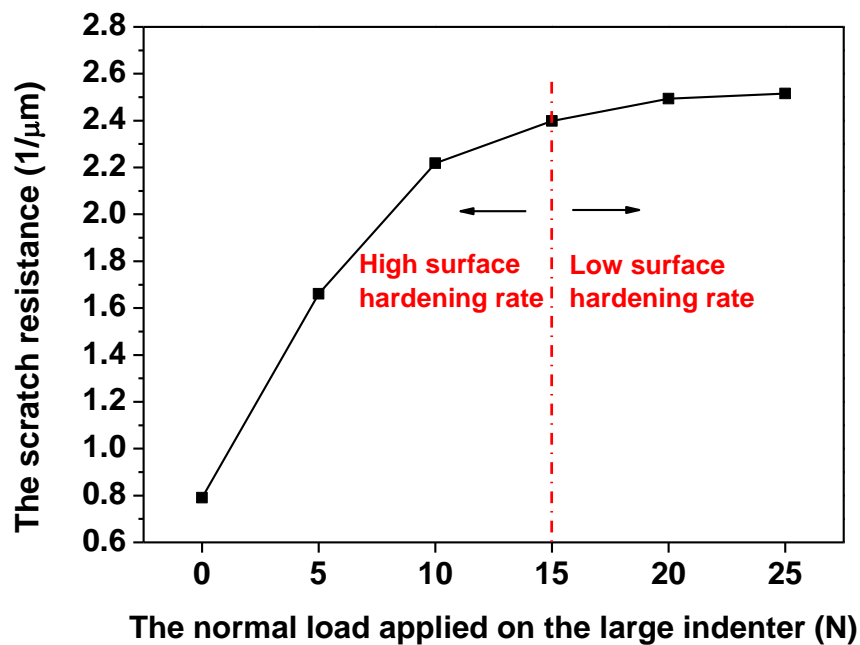


Fig. 6.9 The scratch resistance (the reciprocal of scratch depth) as a function of the normal load applied on the large indenter for the DP-85%M grade (see text).

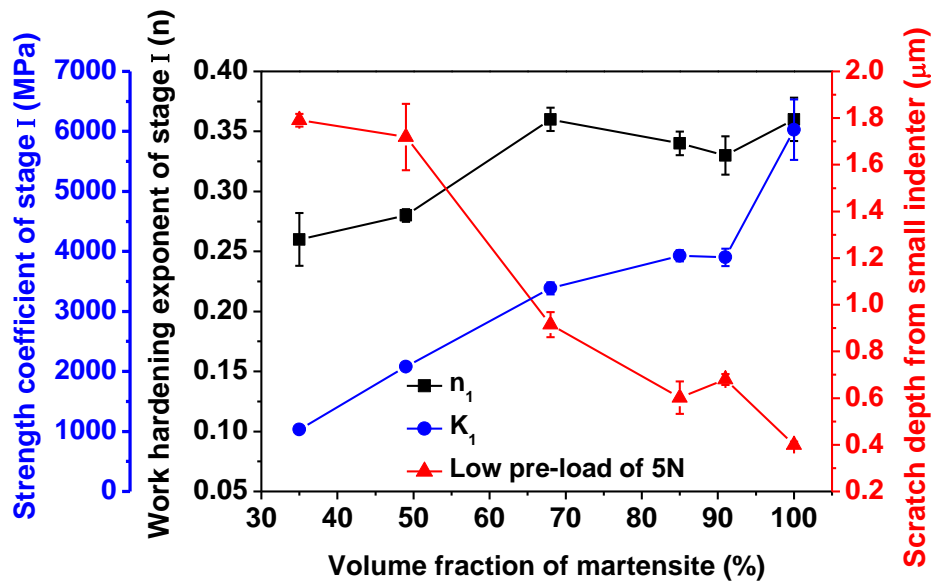


Fig. 6.10 The variation of strain hardening parameters (n_1 and K_1) at the stage I with the corresponding scratch depth at the low pre-loading condition as a function of the martensite volume fraction.

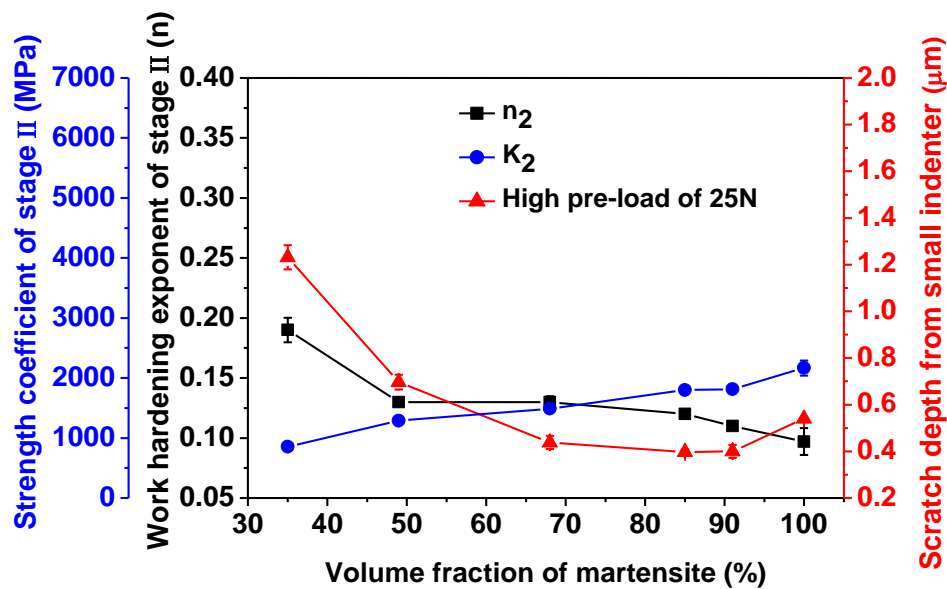


Fig. 6.11 The variation of strain hardening parameters (n_2 and K_2) at the stage II with the corresponding scratch depth at the high pre-loading condition as a function of the martensite volume fraction.

6.4.3 Validation of the MPDI scratch test against the ASTM G65 abrasion test

In order to benchmark the scratch resistance as determined by MPDI test to the (multi-particle) abrasion resistance, the standard ASTM G65 abrasion test was performed on all microstructural grades presented above. Fig. 6.12 presents the correlation of ASTM G65 weight loss and the MPDI scratch depth under the low load of 5N. The ASTM G65 test weight losses are in good agreement with the scratch depths in the 5N pre-load condition. This is also in line with an earlier conclusion in Chapter 5 that ASTM G65 represents the low pre-load situation in the MPDI test.

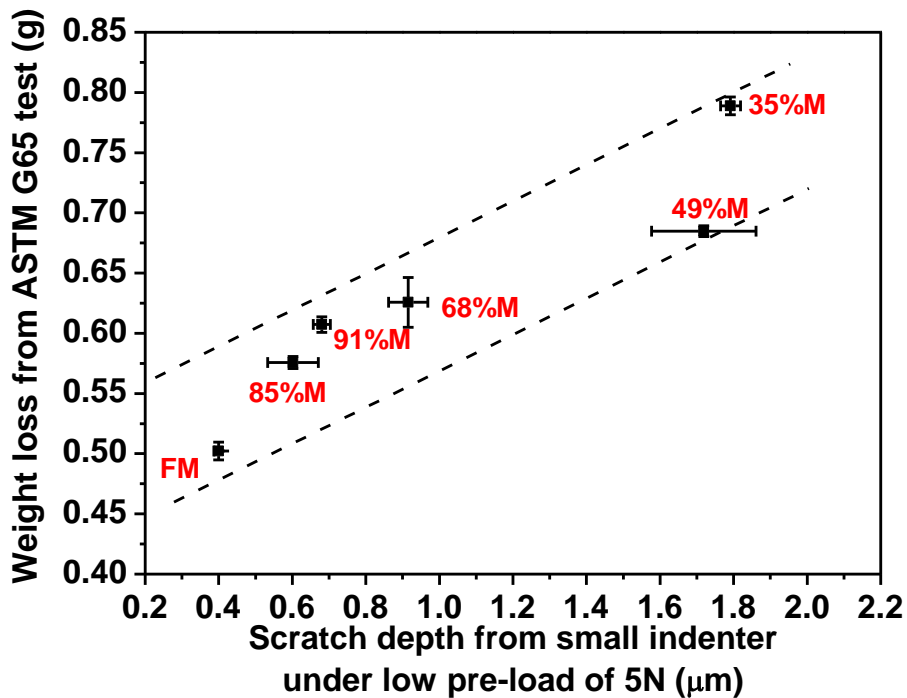


Fig. 6.12 ASTM G65 weight loss versus the MPDI scratch depth for a low pre-load of 5N.

Finally, in applications of abrasion resistant steels, the hardness is still taken as the prime performance predictor and hence engineering steels are classified accordingly. However, the scratch results discussed above clearly demonstrate that the scratch resistance depends on not only the hardness (i.e. the martensite volume fraction) but also the working condition. To show the effect more clearly in Fig. 6.13 the ASTM G65

weight losses and scratch depths under a low load and a high load conditions are plotted versus the hardness. In a mild condition, representing the ASTM G65 test, the hardness is indeed a good indicator and hence a higher hardness results in a better abrasion resistance. However, in a more aggressive condition, e.g. a high contact pressure or impact contact, the presence of some soft constituents in a DP microstructure may increase the scratch/abrasion resistance considerable. The exact amount of the soft phase depends on the working condition and has to be optimized according to the real working condition. Although the relevance of MPDI test methodology with abrasion resistance is only validated for a low preload with the ASTM G65 test, the common natures of MPDI and abrasion process should be valid for the high pressure contact as well, i.e. the MPDI in a high pre-load should represent the abrasion process with a high contact pressure, which is still to be validated by a dedicated experimental setup. Nevertheless, the current investigation on the basis of MPDI scratch test is useful to 1) benchmark different microstructures and rank their scratch/abrasion resistance potentials in different working conditions, e.g. to rank which material works better in a given working condition (not always the highest hardness), and 2) identify the optimal working condition of a given materials, e.g. according to the current study, the full martensite should be used in a mild condition, while the DP steel in a harsh condition.

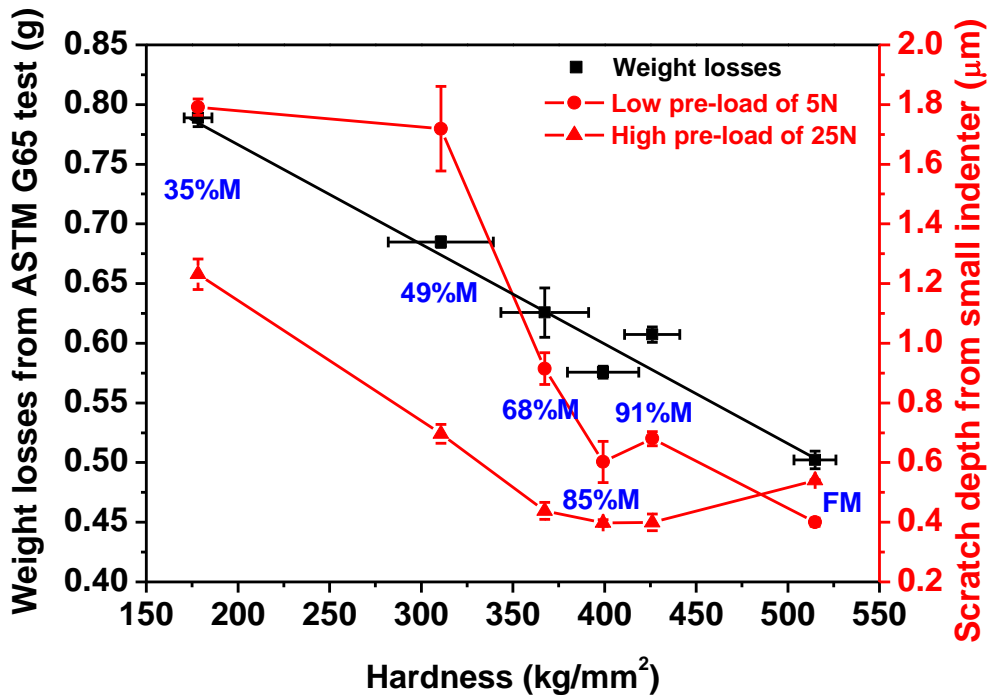


Fig. 6.13 The ASTM G65 weight loss, and MPDI scratch depths under the low load of 5N and the high load of 25N as a function of the initial hardness.

6.5 Conclusions

This paper presents an experimental study of scratch/abrasion behavior of a Fe-0.22C-1.2Mn-0.25Si-0.2Cr steel heat treated to ferrite-martensite dual phase microstructures with different martensite volume fractions using the multi-pass dual-indenter (MPDI) scratch test and the ASTM G65 abrasion test. A two-stage tensile strain hardening model was applied to interpret the scratch resistance under different pre-load condition and resulting failure mechanisms. On the basis of the experimental observations and the strain hardening analysis, the following conclusions can be draw:

- (1) The MPDI test allows separation of the effects of the microstructure and the load condition creating the work hardened surface as formed during steady state abrasion. The scratch resistance of DP steels strongly depends on both the martensite volume fraction and the working condition applied.

-
- (2) The standard ASTM G65 test was found to correlate well MPDI scratch response for mild multi-pass pre-scratching conditions. For these conditions, the scratch depth generally decreases with increasing the martensite volume fraction. The best scratch resistance and best abrasion resistance was obtained for a fully martensitic structure.
 - (3) For conditions leading to a more severely strained surface layer, e.g. high contract pressure or impact, the best scratch resistance (and probably best abrasion resistance) is obtained for DP microstructures with a lower martensite fraction as well as a lower hardness.
 - (4) The two-stage tensile strain hardening model gives a good interpretation on the scratch behavior in the different load conditions and may provide a new insight into correlate the strain hardening with abrasion resistance.
 - (5) The MDPI scratch methodology can be applied to 1) benchmark different microstructures and rank their scratch/abrasion resistance potentials in a given working condition and 2) identify the optimal working condition of a given material and hence to tune the application condition so as to optimize the performance of the component.

References

- [1] R.G. Davies, C.L. Magee, in: R.A. Kott and J.W. Morris (Ed.), *Structure and Properties of Dual-Phase Steels*, TMS-AIME, Warrendale, PA, 1979, pp.1-19.
- [2] M. Mazinani, W.J. Poole, Effect of martensite plasticity on the deformation behavior of a low-carbon dual-phase steel, *Metall. Mater. Trans. A* 38 (2007) 328-339.
- [3] H. Ghassemi-Armaki, R. Maaß, S.P. Bhat, S. Sriram, J.R. Greer, K.S. Kumar, Deformation response of ferrite and martensite in a dual-phase steel, *Acta Mater.* 62 (2014) 197-211.
- [4] M.R. Akbarpour, A. Ekrami, Effect of ferrite volume fraction on work hardening behavior of high bainite dual phase (DP) steels, *Mater. Sci. Eng. A* 477 (2008) 306-310.
- [5] A. Zare, A. Ekrami, Effect of martensite volume fraction on work hardening behavior of triple phase (TP) steels, *Mater. Sci. Eng. A* 528 (2011) 4422-4426.
- [6] J. Zhang, H. Di, Y. Deng, R.D.K. Misra, Effect of martensite morphology and volume fraction on strain hardening and fracture behavior of martensite-ferrite dual phase steel, *Mater. Sci. Eng. A* 627 (2015) 230-240.
- [7] N.J. Kim, G. Thomas, Effects of morphology on the mechanical behavior of a dual phase Fe/2Si/0.1C steel, *Metall. Trans. A* 12 A (1981) 483-489.
- [8] K.J. Kim, C.G. Lee, S. Lee, Effects of martensite morphology on dynamic torsional behavior in dual phase steels, *Scripta Mater.* 38 (1997) 27-32.
- [9] M.J. Molaei, A. Ekrami, The effect of dynamic strain aging on fatigue properties of dual phase steels with different martensite morphology, *Mater. Sci. Eng. A* 527 (2009) 235-238.
- [10] R. Bakhtiari, A. Ekrami, The effect of bainite morphology on the mechanical properties of a high bainite dual phase (HBDP) steel, *Mater. Sci. Eng. A* 525 (2009) 159-165.
- [11] P.H. Chang, A.G. Preban, The effect of ferrite grain-size and martensite volume fraction on the tensile properties of dual phase steel, *Acta Metall. Mater.* 33 (1985) 897-903.
- [12] B.C. Hwang, T.Y. Cao, S.Y. Shin, S.H. Kim, S.H. Lee, S.J. Kim, Effects of ferrite grain size and martensite volume fraction on dynamic deformation behaviour of 0.15C-2.0Mn-0.2Si dual phase steels, *Mater. Sci. Technol.* 21 (2005) 967-975.
- [13] L.F. Ramos, D.K. Matlock, G. Krauss, On the deformation behavior of dual-phase steels, *Metall. Trans. A* 10 (1979) 259-261.
- [14] N.K. Balliger, T. Gladman, Work hardening of dual phase steels, *Met. Sci.* 15 (1981) 95-108.
- [15] V. Colla, M. De Sanctis, A. Dimatteo, G. Lovicu, A. Solina, R. Valentini, Strain hardening behavior of dual-phase steels, *Metall. Mater. Trans. A* 40 (2009) 2557-2567.

- [16] E. Rabinowicz, *Friction and Wear of Materials*, Wiley-Interscience, New York, 1965.
- [17] X. Xu, W. Xu, F.H. Ederveen, S. van der Zwaag, Design of low hardness abrasion resistant steels, *Wear* 301 (2013) 89-93.
- [18] H. Saghafian, S. Kheirandish, Correlating microstructural features with wear resistance of dual phase steel, *Mater. Des.* 61 (2007) 3059-3063.
- [19] O.P. Modi, P. Pandit, D.P. Mondal, B.K. Prasad, A.H. Yegneswaran, A. Chrysanthou, High-stress abrasive wear response of 0.2% carbon dual phase steel: Effects of microstructural features and experimental conditions, *Mater. Sci. Eng. A* 458 (2007) 303-311.
- [20] R. Tyagi, S.K. Nath, S. Ray, Development of wear resistant medium carbon dual phase steels and their mechanical properties, *Mater. Sci. Technol.* 20 (2004) 645-652.
- [21] O.P. Modi, B.K. Prasad, A.K. Jha, R. Dasgupta, A.H. Yegneswaran, Low-stress abrasive wear behaviour of a 0.2% C steel: influence of microstructure and test parameters, *Tribol. Lett.* 15 (2003) 249-255.
- [22] A.P. Modi, Effects of microstructure and experimental parameters on high stress abrasive wear behaviour of a 0.19wt% C dual phase steel, *Tribol. Int.* 40 (2007) 490-497.
- [23] A.K. Jha, B.K. Prasad, O.P. Modi, S. Das, A.H. Yegneswaran, Correlating microstructural features and mechanical properties with abrasion resistance of a high strength low alloy steel, *Wear* 254 (2003) 120-128.
- [24] P. Xu, B. Bai, F. Yin, H. Fang, K. Nagai, Microstructure control and wear resistance of grain boundary allotriomorphic ferrite/granular bainite duplex steel, *Mater. Sci. Eng. A* 385 (2004) 65-73.
- [25] O.P. Modi, B.K. Prasad, S. Das, A.K. Jha, A.H. Yegneswaran, Abrasive Wear Behavior of an Aisi-5132 Steel under Low Stresses, *Mater. Trans. JIM*, 35 (1994) 67-73.
- [26] B.K. Prasad, S.V. Prasad, Abrasion-induced microstructural changes during low stress abrasion of a plain carbon (0.5% C) steel, *Wear* 151 (1991) 1-12.
- [27] L. Fang, Q.D. Zhou, Y.J. Li, An explanation of the relation between wear and material hardness in three-body abrasion, *Wear* 151 (1991) 313-321.
- [28] A. Ball, On the importance of work hardening in the design of wear-resistant materials, *Wear* 91 (1983) 201-207.
- [29] P. J. Mutton, J.D. Watson, Some effects of microstructure on the abrasion resistance of metals, *Wear* 48 (1978) 385 - 398.
- [30] M. Lindroos, K. Valtonen, A. Kemppainen, A. Laukkanen, K. Holmberg, V.T. Kuokkala, Wear behavior and work hardening of high strength steels in high stress abrasion, *Wear* 322-323 (2015) 32-40.

- [31] X. Xu, S. van der Zwaag, W. Xu, A novel multi-pass dual-indenter scratch test to unravel abrasion damage formation in construction steels, *Wear* 322-323 (2015) 51-60.
- [32] S.R. Mediratta, V. Ramaswamy, V. Singh, P. Ramarao, Dependence of strain hardening exponent on the volume fraction and carbon content of martensite in dual phase steels during multistage work hardening, *J. Mater. Sci. Lett.* 9 (1990) 205-206.
- [33] J. Lian, Z. Jiang, J. Liu, Theoretical model for the tensile work hardening behaviour of dual-phase steel, *Mater. Sci. Eng. A* 147 (1991) 55-65.
- [34] Z. Jiang, Z. Guan, J. Lian, Effects of microstructural variables on the deformation behaviour of dual-phase steel, *Mater. Sci. Eng. A* 190 (1995) 55-64.
- [35] P.J. Jacques, Q. Furnemont, F. Lani, T. Pardoën, F. Delannay, Multiscale mechanics of TRIP-assisted multiphase steels: I. Characterization and mechanical testing, *Acta Mater.* 55 (2007) 3681-3693.
- [36] P. Movahed, S. Kolahgar, S.P.H. Marashi, M. Pouranvari, N. Parvin, The effect of intercritical heat treatment temperature on the tensile properties and work hardening behavior of ferrite-martensite dual phase steel sheets, *Mater. Sci. Eng. A* 518 (2009) 1-6.
- [37] H. Chen, X. Xu, W. Xu, S. Van Der Zwaag, Predicting the austenite fraction after intercritical annealing in lean steels as a function of the initial microstructure, *Metall. Mater. Trans. A* 45 (2014) 1675-1679.
- [38] Y. Mazaheri, A. Kermanpur, A. Najafizadeh, A novel route for development of ultrahigh strength dual phase steels, *Mater. Sci. Eng. A* 619 (2014) 1-11.
- [39] G.R. Spiech, R.L. Miller, in: R.A. Kott and J.W. Morris(Ed.), *Structure and Properties of Dual-Phase Steels*, TMS-AIME, Warrendale, PA, 1979, pp.145–182.
- [40] M.A. Moore, R.M. Douthwaite, Plastic-deformation below worn surfaces, *Metall. Trans. A* 7 (1976) 1833-1839.
- [41] A.T. Alpas, H. Hu, J. Zhang, Plastic deformation and damage accumulation below the worn surfaces, *Wear* 162–164, Part A (1993) 188-195.
- [42] X. Xu, S. van der Zwaag, W. Xu, Prediction of the abrasion resistance of construction steels on the basis of the subsurface deformation layer in a multi-pass dual-indenter scratch test, *Wear* 338–339 (2015) 47-53.
- [43] J.H. Hollomon, Tensile deformation, *Trans. AIME*, 162 (1945) 268-290.

Chapter 7

The effect of ferrite-martensite morphology on the scratch and abrasive wear behaviour of a dual phase construction steel

7.1 Introduction

As stated in Chapter 2, in dual phase steels the ferrite-martensite morphology are the critical parameters in controlling the wear resistance. Following the Chapter 6 which has focused on the effect of martensitic volume fraction in DP steels on their abrasion resistance, in the current chapter, we continue to discuss the effect of ferrite-martensite morphology and the spatial distribution of the martensite with respect to its difference in the size, shape and spatial configuration on the scratch and abrasion resistance for a same single lean C-Mn construction steel (a hot rolled 22MnB5 steel). The effect of the ferrite-martensite morphologies produced by different heat treatments on the tensile deformation behaviour [1-4], the quasi-static/dynamic torsional deformation [5, 6], the fatigue resistance [7-9], the impact behaviour [10], and the strain hardening [11-13] has already been studied by others. Given the facts that the abrasion resistance is not an

intrinsic material property but is the complex response of a multi-parameter tribosystem and that the different properties of both phases and the different morphology for ferrite-martensite DP steel will result in complex strain/stress partitioning and different load response, the scratch and abrasion resistance has not been studied in great detail yet.

Some studies [14-16] reported that a DP steel with a continuous ferrite network encapsulating martensite displayed better wear resistance than those with a continuous martensite network encapsulating ferrite at the same martensite fraction. In another study related to the effect of size of martensite colony on abrasion resistance of a DP steel [17], it is demonstrated that for DP steels with coarser martensite colonies (but accompanying the increase of martensite fraction) showed a better performance against abrasive wear than a finer distribution of martensite islands. To separate the effect of martensite fraction and size of martensite colony, Bhowmick, *et al.* [18] produced DP steels with different morphologies at fixed martensite fractions, which showed that the highest abrasion resistance is obtained for the DP steel having large martensite colony. In contrast, some works reported by Khatirkar *et al.* [19] on En24 steel, Baburaj *et al.* [20] on En31 steel, Singh *et al.* [21] on D2 steel and Fu *et al.* [22] on rolling mill liner steels show that a coarser martensite reduces the abrasion resistance. Lindroos *et al.* [23] also pointed out that the morphological features (the prior austenite, packet, block and lath sizes) of the martensitic structure have a strong effect on the strength and work hardening behaviour of the high strength steels and hence influence the wear resistance. Moreover, Deng *et al.* [24] investigated the effect of ferrite morphology on abrasion resistance of DP steel at the same martensite fraction. The results showed that the acicular ferrite-martensite DP steel possesses a better abrasion resistance than the polygonal ferrite-martensite DP steel. While these studies certainly clarified some issues, in these studies either the effect of morphology was determined for one loading (abrasion) condition or the effect of volume fraction was not well separated from that of morphology. Systematic investigations into the effect of ferrite-martensite morphology (shape, size and distribution) on abrasion/scratch resistance of DP steels at different load conditions at fixed martensite fraction are still lacking. Hence, the response of different morphologies in DP steels on scratch and abrasion resistances under different load conditions is still not yet clear.

The objective of this chapter is to clarify the effect of the different ferrite-martensite morphologies on the scratch and abrasive wear behaviour in DP steels at different load levels. In order to separate the effects of the individual parameters (morphology), the volume fractions of the martensite and the properties of ferrite and martensite which are intrinsically coupled were tailored by heat treatments designed on the basis of a local equilibrium (LE) kinetic transformation model [25]. The scratch resistance of resulting microstructures with three different well-characterized morphologies was evaluated using the multi-pass dual-indenter (MPDI) scratch test method. Moreover, the strain hardening analysis using two-stage tensile strain hardening model introduced in Chapter 6 was used to correlate the tensile test strain hardening behaviour with the scratch resistance under different load conditions. Finally, the standard ASTM G65 test was performed to rank the abrasion resistance for the various microstructures and to establish a correlation between the scratch test with the standard ASTM G65 abrasion test.

7.2 Experimental procedures

A same single lean C-Mn construction steel (A hot rolled 22MnB5) as used in Chapter 6 was chosen for the study of this chapter. As same as Chapter 6, the 3mm thick hot-rolled steel sheet was firstly homogenized at 1200°C for 24h in a hydrogen atmosphere followed by air cooling. After homogenization, the isothermal transformation heat treatment was carried out using a Nabertherm furnace - Modell L 5/13/B180. The variation of temperature on the sample sheet is measured to be within $\pm 5^\circ\text{C}$. Three different isothermal transformation experiments (as seen in Fig. 7.1) were performed to generate DP steels with different morphologies: (a) full **A**ustenisation, then **I**ntercritical annealing to form ferrite necklace structures followed by **Q**uenching (AIQ); (b) **I**ntercritical annealing, directly from the **F**errite/pearlite starting microstructure followed by **Q**uenching (FIQ); and (c) **I**ntercritical annealing from an almost fully **M**artensitic starting state followed by **Q**uenching (MIQ). The detailed heat treatments are described below:

- AIQ: full austenisation followed by intercritical annealing at 700°C, 725°C, 750°C and 760°C for 1h followed by water quenching, as shown in Fig. 7.1a.
- FIQ: intercritical annealing of the initial ferrite-pearlite microstructure at 750°C, 775°C, 790°C and 800°C for 1h and water quenching, as shown in Fig. 7.1b.
- MIQ: first full austenisation followed by water quenching; then intercritical annealing at 750°C, 775°C, 790°C and 800°C for 1h followed by water quenching, as shown in Fig. 7.1c.

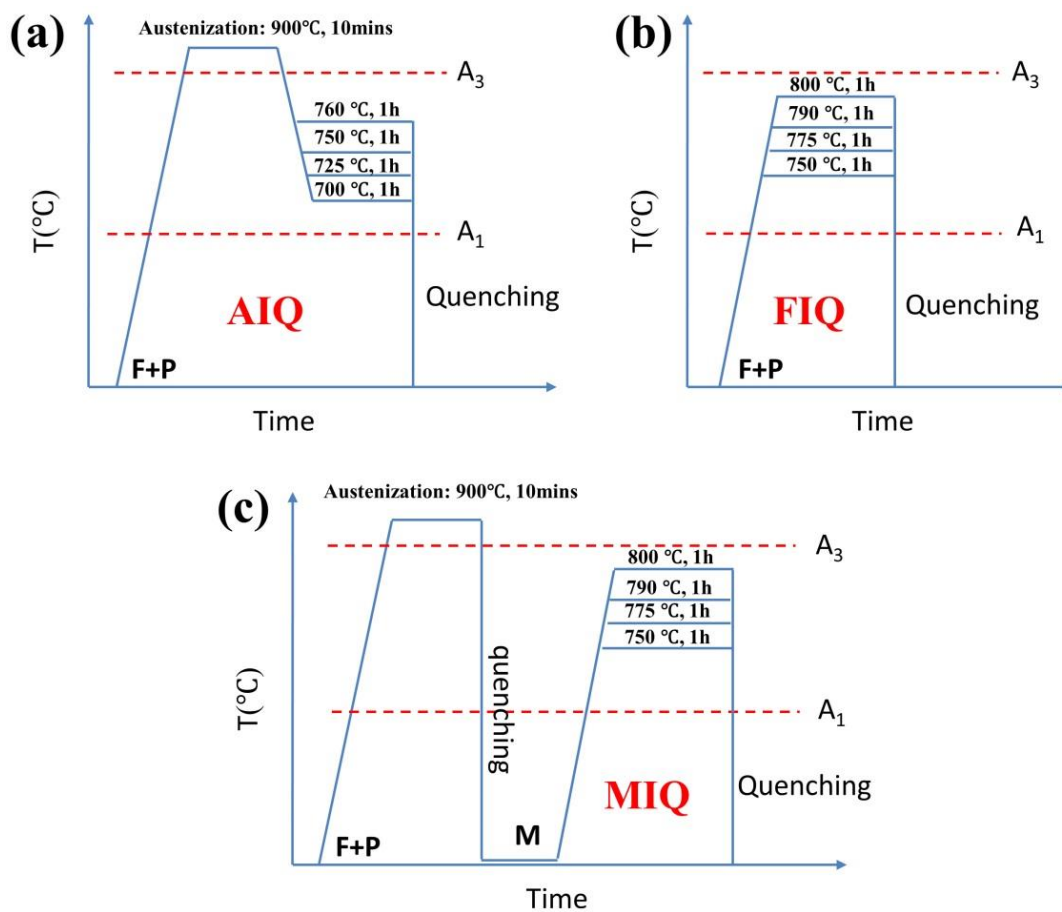


Fig. 7.1 The schematic drawing of the three isothermal transformations: (a) AIQ-austenite to ferrite transformation; (b) FIQ- ferrite + pearlite to austenite; and (c) MIQ- martensite to austenite transformation.

The heat treatment parameters and resulting microstructures are summarized in Table 7.1. After annealing, the preparation of specimens for scratch testing, ASTM G65 testing, and tensile testing follows the description in Chapter 6. The MPDI scratch test procedure including the test conditions and the standardized ASTM G65 test are same as Chapter 6. The micro-hardness measurements and tensile test were carried out following the same procedure as shown in Chapter 6. Samples for metallurgical characterisation of all sample grades created were polished to a high standard and subsequently etched with a 2% Nital solution. A Leica optical microscope, scanning electron microscopy (SEM) operating at 5kV and X-ray diffraction (XRD) test with Co K α radiation were used for the microstructural examinations. The volume fractions of the various phases were determined following the same procedure as shown in Chapter 6, and the results are listed in Table 7.1. After scratch test, SEM was employed to investigate the morphology of the worn surface.

Table 7.1 Heat treatment conditions and the resulting microstructures

Heat treatment cycles		Volume fractions of martensite (experimental value)
Thermal paths	Annealing temperature (°C)	
AIQ	700°C	49(±5) %
AIQ	725°C	68(±4) %
AIQ	750°C	85(±3) %
AIQ	760°C	91(±2) %
FIQ	750°C	48(±4) %
FIQ	775°C	65(±6) %
FIQ	790°C	84(±4) %
FIQ	800°C	92(±2) %
MIQ	750°C	53(±4) %
MIQ	775°C	71(±4) %
MIQ	790°C	85(±4) %
MIQ	800°C	90(±3) %

7.3 Results

7.3.1 Microstructures

The typical optical micrographs of the rather different microstructures (i.e. ~ 65%M and ~90%M) created by the three different heat treatments are shown in Fig. 7.2. In the AIQ route the microstructure before entering into the two-phase region is austenite. Upon lowering the temperature to the two-phase region, ferrite nucleates at the prior austenite grain boundaries and grows into the austenite. The resulting microstructure after quenching is that of martensite islands (black region) surrounded by the necklace ferrite (white region), as shown in Fig. 7.2(a). In the FIQ route the starting microstructure is hypoeutectoid ferrite and pearlite formed during homogenization in combination with air cooling. Upon intercritical annealing, austenite nucleates at the ferrite/carbide interface and grows. The resulting microstructure is that of coarse martensite and ferrite islands as shown in Fig. 7.2(b). The final microstructure inherits the large prior ferrite grain size resulting from the homogenization treatment at 1200°C for 24 hours, and thus tends to be coarser than the AIQ microstructure formed via re-austenisation treatment before entering into the two-phase region. In the MIQ route the starting structure prior to intercritical annealing is an almost fully martensitic microstructure formed by water quenching from austenisation. Then the annealing in the two-phase field region results in the nucleation of austenite along the lath boundaries of prior martensite. After water quenching, the final microstructure is that of a more or less homogeneous distribution of fine fibrous martensite in a ferrite matrix, as shown in Fig. 7.2 (c).

Fig. 3 gives the SEM micrographs for all heat treatment conditions. For each heat treatment route, not only the martensitic fraction but also the size of martensitic islands increases with increasing intercritical annealing temperature due to the growth of austenite grains during the intercritical annealing. In addition, no evident retained austenite or precipitates can be observed in SEM micrographs. XRD measurements were performed for AIQ, FIQ and MIQ-DP steels with lowest and highest martensite volume fraction. XRD results also show that there are no detectable fractions of retained austenite and precipitates.

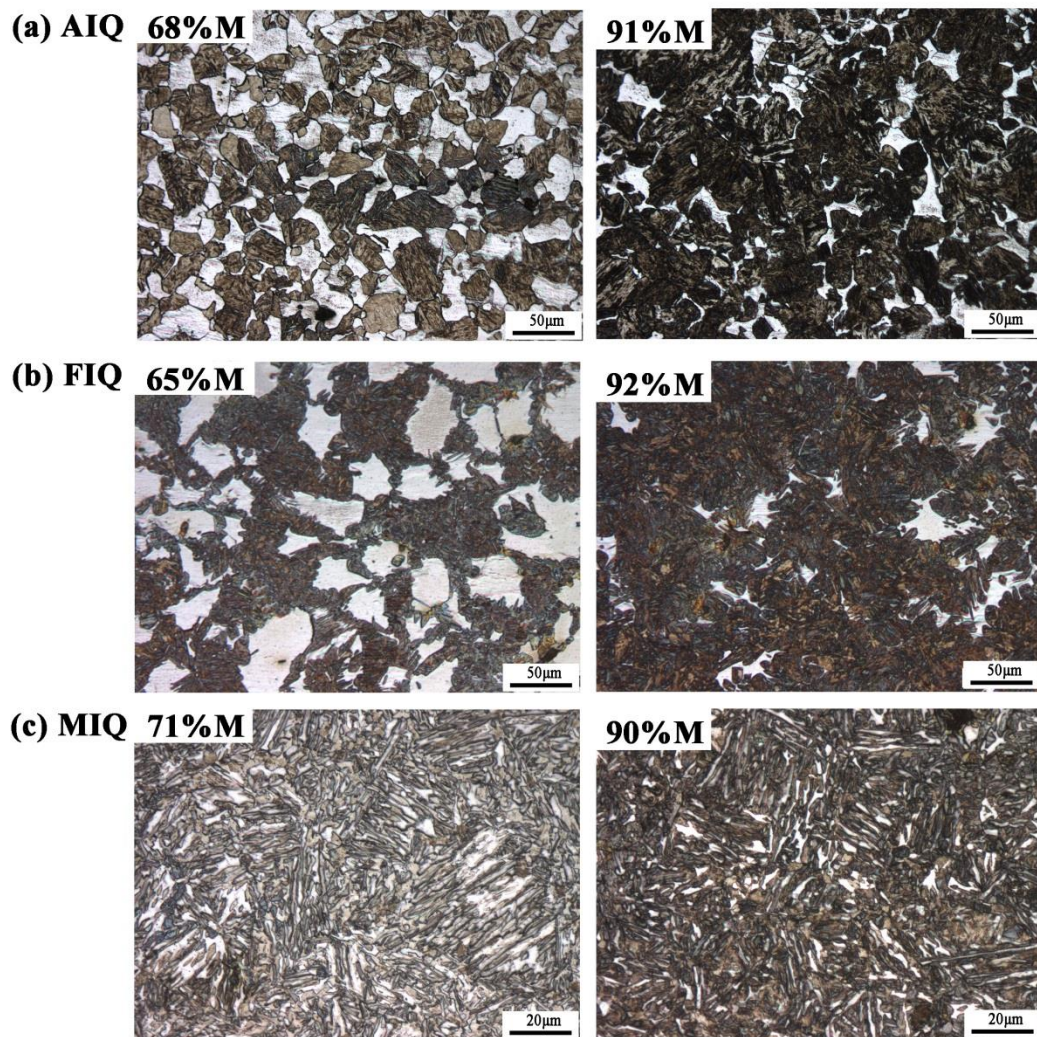


Fig. 7.2 Optical micrographs of dual phase microstructures: (a) AIQ-DP steels with 68%M and 91%M, (b) FIQ-DP steels with 65%M and 92%M, (c) MIQ-DP steels with 71%M and 90%M (Note: a higher magnification for the image of Fig. 7.2c in order to show clearly the microstructural feature).

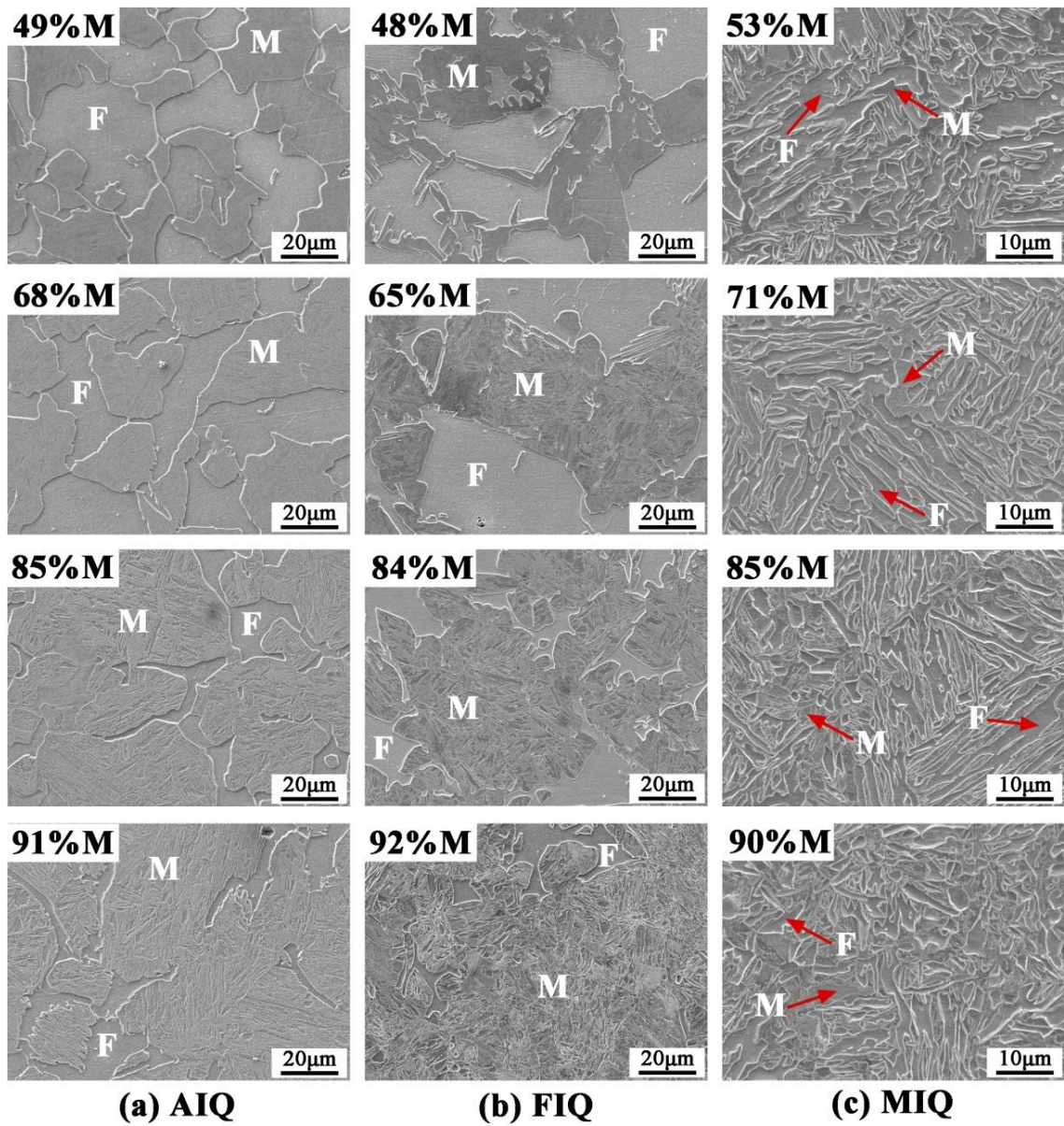


Fig. 7.3 SEM images of all samples with different morphologies: (a) AIQ-DP steels, (b) FIQ-DP steels, (c) MIQ-DP steels (Note: a higher magnification for the images of MIQ-DP steels).

7.3.2 Mechanical properties and hardness

Figure 7.4 shows the tensile strength and uniform elongation (i.e. the strain at UTS) as a function of martensite fraction for the DP steels of the AIQ, FIQ and MIQ routes. The tensile strength and uniform elongation of dual phase steel strongly depend on the martensitic volume fraction. The size and morphology of martensitic islands also plays a significant role on the mechanical behaviour. At the same martensite fraction, the coarse dual phase microstructure (FIQ) has the highest ultimate tensile strength (UTS) and yield strength (YS) but the lowest uniform elongation. The AIQ route yielding a fine granular martensite has a relatively lower UTS and YS at low martensite fraction levels but higher UTS and YS at high martensite fraction levels than the MIQ grades with fine fibrous martensite, as shown in Fig. 7.4a, while the MIQ grades have the largest uniform elongation at the same martensite fraction (Fig. 7.4b). Fig. 7.5 shows the bulk hardnesses (Fig. 7.5a) for the AIQ, FIQ and MIQ grades as well as the hardness of the isolated martensite (Fig. 7.5b) at high martensite fraction levels. As can be seen in Fig. 7.5a, the FIQ grades have the highest bulk hardness, while the AIQ and MIQ grades have the similar bulk hardness but lower than FIQ grades given a same martensite fraction. It can also be noted (see Fig. 7.5b) that the isolated martensite islands in AIQ and FIQ have the same hardness levels, which are to be expected as the martensite fractions, and hence the carbon concentrations in the martensite, are the same. As expected, the hardness of the isolated martensite in DP steel decreases with increasing martensite fraction due to the reduction of carbon concentration. Given the same martensite fractions and martensitic hardness, the difference in mechanical properties of AIQ and FIQ is attributed to the different morphology of ferrite-martensite mixture. As shown in Fig. 7.2 and Fig. 7.3, in the AIQ condition the ferrite surrounds the martensitic islands, while the ferrite in FIQ steels is embedded in the martensitic islands. For the MIQ grades, due to the fine distribution of the martensite, the micro-hardness of isolated martensite could not be determined.

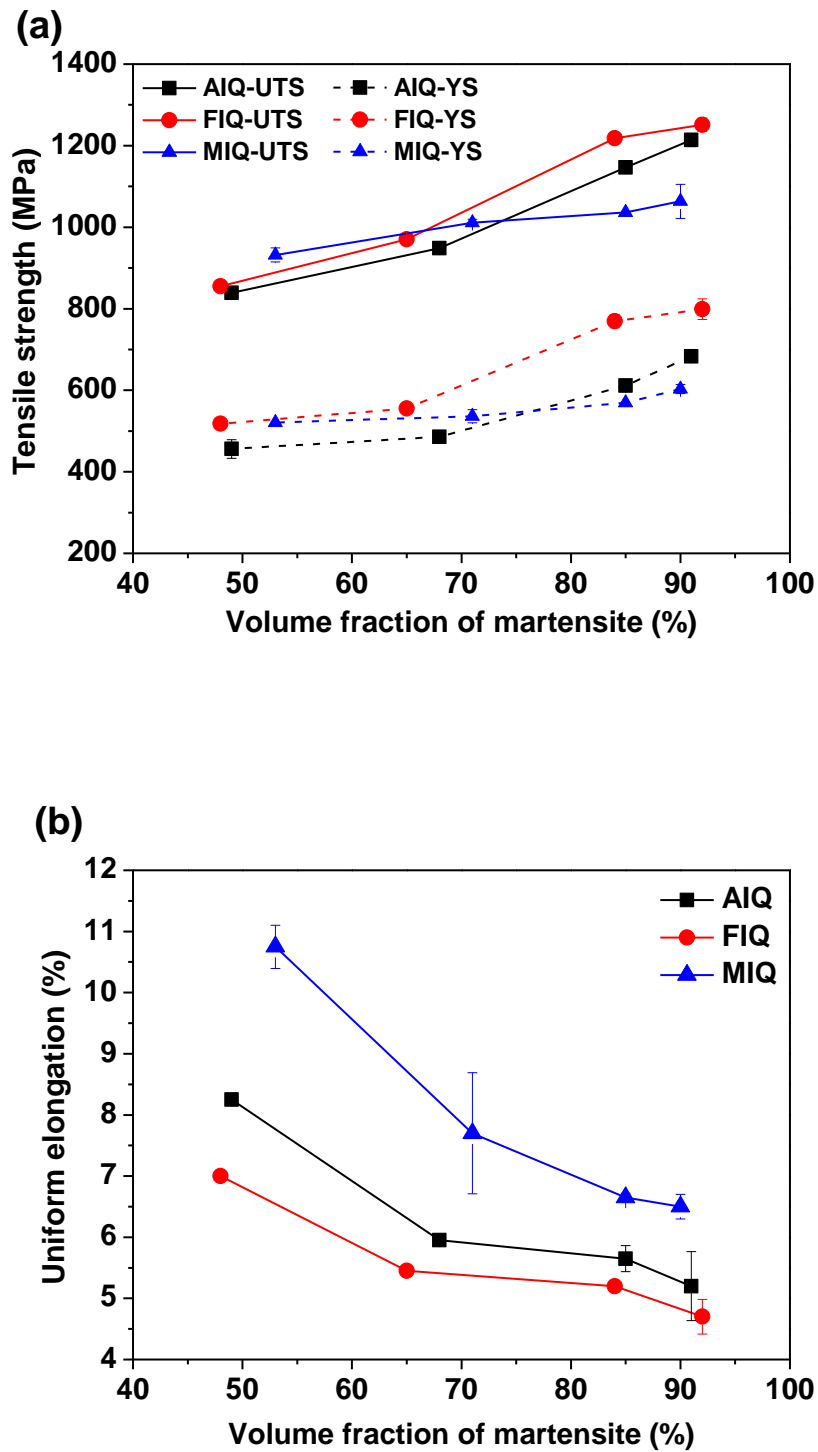


Fig. 7.4 Ultimate tensile strength, yield strength and uniform elongation of AIQ, FIQ and MIQ-DP steels as a function of martensite fraction.

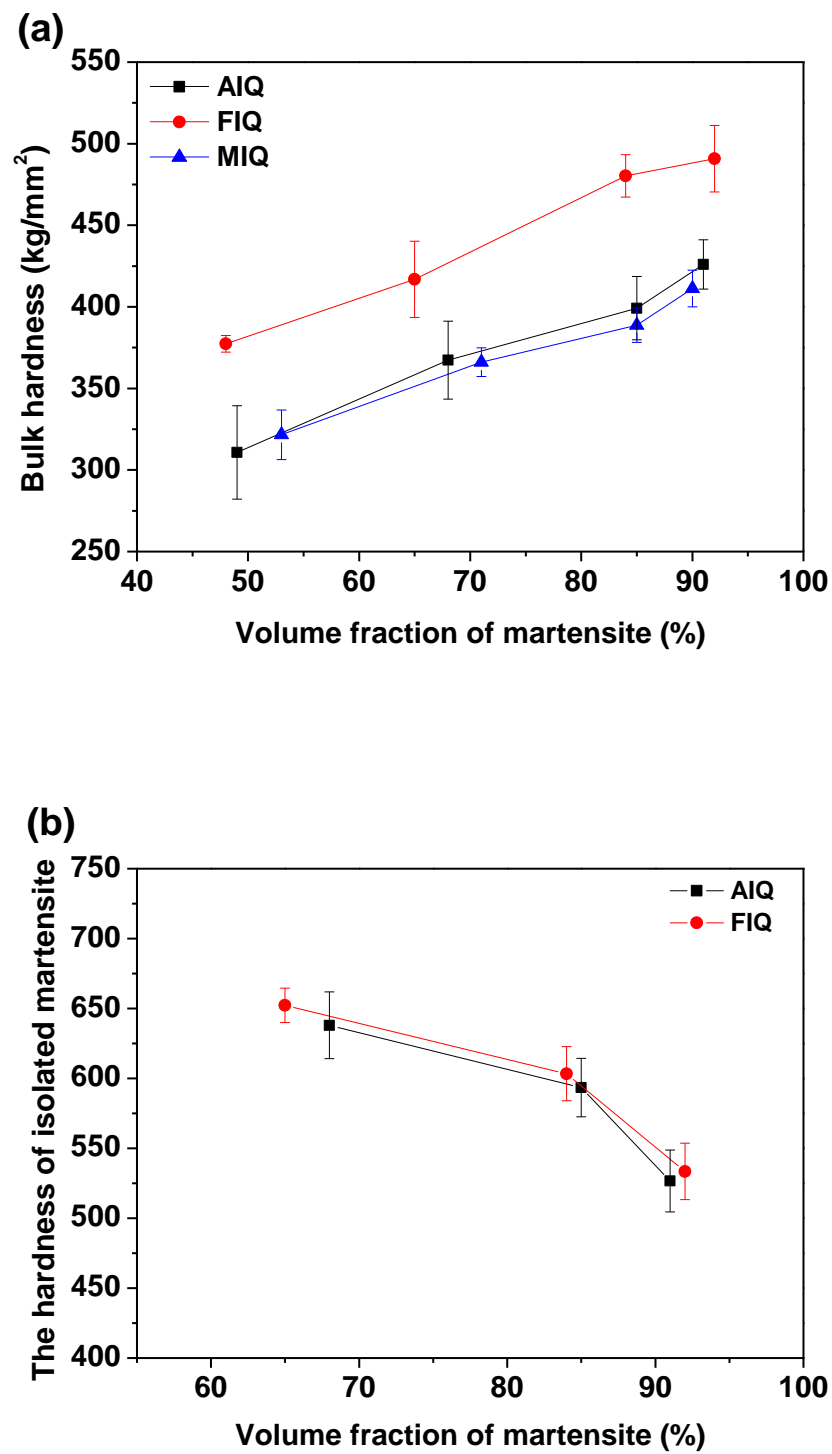
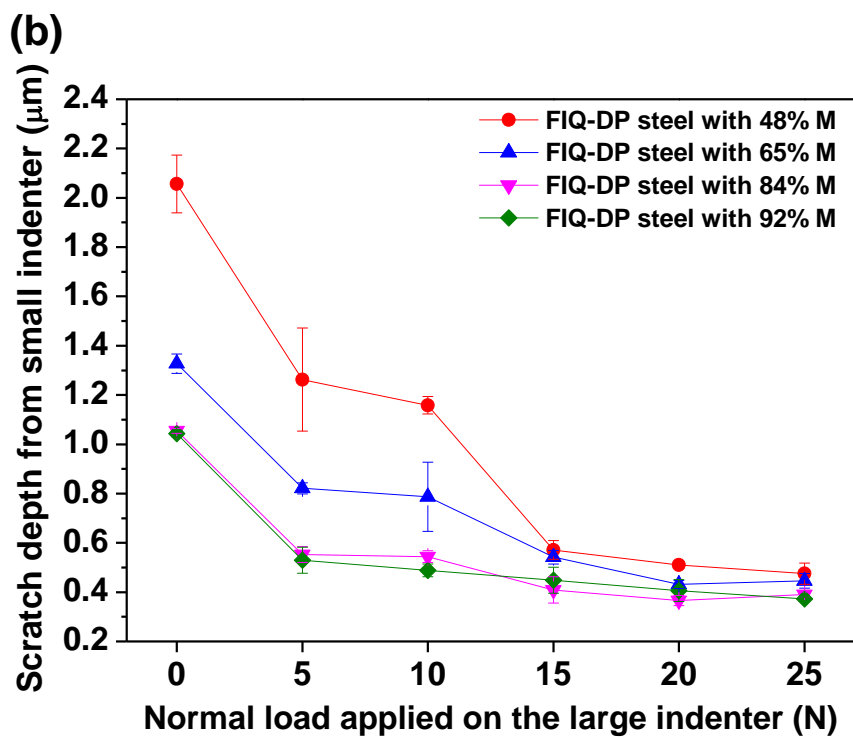
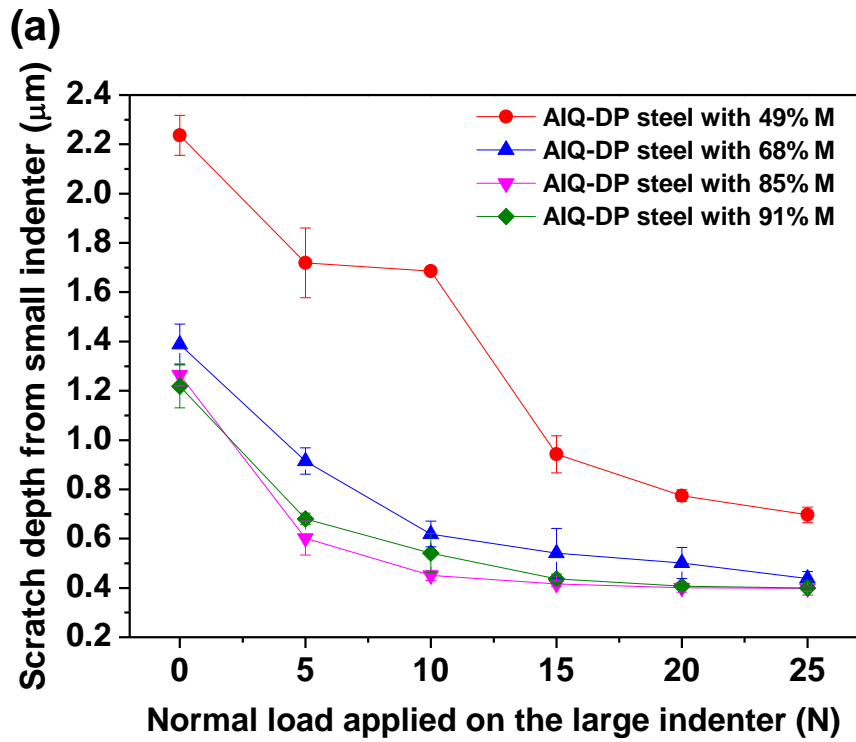


Fig. 7.5 The bulk hardness (a) and the hardness of isolated martensite (b) as a function of martensite fraction for AIQ and FIQ-DP steels.

7.3.3 MPDI scratch test

Fig. 7.6 shows the averaged depth of the scratch produced by the small indenter as a function of the pre-load applied on the large indenter for various DP steels (AIQ, FIQ and MIQ). The scratch depth at 0N load is the depth of a scratch produced by the small indenter on the surface of steels in the initial polished state, as described in Chapter 4. It can be seen that the scratch depth as a function of the applied load during pre-scratching on the blunt indenter follow the same trend for the AIQ, FIQ and MIQ grades, i.e. the scratch depth decreases with increasing pre-scratching load. The decrease is relatively sharp in the low load region, while upon further increase of the pre-load, the decrease of the scratch depth by small indenter becomes marginal. It is worth noting that for all DP steels the evolutions of the scratch depths versus pre-load do not show a characteristic shape as reported in Chapter 4 involving a wider range of steel grades, i.e. scratch depth first decreases due to sub surface strain hardening and then increases due to local damage/material abrasive removal with the pre-load increases. The transition load depends on the strain hardening capability of the material. No transition load can be found in all DP microstructures suggesting that the DP microstructures possess good hardenability and resistance to scratch and that the transition load is beyond the maximum load which can be imposed with the current automated scratching set-up. The drop in scratch depth with increasing martensite fraction is slightly different for the three morphology families which may be attributed to differences in their strain hardening behaviour.



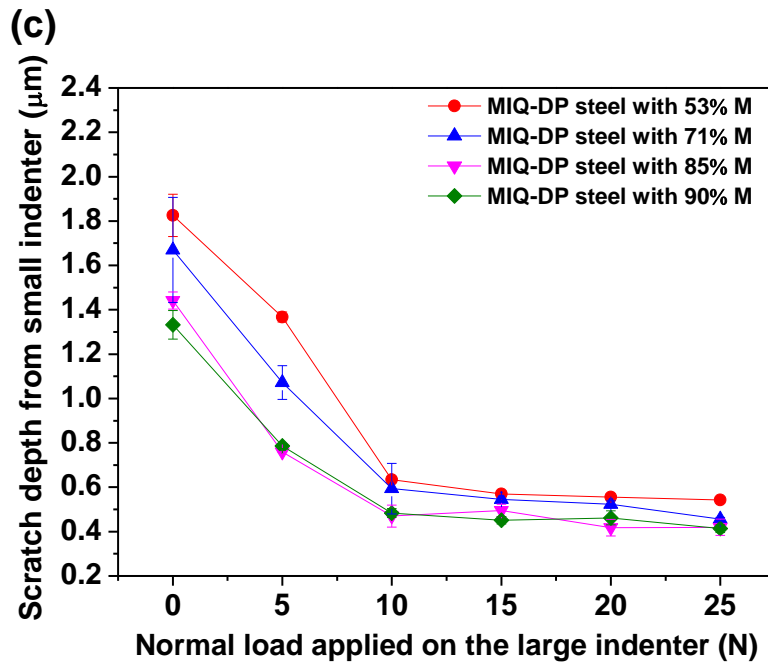


Fig. 7.6 The scratch depth produced on (a) AIQ-DP steels, (b) FIQ-DP steels and (c) MIQ-DP steels by the small indenter with a single pass as a function of the normal load applied on the large indenter during pre-scratching.

7.3.4 ASTM G65 tests

The average weight losses of the same samples in the ASTM G65 wear tests are plotted in Fig. 7.7 as a function of the martensitic volume fraction. There are noticeable differences in weight losses amongst the AIQ, FIQ and MIQ grades. The MIQ grade with fine fibrous martensite suffers from maximum wear loss at a fixed martensite fraction, which is much larger than that of either the AIQ or FIQ grades. The FIQ grades show the lowest weight loss. It seems that for each type (AIQ, FIQ or MIQ) there is a critical martensitic volume fraction beyond which a further increase in martensite fraction does not result in a further increase in abrasion resistance. The drop in weight loss with increasing martensite fraction is smallest for the MIQ grades, which is consistent well with the results shown in Fig. 7.6.

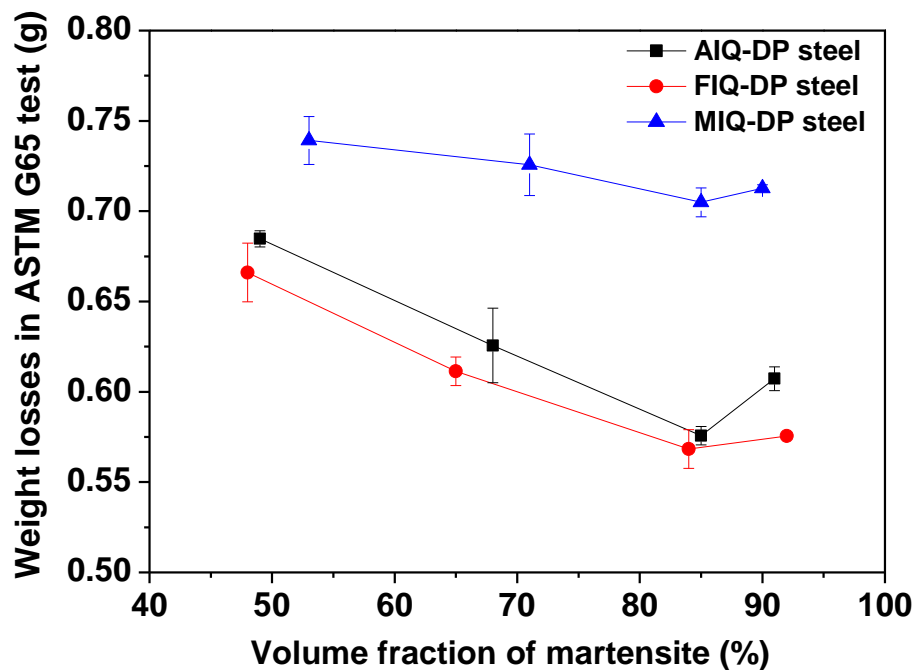


Fig. 7.7 The weight losses of all DP steels subjected to the ASTM G65 test as a function of the martensite volume fraction.

7.4 Discussions

7.4.1 Effect of ferrite-martensite morphology

In general, there are three main factors which affect the mechanical properties (including the wear resistance) of DP steels [3,26]: 1) the volume fraction of martensite, 2) the morphology, 3) the properties of the ferrite and martensite phases. The effect of martensite fraction on abrasion resistance in DP steel has been investigated in Chapter 6. As for the property of the ferrite and martensite, Kim [3] reported that for the same martensite fraction there is no significant change in mechanical behaviour of the isolated martensite and isolated ferrite with morphology. This is due to the fact that the carbon concentration/distribution in the isolated martensite and the isolated ferrite islands is a function of the martensite fraction only. This conclusion in the literature is supported by the results in Fig. 7.5b which shows nearly same hardness of isolated

martensite for the AIQ and FIQ grades. Therefore, at a fixed martensite fraction, the different responses of the DP steels on the scratch and abrasion resistance are solely attributable to the different ferrite-martensite morphologies (and the applied local loads).

Fig. 7.8 shows the scratch depths produced by small indenter as a function of the martensite fractions for pre-scratches made at a low pre-load of 5N (Fig. 7.8a) and at a high pre-load of 25N (Fig. 7.8b), respectively. As seen in Fig. 7.8a, at the low load of 5N the FIQ grades with coarse granular martensite yield the lowest scratch depths (i.e. the best scratch resistance), which is consistent with its largest yield strength, tensile strength and hardness, while the MIQ grades with their fine fibrous martensite display the largest scratch depths, i.e. the worst scratch behaviour. The order of scratch resistance is in good agreement with their corresponding failure mechanisms. As seen in Fig. 7.9 (a1, b1 and c1), the MIQ grades present the largest scratch width and the failure mechanism is that of ploughing in combination with debris formation. The FIQ grades show the smallest scratch width and the scratch is relatively smooth, showing only ploughing. As reported in [4, 5, 27], the ferrite-martensite morphology in DP steels influences the load transfer or stress/strain partitioning between two phases, and hence affects the tensile strength. It certainly influences the abrasion/scratch behaviour as well. According to Mazinani's analysis [5], the granular martensite (corresponding to the AIQ and FIQ-DP steels in present chapter) bearing the majority of load, is harder to deform plastically than the fine fibrous martensite DP steels (MIQ grades). Furthermore, taking into account that upon the pre-load the plastic deformation initiates and develops maximally in the soft ferrite phase but is constrained by the adjacent martensite, the rigid response of the martensite will in turn cause large misfit strains between ferrite and martensite and hence result in a build-up of large stress concentration. This will further strengthen the ferrite and the ferrite/martensite interface in granular martensite DP steel. As a result, combining these effects, the granular martensite DP steels (AIQ and FIQ grades) present a lower scratch depth than that of MIQ-DP steels. In addition, the different morphologies will generate the different spacing between the ferrite and martensite, and hence influences the dislocation density and the stress concentration. The degree of effect on stress concentration is stronger in coarse DP microstructure than that in the fine DP microstructures [3]. Therefore, upon pre-scratching the coarse DP microstructure (FIQ grades) can be strengthened to a higher degree, hence showing a

better scratch resistance than that of the fine DP microstructure (AIQ grades), which is consistent with Bhowmick's result. The difference in martensite island spacing between AIQ and FIQ grades at the same martensite fraction will become smaller with increasing martensite fraction due to the increase in martensitic islands size, which will weaken the effect of spacing and hence result in a smaller difference in scratch depth for AIQ and FIQ grades at the higher martensite fraction levels, as confirmed in Fig. 7.8a. In contrast to the low pre-load condition, the DP steels of three morphology types under the high pre-load condition have comparable levels of scratch resistance despite of their initial different morphologies, especially at the high martensite fraction levels, as seen in Fig. 7.8b. This may be attributed to the fact that under the high pre-load condition, the subsurface microstructures after a large amount of plastic deformation are all reshaped to a comparable "band or laminar" morphology, as shown clearly in Chapter 4. Consequently, they show similar performance on scratch resistance, as also shown in Fig. 7.9 (a2, b2 and c2) with the same failure mechanism, i.e. pure ploughing. In addition, it should be noted that the worn surfaces of the samples subjected to ASTM G65 test look very similar and do not visualize any evident difference in behaviour.

The results discussed above clearly point out that the effect of morphology on the scratch resistance is dependent on the scratching/abrasion conditions. For low local load conditions, the ferrite-martensite morphology plays an important role in determining the scratch resistance. While under the high pre-load condition, the morphology has little influence on scratch resistance.

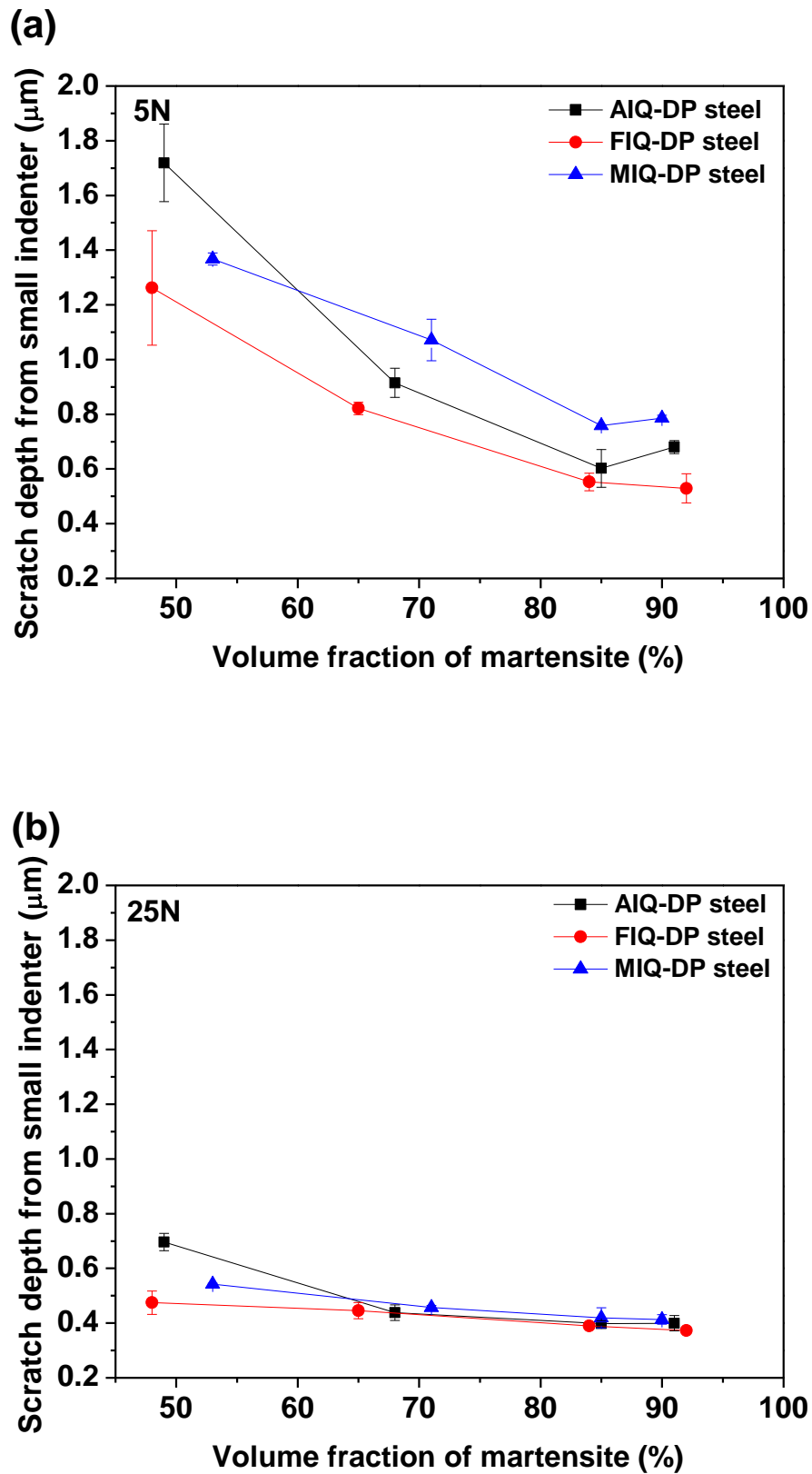


Fig. 7.8 Comparison of the scratch depth amongst AIQ, FIQ and MIQ-DP steels as a function of the martensite fraction under (a) low load condition of 5N and (b) high load condition of 25N.

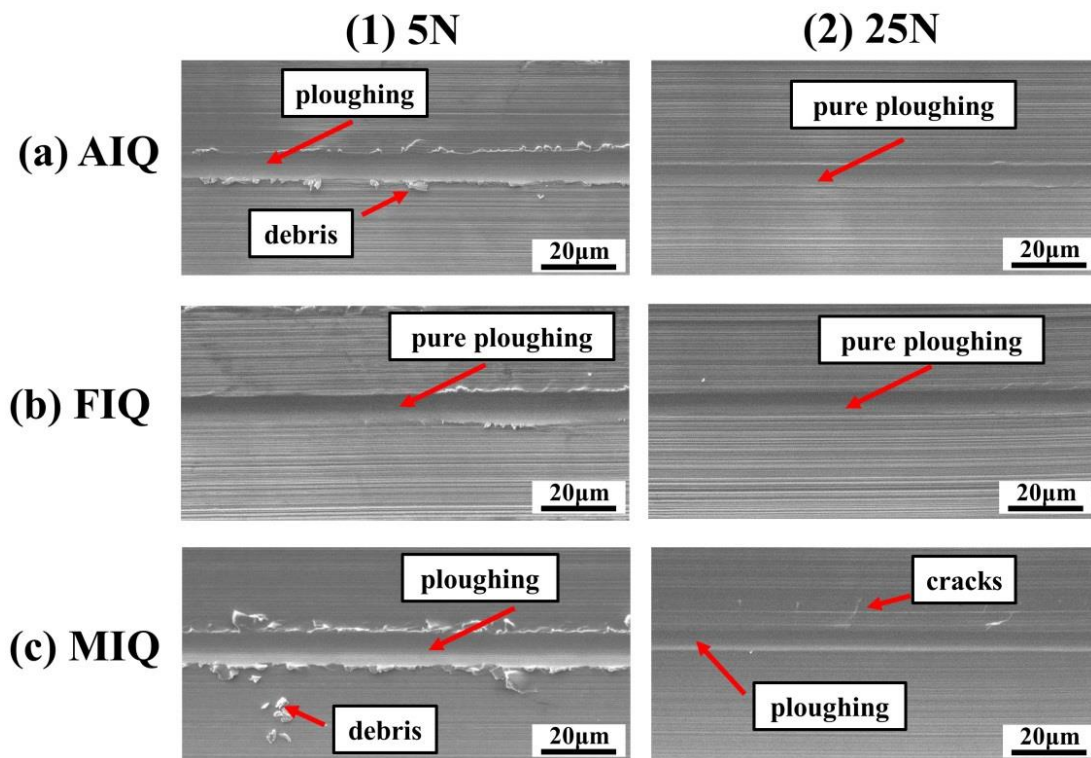


Fig. 7.9 Scratch tracks of AIQ, FIQ and MIQ-DP steels at fixed martensite fraction of $\sim 85\%M$ subjected to MPDI scratch methodology: single pass scratching with small indenter at 0.2 N, and 10 passes pre-scratching with large indenter at low load of 5N and high load of 25N. Note: the scratch tracks presented are grooves produced by the small indenter, while the entire field of view is within the central zone of the big pre-scratches by the large indenter, as described in Chapter 4.

7.4.2 The relation of tensile strain hardening to abrasion resistance

It is well-known that the strain hardening capability of materials plays a very important role in determining the abrasion resistance. In order to quantitatively interpret the effect of strain hardening on the scratch behaviour under different load conditions, a two-stage tensile strain hardening model, which has been introduced in Chapter 6, was applied to correlate the scratch resistance with tensile strain hardening at different loads. In line with this model, in this chapter, the scratch resistance, i.e. the reciprocal of the scratch

depth, is related to the strength coefficient K in the Hollomon equation, i.e. $\sigma = K\varepsilon^n$, where σ and ε are the true stress and strain, and n and K are strain hardening exponent and strength coefficient, respectively [28]. The value of K is derived from the intercept (i.e. the stress where $\varepsilon = 1$ or $\ln\varepsilon = 0$) by linear fitting the plot of $\ln\sigma$ v.s. $\ln\varepsilon$.

Fig. 7.10 gives the variation of scratch resistance and the corresponding strength coefficient K as functions of martensite fraction for the DP steels with different morphology at different load levels. As can be seen, the change in strength coefficient K with increasing martensite fraction matches well with change in scratch resistance for all DP steels. Fig. 7.11 shows the correlation of scratch resistance and the strength coefficient K . It shows nearly linear correlation between scratch resistance and strength coefficient K under the low load and high load condition, respectively. As described in Hollomon equation [28], the strength coefficient K is equal to the stress where the true strain is equal to 1. It represents the strength of materials to resist the plastic deformation. Therefore, it is not surprising that the higher strength coefficient of a material imparts a higher scratch resistance. The results suggest that the strength coefficient K may be considered as a parameter to rank the scratch resistance of DP steel depending on the work condition. Moreover, it seems that the dependence of the scratch resistance on the strength coefficient under the high condition is stronger than that under the low load condition.

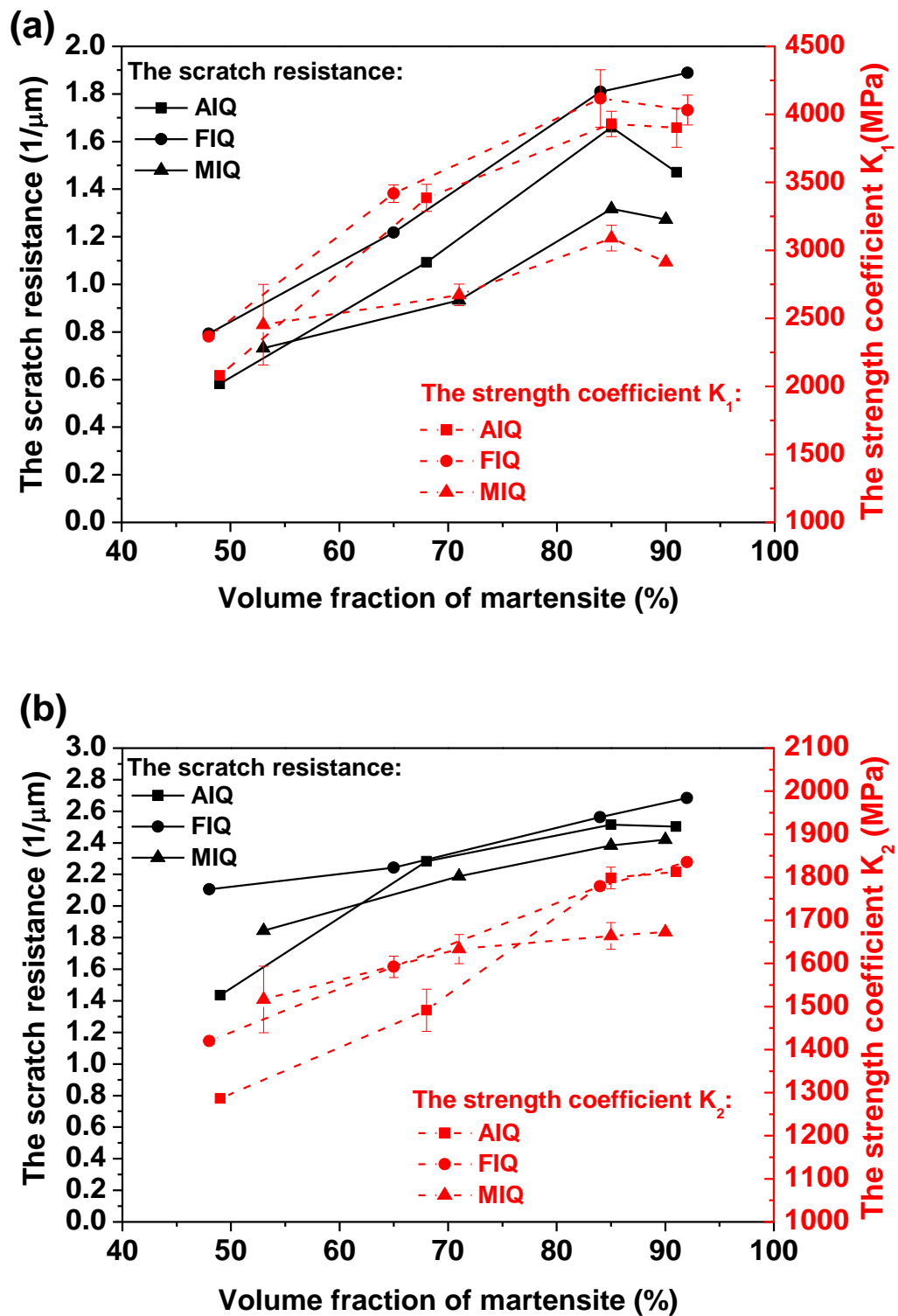


Fig. 7.10 The variation of scratch resistance with the corresponding strength coefficient K at low load of 5N (a) and high load of 25N (b) as functions of martensite volume fraction.

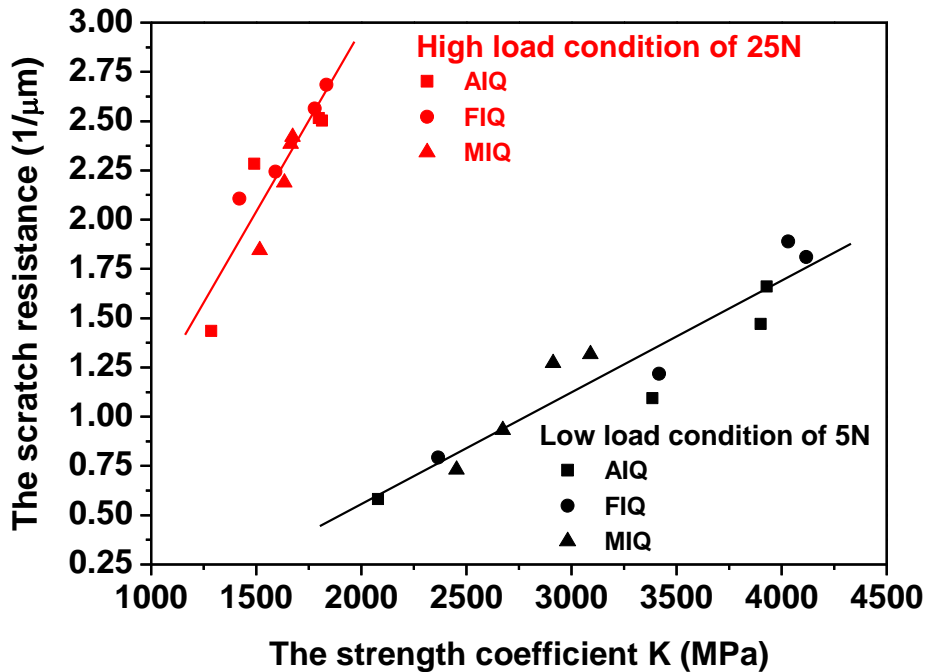


Fig. 7.11 The correlation of the scratch resistance and the strength coefficient K .

7.4.3 Relating the scratch and abrasion resistance to the initial hardness

Given the current industrial target to design low-hardness, high-abrasion-resistant steels for demanding industrial applications as proposed in Chapter 2, we explore the relation between the hardness of the undeformed materials and the scratch/abrasion resistance for AIQ, FIQ and MIQ grades. To this aim the data in Fig. 7.8 are re-plotted using the initial hardness as variable, as shown in Fig. 7.12. To more clearly mark the effect of ferrite-martensite morphology on scratch and abrasion resistance as a function of the initial hardness, in Fig. 7.12 two terms are defined: one is “scratch depth gap” which refers to the difference in scratch depth under the same initial hardness condition, and the other is “hardness gap” which corresponds to the difference in the initial hardness under the same scratch depth condition. Accordingly, at a low load of 5N referring to a mild condition, as shown in Fig. 7.12a, a big “hardness gap” and “scratch depth gap”

exist between the fine granular martensite AIQ grades and the coarse granular martensite FIQ grades. It implies that the AIQ-DP steels with much lower hardness can have an equivalent scratch resistance as the harder FIQ-DP steels. Alternatively, for the same initial hardness the AIQ-DP steel possesses lower scratch depth than the FIQ-DP steels. For the fine granular martensite AIQ-DP steel and fine fibrous martensite MIQ-DP steel, there is a marginal “hardness gap” between both but a somewhat big “scratch depth gap” which suggests that the AIQ-DP grades give a better performance against scratching than the MIQ-DP grades. The ASTM G65 test representing mild local contact condition shows the similar results, as shown in Fig. 7.13.

However, under the high load condition representing a more aggressive work condition, as shown in Fig. 7.12b, the “scratch depth gap” becomes marginal but the “hardness gap” is still big between AIQ and FIQ-DP steels, in particular at the high hardness level, which means that a much lower hardness AIQ-DP steel can perform a comparable level of scratch resistance to the harder FIQ-DP steel. But for AIQ and MIQ-DP steel, the curves nearly overlap and the “scratch depth gap” and “hardness gap” are almost absent suggesting that the effect of morphology on the relation between scratch resistance and hardness is very weak.

On the basis of the comparative analysis on the correlation of scratch resistance and the initial hardness amongst the DP steels with different morphology types, it can be concluded that altering the morphology of microstructure by tailoring the heat treatment is an attractive option to obtain low hardness materials without sacrificing the scratch/abrasion resistance. As can also be seen, the hardness at relatively high level can vary widely at a given comparable level of scratch resistance. Assuming such a dependence to hold for other DP steel compositions as well, it suggests that at low load condition, the AIQ-DP steel is a good alternative to be used as abrasion resistant steel in industrial application. While for the high load condition, the AIQ and MIQ grades are the best option. The results further suggest that the design of abrasion resistant steels should not be oriented towards the initial hardness only, but also to the microstructural features most appropriate for the steady state working conditions.

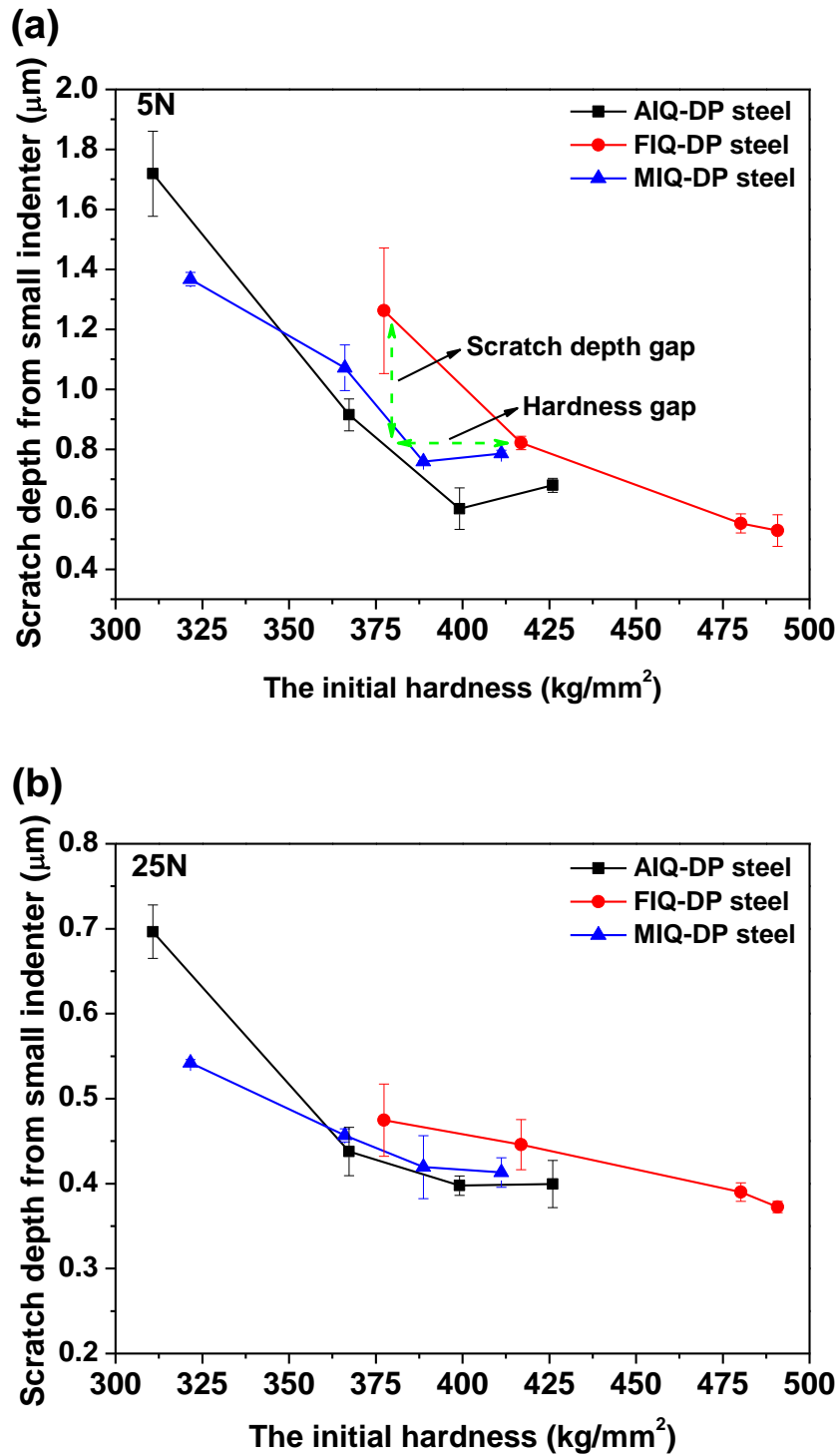


Fig. 7.12 Comparison of the scratch depths amongst AIQ, FIQ and MIQ-DP steels as a function of the initial hardness under low load condition of 5N (a) and high load condition of 25N (b).

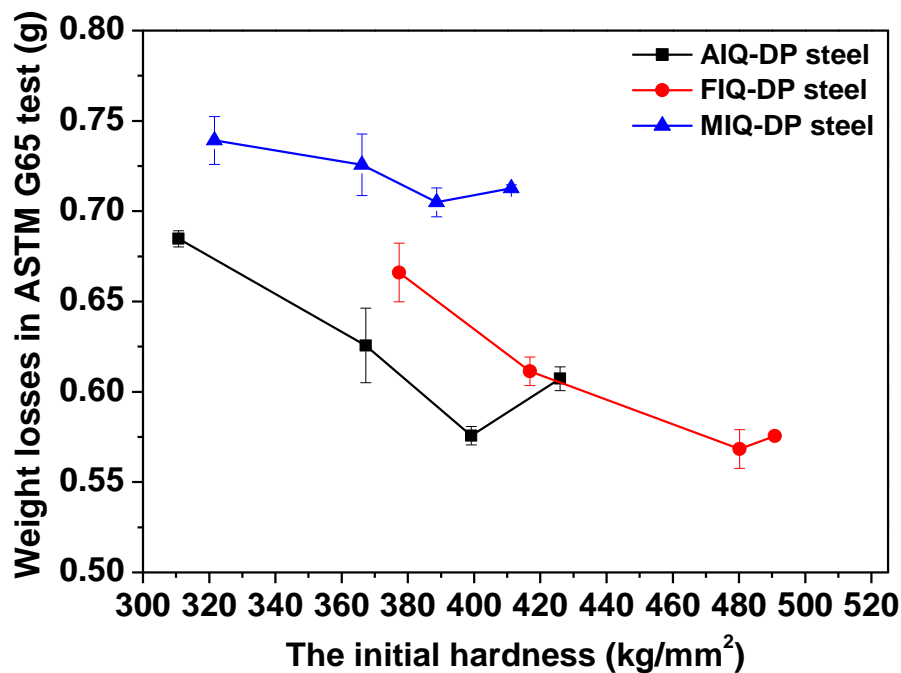


Fig. 7.13 Comparison of weight losses amongst AIQ, FIQ and MIQ-DP steels as a function of the initial hardness.

7.4.4 Correlation of scratch test against the ASTM G65 abrasion test

Finally, in order to benchmark the results of MPDI scratch test, the standard ASTM G65 abrasion test was performed on same steels examined to compare the abrasion resistance with scratch resistance. Fig. 7.14 gives the correlation of ASTM G65 weight loss and the MPDI scratch depth under the low load of 5N. As seen, for all DP steels the ASTM G65 test weight losses are in good agreement with the scratch depths at the low load of 5N irrespective of the martensite morphology, suggesting that the low pre-load MPDI scratch test can be used as a fast screening method for the ASTM G65 experiments. A similar conclusion was drawn elsewhere too in Chapter 6.

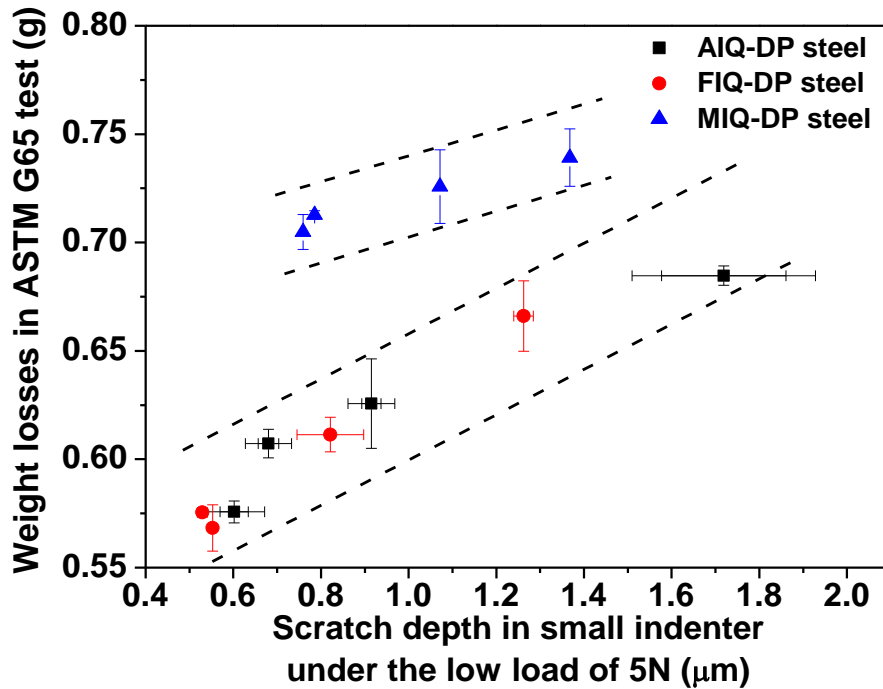


Fig. 7.14 The correlation of the weight losses and scratch depth under the low load condition of 5N.

7.5 Conclusions

This chapter presents an experimental investigation on the scratch and abrasion behaviour of a fixed composition low alloyed steel heat treated to ferrite-martensite DP microstructures with different morphologies. It shows that the effect of the ferrite-martensite morphology on the scratch and abrasion resistance depends on the working conditions. At low contact loads the FIQ grades having relatively coarse granular martensite islands show the best scratch and abrasion resistance, while the MIQ grades with a homogeneous fine fibrous martensite display the worst scratch and abrasion resistance for a given martensite fraction. The scratch resistance of the AIQ grades with fine granular martensite islands is at an intermediate level. However, under high load conditions, all DP morphologies show comparable levels of scratch resistance only affected by the martensite fraction. The strength coefficient K in a simple two-stage

tensile strain hardening model corresponds well with that of scratch resistance regardless of the loading conditions.

Altering the morphology of microstructure by tailoring the heat treatment is an attractive option to obtain low hardness materials without sacrificing the scratch/abrasion resistance. DP steels with fine granular martensite islands are the best microstructure for low-hardness abrasion resistant steel for mild abrasion conditions, while in an aggressive work condition the DP steels with fine (granular or fibrous) martensite structures are to be preferred. The results of the MPDI scratch test under mild conditions are in good agreement with those for the ASTM G65 multi-body abrasion test.

References

- [1] Y. Tomota, Effects of morphology and strength of martensite on cyclic deformation-behaviour in dual-phase steels, *Mater. Sci. Technol.* 3 (1987) 415-421.
- [2] E. Ahmad, T. Manzoor, M.M.A. Ziai, N. Hussain, Effect of martensite morphology on tensile deformation of dual-phase steel, *J. Mater. Eng. Perform.* 21 (2012) 382-387.
- [3] N.J. Kim, G. Thomas, Effects of morphology on the mechanical behavior of a dual phase Fe/2Si/0.1C steel, *Metall. Trans. A* 12 12 A (1981) 483-489.
- [4] M. Sarwar, R. Priestner, Influence of ferrite-martensite microstructural morphology on tensile properties of dual-phase steel, *J. Mater. Sci.* 31 (1996) 2091-2095.
- [5] S. Kim, S. Lee, Effects of martensite morphology and volume fraction on quasi-static and dynamic deformation behavior of dualphase steels, *Metall. Mater. Trans. A* 31 (2000) 1753-1760.
- [6] K.J. Kim, C.G. Lee, S. Lee, Effects of martensite morphology on dynamic torsional behavior in dual phase steels, *Scripta Mater.* 38 (1997) 27-32.
- [7] V.B. Dutta, S. Suresh, R.O. Ritchie, Fatigue crack propagation in dual-phase steels: effects of ferritic-martensitic microstructures on crack path morphology, *Metall. Trans. A* 15 A (1984) 1193-1207.

- [8] M.J. Molaei, A. Ekrami, The effect of dynamic strain aging on fatigue properties of dual phase steels with different martensite morphology, *Mater. Sci. Eng., A* 527 (2009) 235-238.
- [9] S.R. Mediratta, V. Ramaswamy, P.R. Rao, Influence of ferrite-martensite microstructural morphology on the low cycle fatigue of a dual-phase steel, *Int. J. Fatigue* 7 (1985) 107-115.
- [10] A. Bag, K.K. Ray, E.S. Dwarakadasa, Influence of martensite content and morphology on tensile and impact properties of high-martensite dual-phase steels, *Metall. Mater. Trans. A* 30 (1999) 1193-1202.
- [11] Y. Tomita, Effect of morphology of second-phase martensite on tensile properties of Fe-0.1C dual phase steels, *J. Mater. Sci.* 25 (1990) 5179-5184.
- [12] D. Das, P.P. Chattopadhyay, Influence of martensite morphology on the work-hardening behavior of high strength ferrite-martensite dual-phase steel, *J. Mater. Sci.* 44 (2009) 2957-2965.
- [13] J. Zhang, H. Di, Y. Deng, R.D.K. Misra, Effect of martensite morphology and volume fraction on strain hardening and fracture behavior of martensite-ferrite dual phase steel, *Mater. Sci. Eng., A* 627 (2015) 230-240.
- [14] S.F. Wayne, S.L. Rice, K. Minakawa, H. Nowotny, The role of microstructure in the wear of selected steels, *Wear* 85 (1983) 93-106.
- [15] A. Bayram, A. Uguz, Effect of microstructure on the wear behaviour of a dual phase steel, *Mater. Technol. Testing.* 32 (2001) 249-252.
- [16] M. Sawa, D.A. Rigney, Sliding behavior of dual phase steels in vacuum and in air, *Wear* 119 (1987) 369-390.
- [17] O.P. Modi, P. Pandit, D.P. Mondal, B.K. Prasad, A.H. Yegneswaran, A. Chrysanthou, High-stress abrasive wear response of 0.2% carbon dual phase steel: Effects of microstructural features and experimental conditions, *Mater. Sci. Eng., A* 458 (2007) 303-311.
- [18] S. Bhowmick, B.K. Show, Effect of prior heat treatment on wear behaviour of 0.23% carbon dual phase steel, *Can. Metall. Quart.* 53 (2014) 93-99.
- [19] R.K. Khatirkar, P. Yadav, S.G. Sapate, Structural and wear characterization of heat treated En24 steel, *ISIJ Int.* 52 (2012) 1370-1376.
- [20] A. Baburaj, K.B.S.S. Chaudhary, R.K. Khatirkar, S.G. Sapate, Abrasive wear behaviour of heat treated En31 steel, *ISIJ Int.* 53 (2013) 1471-1478.
- [21] K. Singh, R.K. Khatirkar, S.G. Sapate, Microstructure evolution and abrasive wear behavior of D2 steel, *Wear* 328-329 (2015) 206-216.
- [22] H. Fu, Q. Xiao, H. Fu, Heat treatment of multi-element low alloy wear-resistant steel, *Mater. Sci. Eng., A* 396 (2005) 206-212.

- [23] M. Lindroos, K. Valtonen, A. Kemppainen, A. Laukkanen, K. Holmberg, V.T. Kuokkala, Wear behavior and work hardening of high strength steels in high stress abrasion, *Wear* 322-323 (2015) 32-40.
- [24] X. Deng, Z. Wang, Y. Tian, T. Fu, G. Wang, An investigation of mechanical property and three-body impact abrasive wear behavior of a 0.27% C dual phase steel, *Mater. Des.* 49 (2013) 220-225.
- [25] H. Chen, X. Xu, W. Xu, S. van Der Zwaag, Predicting the austenite fraction after intercritical annealing in lean steels as a function of the initial microstructure, *Metall. Mater. Trans. A* 45 (2014) 1675-1679. 45 (2014) 1675-1679.
- [26] X. Xu, W. Xu, F.H. Ederveen, S. van der Zwaag, Design of low hardness abrasion resistant steels, *Wear* 301 (2013) 89-93.
- [27] M. Mazinani, W.J. Poole, Effect of martensite plasticity on the deformation behavior of a low-carbon dual-phase steel, *Metall. Mater. Trans. A* 38 (2007) 328-339.
- [28] J.H. Hollomon, Tensile deformation, *Trans. AIME*, 162 (1945) 268-290.

Chapter 8

The scratch and abrasive wear behaviour of a tempered martensitic construction steel and its dual phase variants

8.1 Introduction

Lowly alloyed martensitic steels are used widely as cost-effective materials for applications requiring a high abrasion resistance because of their high hardness [1-3], which is supposed to lead to a higher abrasion resistance [4, 5]. In order to improve the wear resistance, such steels are generally tempered to modify the balance between the various mechanical properties, and in particular to improve the toughness/ductility [6-8] while keeping a relatively high hardness. The wear behaviour of (tempered) martensitic steels has been studied extensively as a function of many main factors, such as carbon concentration [9, 10], tempering temperature [11-13] and working conditions (such as applied load and sliding speed) [14-16]. The work reported by Xu, *et al.* [9] and Moore [10] showed that the wear resistance of martensitic steels can be improved by increasing the carbon content. However, if the carbon concentration exceeds a critical level, the wear resistance decreases although the hardness increases. The change in behaviour is because the ductility and toughness decrease dramatically and the resulting

microstructure becomes susceptible to crack nucleation and brittle delamination, especially under harsh conditions [17-19]. Studies on the effect of the tempering temperature on wear resistance [13, 20-22] showed that with increasing tempering temperature both the hardness and wear resistance decrease. In contrast, El-Rakayby, *et al.* [11] and Fu, *et al.* [23] showed that for their steels the wear resistance first increases and then drops with the temperature rises and they attributed this dependence to the carbide precipitation during tempering. Finally, many studies reported that the wear rate displays a linear relationship between the abrasion rate and the work conditions in particular applied load and sliding speed [14, 15, 24]. However, Rai, *et al.* [16] reported that the wear rate first increases with applied load or sliding speed up to a transition value beyond which the wear rate decreases as a result of oxidative wear. While the relationship between microstructure, load conditions and abrasion resistance is not yet very clear and unambiguous, the situation becomes even less clear when the abrasion resistance of low alloyed martensitic steels is compared to that of other steel grades, such as ferritic, pearlitic steel and bainitic steels [17, 25, 26] and Hadfield austenitic steels [1, 2]. Most studies showed that the martensitic microstructure displays a better abrasion resistance than ferrite, pearlite and bainite or high Mn austenite. However, systematic investigations on the abrasion resistance of a single steel of a fixed chemical composition yet heat treated to produce different microstructures such as a range of tempered martensitic microstructures as well as ferrite-martensite (DP) microstructures with different martensite volume fractions and morphologies are still lacking. The only work coming close to the objective of the present work is that of Jha *et al.* [27] who reported that the abrasion resistance of a steel in the ferrite-martensite state can be better than that in the martensitic state, but they did not examine the relative abrasive performance for both microstructural variants for a wider range of conditions.

The aim of this chapter is to clarify the response of tempered martensitic microstructures produced by different tempering temperature on scratch and abrasion behaviour for different load conditions, and to compare this to the scratch and abrasion behaviour of the same steel yet produced to distinctly different DP microstructures (as seen in Chapter 6 and 7). The scratch resistance and the corresponding failure mechanism of the tempered martensitic microstructure at the different load conditions were unravelled using the multi-pass dual-indenter (MPDI) scratch methodology. In this

test the work hardened state of the surface layer can be varied by changing the load employed, making it possible to mimic a wide range of abrasion conditions ranging from a mild to harsh condition. Moreover, the strain hardening analysis introduced in Chapter 6, was utilized to correlate the tensile test strain hardening behavior with the scratch resistance under different loading conditions. Finally, the MPDI scratch test at mild conditions was correlated with the standard ASTM G65 test commonly used to screen steel grades for abrasive applications.

8.2 Experimental procedures

A same material as used in Chapter 6 and 7 was selected for this study, which was initially homogenized at 1200°C for 24h in a hydrogen atmosphere followed by air cooling. After homogenization, a quenching and tempering (Q&T) treatment (after austenization at 900 °C for 10 minutes) was performed to produce tempered martensitic (TM) microstructures. The tempering temperatures were 200°C, 300°C, 400°C and 500°C with a fixed time of 1 h. After tempering the material was quenched again in water. The heat treatment cycles are shown in Fig. 8.1. After the heat treatment, the procedures for metallurgical characterisation of samples, micro-hardness measurements and tensile test are same as described in Chapter 6 and 7, respectively. The MPDI scratch test conditions and ASTM G65 abrasion testing procedure are same as shown in Chapter 6 and 7. Finally, scanning electron microscope (SEM) operating at 5 kV was employed to investigate the characteristics of the worn surface.

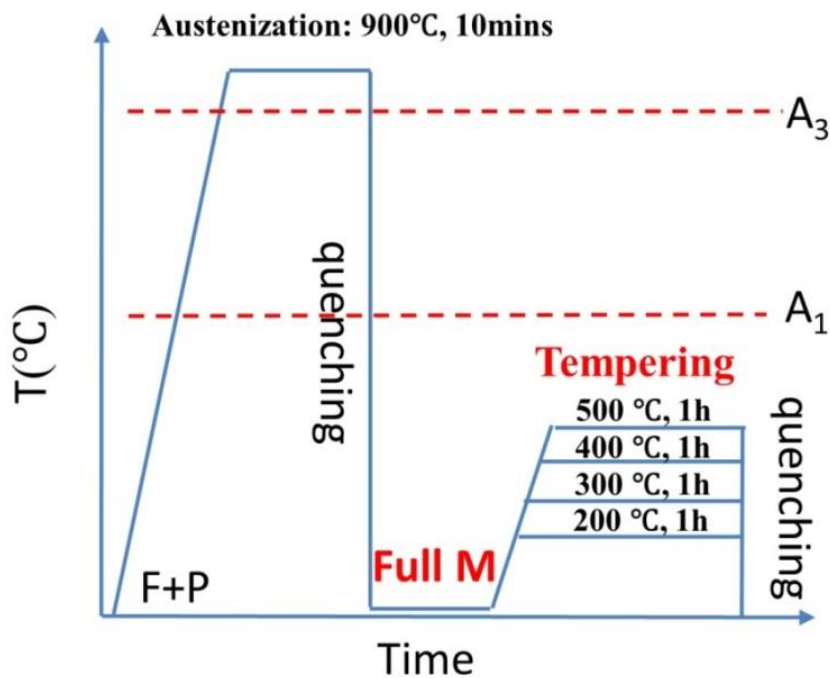


Fig. 8.1 Schematic representation of the various heat treatment procedures.

8.3 Results

8.3.1 Microstructures and mechanical properties

Characteristic microstructures generated by tempering at different temperatures are shown in Fig. 8.2. It can be seen that all samples display a fully lath martensitic microstructure with some carbides but without notable fractions of retained austenite. Among them, there are no visible differences in morphology, except for an increase in carbides precipitate density along the lath boundary with increasing tempering temperature. Fig. 8.3 gives the yield strength (YS), the ultimate tensile strength (UTS), the uniform elongation (UE) and the micro-hardness as a function of the tempering temperature. As expected there are major differences in mechanical properties as a function of the tempering conditions. With increasing tempering temperature, the YS, UTS and hardness decrease as a result of martensite softening. In contrast, the uniform elongation increases due to the combined effects of recovery and softening of the martensite.

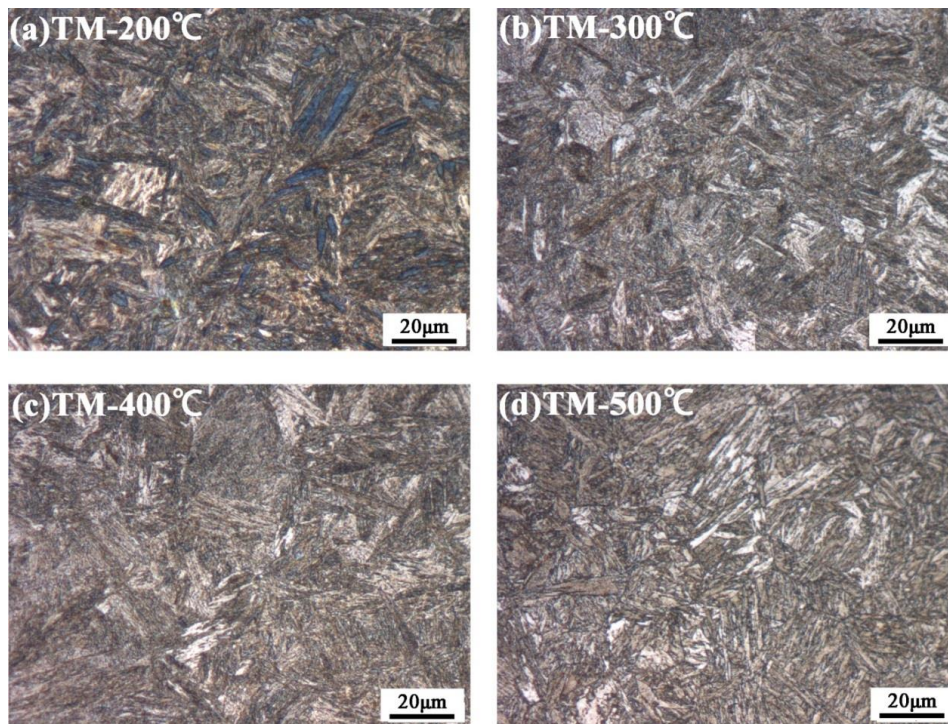


Fig. 8.2 Optical micrographs of tempered martensitic microstructures for various tempering temperatures: (a) 200°C, (b) 300°C, (c) 400°C, (d) 500°C.

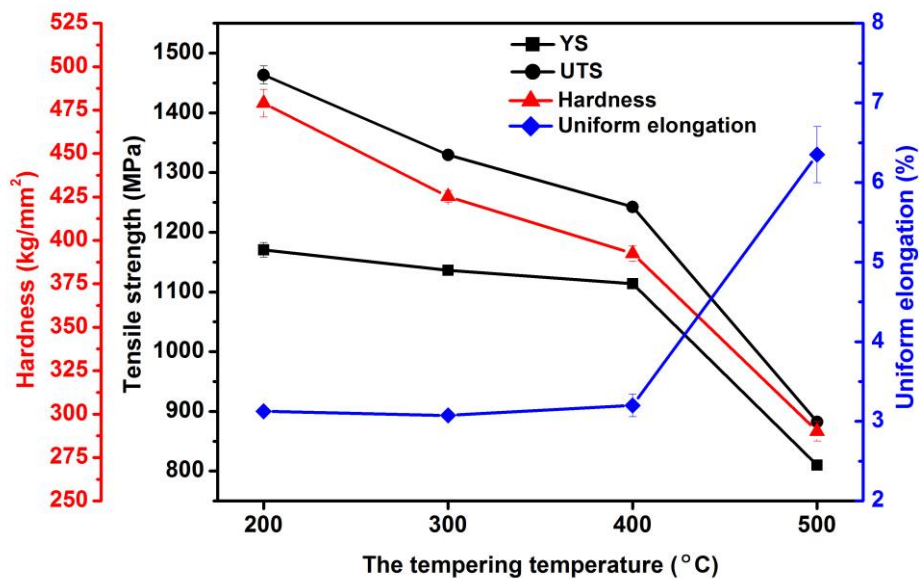


Fig. 8.3 The yield strength, ultimate tensile strength, uniform elongation and Vicker's hardness as a function of the tempering temperature.

8.3.2 MPDI scratch test

In accordance with the MPDI scratch test protocol, the average additional scratch depth due to sliding of the small indenter within the wear track made by the large indenter is plotted in Fig. 8.4 as a function of the normal pre-load applied on the large indenter. The scratch depth plotted at 0N normal load is the depth of a scratch by small indenter on the pristine surface of the steel grade examined (seen in Chapter 4). A low scratch depth implies a high scratch resistance. As described and analyzed extensively in the Chapter 4, a plot of the scratch depth as a function of the normal pre-load has a characteristic “V”-shape, i.e. firstly the depth decreases with normal load on the big indenter due to increased strain hardening of the wear track made during pre-scratching. Beyond a critical (transition) load, the scratch depth increases again with pre-load due to the interaction of the small indenter with pre-existing damage in the wear track leading to material removal. The transition load depends on the strain hardening and strain accumulation capability of a material. In Fig. 8.4, it can be observed that such a transition only takes place for TM-400°C and TM-500°C martensitic steel. For these steels the transition load is around 10N. However, no evident transition loads can be found for TM-200°C and TM-300°C martensitic steel and the scratch depth continuously decreases with increasing pre-load. The result indicates that the TM-200°C and TM-300°C martensitic steels possess a good strain hardening capability and scratch resistance, such that the transition load is beyond the maximum load which can be imposed with the current scratching set-up. The figure clearly shows that the tempering temperature has a significant influence on the scratch resistance of martensitic steels tempered to different temperatures and that this effect depends on the working conditions. Under low load conditions, only small differences in scratch depth versus tempering temperature exist. However, under high load conditions, significant differences in scratch depth exist between the four tempered conditions, i.e. comparable levels of scratch depth are obtained for the TM-200°C and TM-300°C, which are much lower than that of the TM-400°C grade and even more so than that of TM-500°C grade.

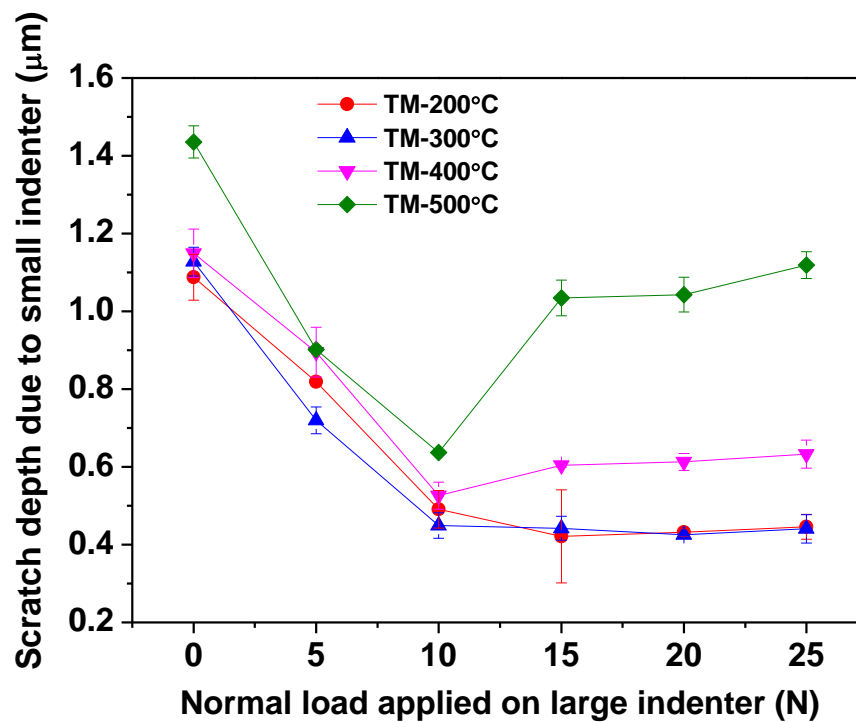


Fig. 8.4 The scratch depth produced by a single pass with the small indenter as a function of the normal load applied on the large indenter during pre-scratching for 4 tempering temperatures.

8.3.3 Scratch morphology and failure mechanisms

The results of the morphological investigations of scratch tracks made by the small indenter on wear tracks produced by the large indenter reflecting the resulting failure mechanisms under different pre-loads are shown in Fig. 8.5. The representative scratch tracks presented in these figures are the grooves produced by the small indenter, while the entire file of view is within the central zone of wear track made by the large indenter, as stated in Chapter 4.

Fig. 8.5a illustrates the damage mechanism of the softest grade, i.e. TM-500 °C. The scratch track for a low load of 5N reveals that the failure mechanism is ploughing with the occasional formation of debris, as shown in Fig. 8.5(a1). As the pre-load increases to 10N (i.e. near the transition load, as shown in Fig. 8.4), cracks start to propagate on the edge of the new scratch and delamination takes place but the width (and hence depth)

of scratch track is still smaller than that under 5N pre-load as a result of the increase in accumulated strain hardening due to pre-scratching (Fig. 8.5(a2)). A further increase in the pre-load on the large indenter to 25N (i.e. within the abrasive damage/materials removal regime) results in severe plastic deformation in the pre-scratched surface, which further leads to the propagation of cracks. Upon subsequent scratching with the small indenter, the cracks connect with each other leading to a significant delamination and detachment of debris (Fig. 8.5(a3)). As a result, the scratch depth is significantly increased. The evolutions of damage with pre-load are in line with the changes of the resulting scratch depths shown in Fig. 8.4.

The TM-400°C grade displays a similar damage evolution with increasing pre-load but a milder damage than that in TM-500°C grade, as shown in Fig. 8.5b. Under the low load of 5N, only mild delamination occurs (Fig. 8.5(b1)). For the 10N pre-load condition, the delamination and the propagation of cracks increases but the width of scratch becomes smaller due to the effect of strain hardening, as shown in Fig. 8.5(b2). As the pre-load further increases and enters into the damage region, the pre-scratched surface experiences severe plastic deformation. Upon scratching with the small indenter, cracks propagate perpendicular to the new scratch and severe delamination was seen (Fig. 8.5(b3)), which indicates that the worn surface promoted serious damage, hence resulting in a higher scratch depth.

The TM-300°C and TM-200°C steel possessing a good combination of strength and ductility show very mild damage compared to the TM-400°C and TM-500°C steels as shown in Fig. 8.5c and Fig. 8.5d, respectively, in particular at high load level. The SEM image for the low load of 5N for TM-300°C demonstrates that the failure mechanism is mainly ploughing, as shown in Fig. 8.5(c1). As the pre-load increase to 10N, some mild delamination can be observed at the edges of the new scratch track (Fig. 8.5(c2)). It is interesting to note that even when the pre-load further increases to 25N, the scratch track remains quite smooth and only small cracks are observed (Fig. 8.5(c3)). The evolution of damage with pre-load is highly consistent with the change in the scratch depth shown in Fig. 8.4. With increasing the load on the large indenter to the maximum load which can be applied in the current set-up, an intact yet more extensively strengthened strain hardening subsurface layer is formed (see Chapter 4). As a result, the scratch damage becomes milder and the resulting scratch depth and width become

smaller. The behaviour of the TM-200 °C grade (Fig. 8.5d) is very similar to that of the TM-300 °C grade. Even at the highest load of 25N, the scratch groove looks smooth and only displays minor crack formation, as shown in Fig. 8.5d (3).

The systematic observation on the set of scratch tracks reveals clearly the dependence of the damage mechanisms of tempered martensitic steel on the loading condition and the microstructure controlled by tempering temperature. The evolution of failure mechanisms is in good agreement with the changes in the corresponding scratch depth values.

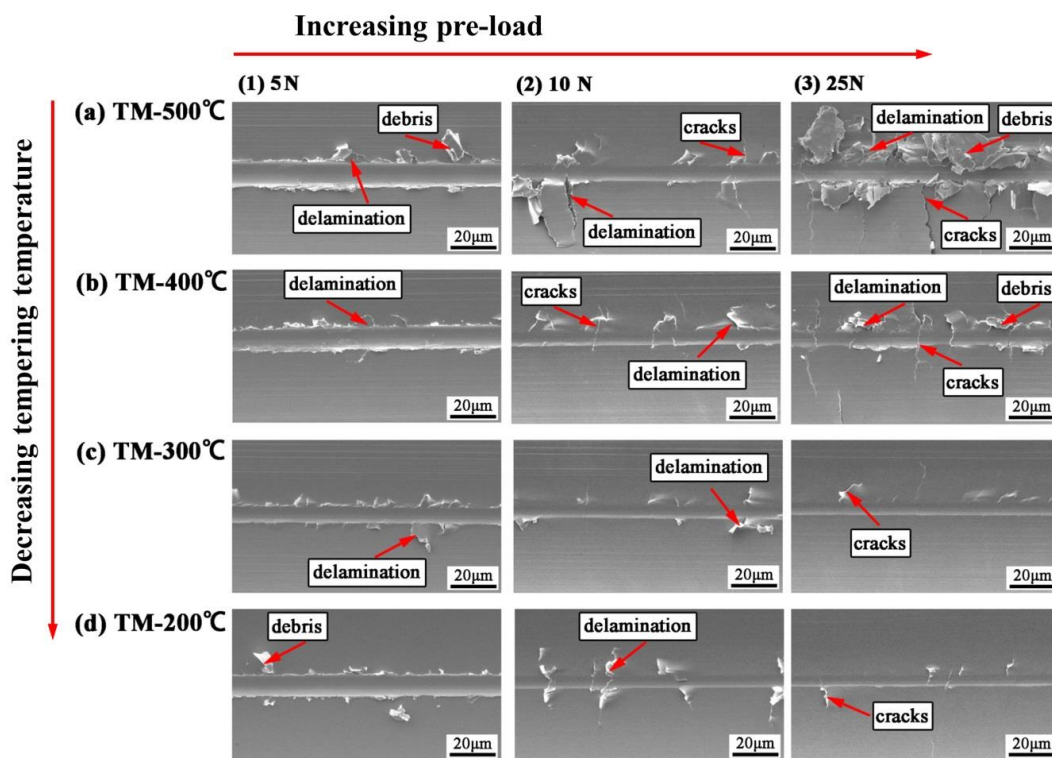


Fig. 8.5 Scratch tracks of all steels subjected to MPDI scratch methodology: single pass scratching with small indenter at 0.2 N, and 10 passes pre-scratching with large indenter at 5N, 10N and 25N load.

8.4 Discussions

8.4.1 The dependence of scratch and abrasion resistance on tempering temperature and loading condition

As stated earlier, the martensitic microstructure in its virgin condition is rather brittle, leading to rapid crack initiation and propagation during an abrasive process hence leading to severe delamination and rapid material removal, in particular under harsh conditions, despite its high hardness [28]. In order to modify the virgin martensitic microstructure, a quenching and tempering (Q&T) treatment is most frequently used in industry as the Q&T treatment is a versatile and cost-effective way to produce desired combinations of ductility or toughness and strength [29-32]. As tempering proceeds, the martensite rejects excess dissolved carbon and carbide precipitation occurs, which alters the mechanical behaviour including the wear resistance. With increasing tempering temperature, the cementite size and inter-particle distance increases and the ferritic matrix becomes progressively softer. The resulting changes are a strong function of the tempering temperature [33, 34]: between 200°C and 350°C, a very fine dispersion of cementite and a slightly supersaturated ferritic matrix is formed, while above 350°C, the ferritic matrix becomes much softer and carbides coarsen and spheroidize. These microstructural changes will have their impact on the scratch and abrasion resistance as well as its working conditions dependence.

Fig. 8.6 shows the scratch depths of the four tempering conditions for a low load of 5N and a high load of 25N as well as the ASTM G65 test weight loss as a function of the initial hardness. In addition, the weight loss and scratch depths of the virgin (un-tempered) full martensite (FM), already presented in Chapter 6, are also plotted. As can be seen, the scratch depths by the MPDI scratch test under the low load of 5N generally increases with the hardness decreases, in line with the consistent increase of tempering temperature. Similarly, the weight loss continuously increase with the decrease of hardness (i.e. the increase of tempering temperature), which is in good agreement with the scratch depths by MPDI scratch test in the low load condition. So, in the ASTM G65 test condition and in the low load regime of the MPDI test, the hardness is a good indicator for abrasion resistance and a higher hardness results in a better scratch/abrasion resistance. In this regime, the hardness and strength of the material play

a dominant role and toughness is less important. However, under the high load of 25N representing an aggressive abrasive condition, the relation between hardness and abrasion resistance is non-monotonous and that a “V” shaped correlation exist. In such working conditions, there is an optimal tempering temperature at which a higher scratch resistance is obtained despite a lower initial hardness. It means that, under high load condition, the scratch and abrasion resistance depends not only on the strength of the ferritic matrix, but also on the combination of the ductility of matrix and the morphology effect (size, distribution and amount) of the second phase (cementite). Under harsh abrasive conditions, for the as-quenched (FM) condition cracks initiate and propagate easily hence deteriorating the abrasion resistance. Upon tempering treatment in the temperature range between 200°C and 350°C, as stated above, the combination of a fine dispersion of cementite and a somewhat supersaturated ferritic matrix imparts a good balance of strength (resisting penetration of abrasives/indenter) and ductility (resisting crack initiation and propagation) of materials [35]. This also explains that in Fig. 8.4 no transition loads are observed for TM-200°C and TM-300°C steels. As a consequence, the TM-200°C and TM-300°C steels show a super performance against scratching/abrasive wear, as also shown in Fig. 8.5 (c3-d3) where the scratch track is quite smooth and only occasionally cracks are found. At a further increase of tempering temperature to 400°C and 500°C, the carbon level in the ferrite drops to the equilibrium values and the ferritic matrix becomes very soft while the carbides coarsen. Hence upon scratching the material deforms extensively and becomes susceptible to the initiation and propagation of cracks along the brittle interconnected carbide, as shown in Fig. 8.5 (a3) and (b3) where big cracks form and severe delamination occurs. Although their uniform elongation values are highest, the TM-400°C and TM-500°C steels show an inferior scratch resistance.

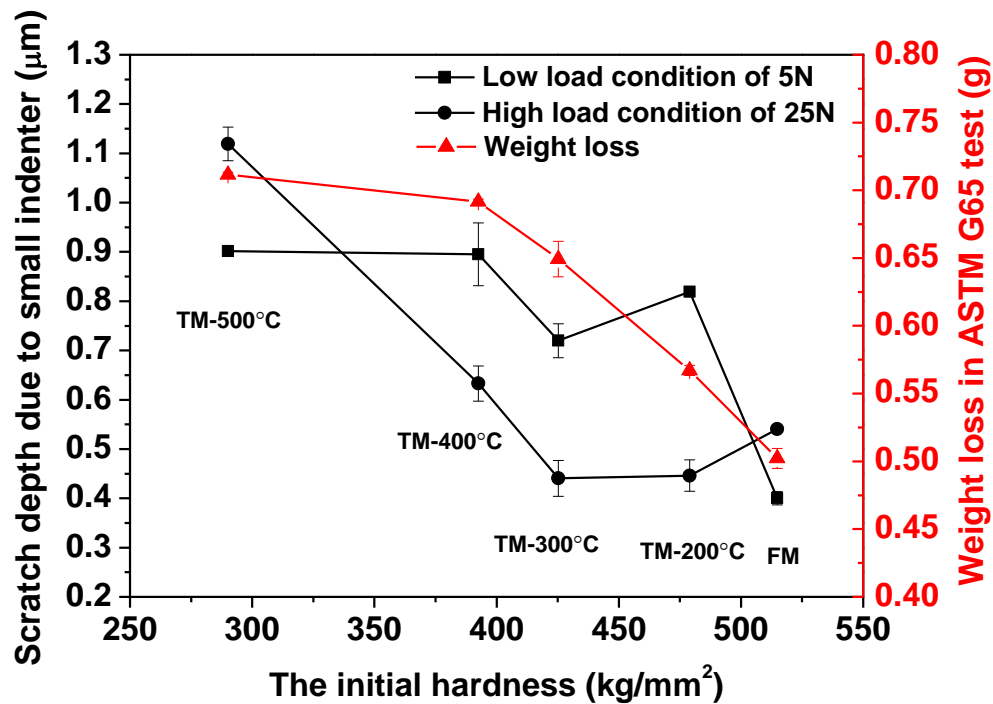


Fig. 8.6 The ASTM G65 weight loss and the MPDI scratch depth under a low load of 5N and a high load of 25N as a function of the initial hardness.

8.4.2 Relating the scratch and abrasion resistance to the initial hardness: comparison of martensitic steels and dual phase steels

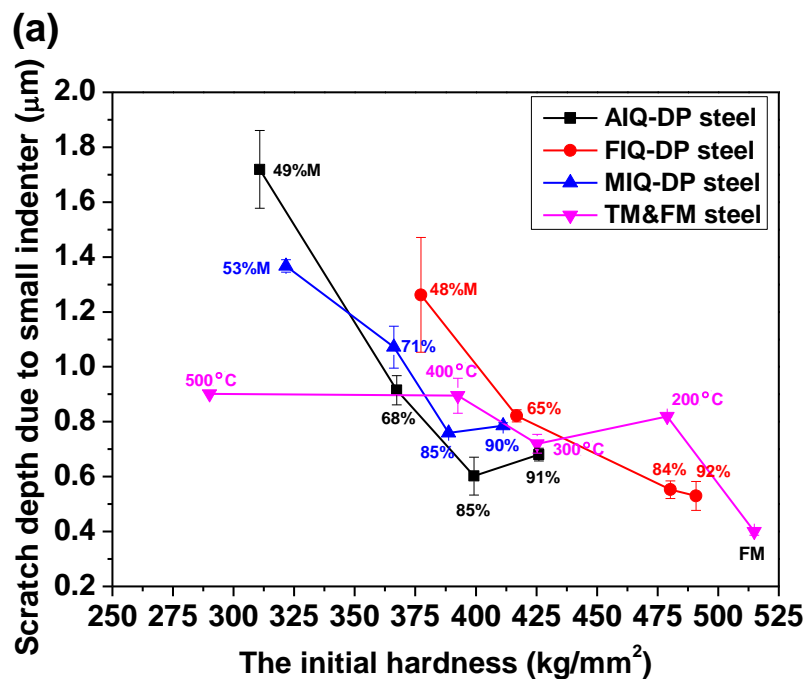
As stated in Chapter 2, in the steel industry the material hardness is taken as the main indicator for abrasion resistance and hence engineering steels are classified accordingly. As a consequence, the design of abrasion resistant steel orients toward a high hardness as the first goal [4, 5]. However, many investigations have shown that the monotonous relation between hardness and wear resistance does not always hold true [9, 25, 36] and “V” and “S” shaped relations between hardness and wear resistance have been reported [37-39]. Furthermore, considering the fact that the abrasion resistance is not an intrinsic property but is the response of multi-parameter tribosystem and that the microstructures will develop during abrasion process, it is difficult to build a general and quantitative

description of the abrasion resistance as a function of other mechanical properties, as described in Chapter 2. Both the hardness and the other (non-elastic) mechanical properties including the abrasion resistance are ultimately determined by the microstructural features. Given the current industrial target to design low-hardness high-abrasion resistant steels for demanding industrial applications [19], as proposed in Chapter 2, therefore, it is essential to directly link the abrasion resistance to the microstructural features.

Systematic experimental investigations have already been conducted to study the response of dual-phase microstructures with different volume fractions (up to 100% martensite) and morphologies on scratch and abrasion resistance. A wide range of DP microstructures was made by varying the starting condition prior to intercritical annealing and quenching. Three process routes were distinguished: 1) full austenisation, then intercritical annealing and quenching (AIQ), 2) a normalized ferritic-pearlitic microstructure, then intercritical annealing and quenching (FIQ) and 3) a martensitic starting structure, then intercritical annealing and quenching (MIQ). Full details can be found in Chapter 7. To make a comparison between the DP microstructures and tempered martensitic microstructures with regard to their scratch and abrasion resistance, the scratch depths at different load levels and weight loss values were collected and correlated against the indentation hardness, and the results are shown in Fig. 8.7 and Fig. 8.8. It should be stressed that all microstructures were created from the same hot rolled steel strip and all samples there have exactly the same chemical composition. As shown in Fig. 8.7a, under the 5N low load condition the best scratch resistance is obtained for un-tempered full martensite. Furthermore, it can be observed that the DP steels having a high martensite fraction level (more than 85%) all show comparable or even lower scratch depths than all tempered martensite grades. The AIQ-DP steel (having a fine granular martensite island microstructure with a high martensitic fraction) yields the best combination of scratch resistance and hardness, and hence presents a good optimum for low-hardness high-abrasion resistant steels. In addition, the ASTM G65 test shows similar results in which the AIQ-DP steels with a high martensite fraction level shows a superior abrasion resistance in combination with a low hardness as shown in Fig. 8.8. However, under the high load condition, representing a more severe abrasive condition, Fig. 8.7b shows that the virgin full martensite is considerably less scratch

resistant than most DP steels and the TM-200°C and TM-300°C grades, despite the fact that the hardness of the latter is clearly lower. Moreover, for the same initial hardness, the tempered martensitic grades show a worse scratch resistance than any of the DP grades. Alternatively, the DP grades with a much lower hardness can have a scratch resistance equivalent to that of the harder TM grades.

The results of this study validate our original hypothesis in Chapter 2 that a dual phase microstructure is the attractive microstructure leading to a modest hardness and a high abrasion resistance. Nonetheless, the optimal volume fraction and morphology for DP steel depends on the working condition and has to be optimized according to the real working conditions.



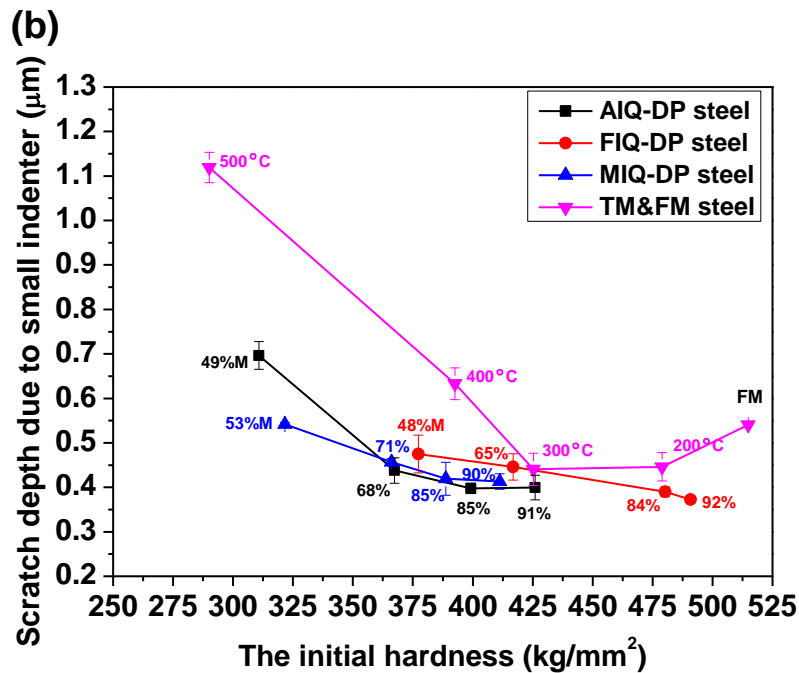


Fig. 8.7 Comparison of the scratch depths for various steels as a function of their initial hardness under low load condition of 5N (a) and high load condition of 25N (b). Note: 1) AIQ, FIQ and MIQ-DP steels refer to the DP steel described in Chapter 7, 2) the values indicated are the martensite fraction for each DP steel and the tempering temperature for each tempered martensite. All steels have the same chemical composition.

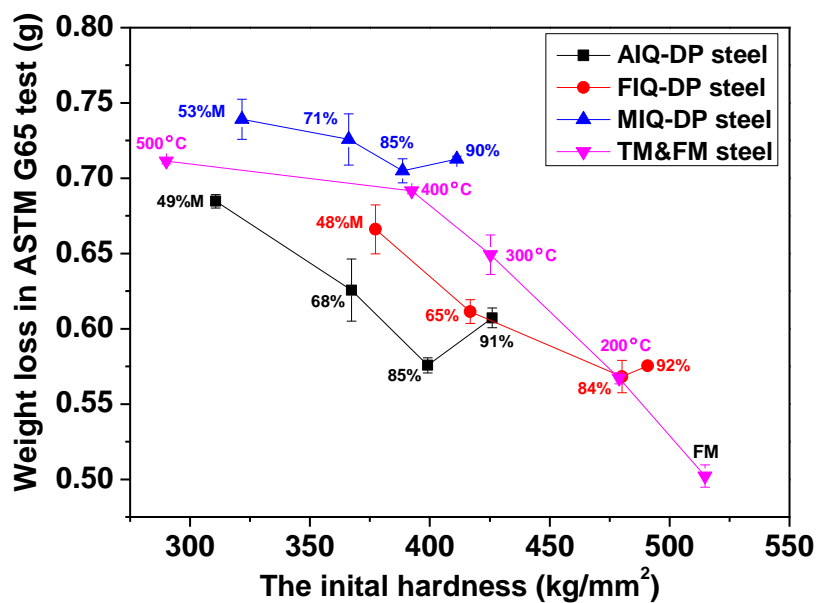


Fig. 8.8 Comparison of weight loss amongst AIQ, FIQ and MIQ-DP steels subjected to ASTM G65 test as a function of the initial hardness.

8.4.3 The relation of tensile strain hardening to scratch resistance

During the steady state of the actual abrasion process, plastic deformation occurs in the surface layer and it is the work hardened (sub) surface layer which is tested [40, 41]. In essence, the abrasion resistance is controlled by the property of (sub) surface layer generated, which itself strongly depends on the strain hardening capability of the material substrate [42-45]. In order to quantitatively interpret the effect of strain hardening on the scratch behavior of tempered martensite under different loading conditions, the strain hardening model [46-50], which has been linked successfully to the abrasion resistance of DP steels, was also employed to correlate the scratch resistance at different loads with tensile strain hardening. As describe in Chapter 7, on the basis of this model, the scratch resistance, i.e. the reciprocal of the scratch depth, is related to the strength coefficient K in the Hollomon equation, i.e., $\sigma = K\varepsilon^n$, where σ and ε are the true stress and strain, and n and K are strain hardening exponent and strength coefficient, respectively [51].

Fig. 8.9 gives the change of the scratch resistance and the strength coefficient K as a function of the tempering temperature employing different load levels on the large indenter to create different work hardening states. It can be seen that the variation in strength coefficient K with tempering temperature matches with that in scratch resistance irrespective of the load conditions, as has been reported for DP steels in Chapter 7. To show the relation between the strength coefficient K and the scratch resistance, the scratch resistance is shown versus the strength coefficient K for three families of steel microstructures (the (tempered) martensite grades (FM & TM grade), the AIQ & FIQ grades and the MIQ grade shown in Chapter 7) for two pre-load scratching conditions. As shown in Fig. 8.10 the various steels obtained from one single steel composition all fall on two linear dependences. On the basis of the investigation, it may be proposed that the strength coefficient K can be considered as a parameter to rank the scratch resistance of low alloyed steels taking into account the working condition. It seems that the dependence of the scratch resistance on the strength coefficient under a high condition is stronger than that under a low load condition.

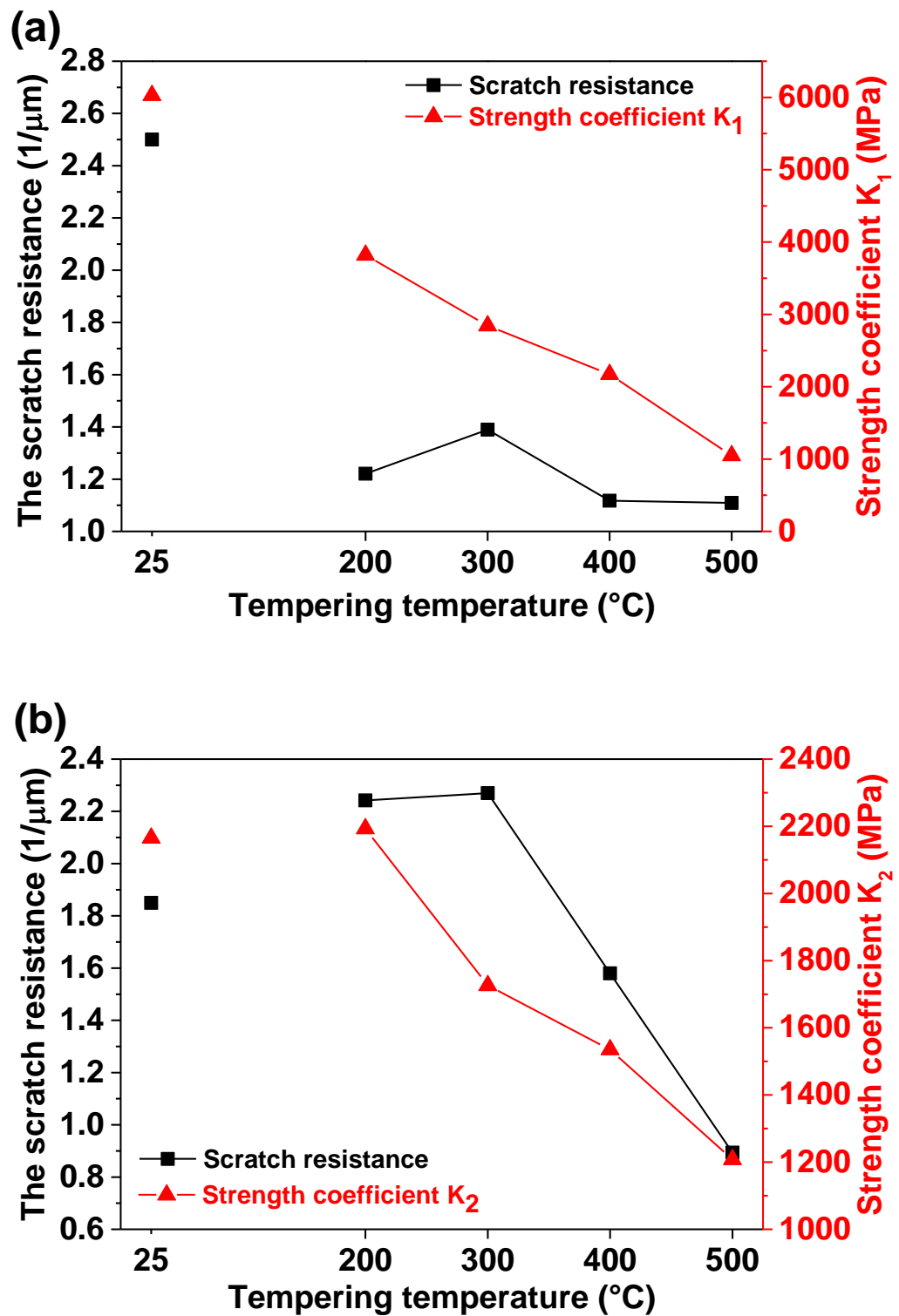


Fig. 8.9 The variation of scratch resistance with the corresponding strength coefficient K at low load of 5N (a) and high load of 25N (b) as functions of tempering temperature. Note: the 25°C in tempered temperature refers to the un-tempered martensite (FM).

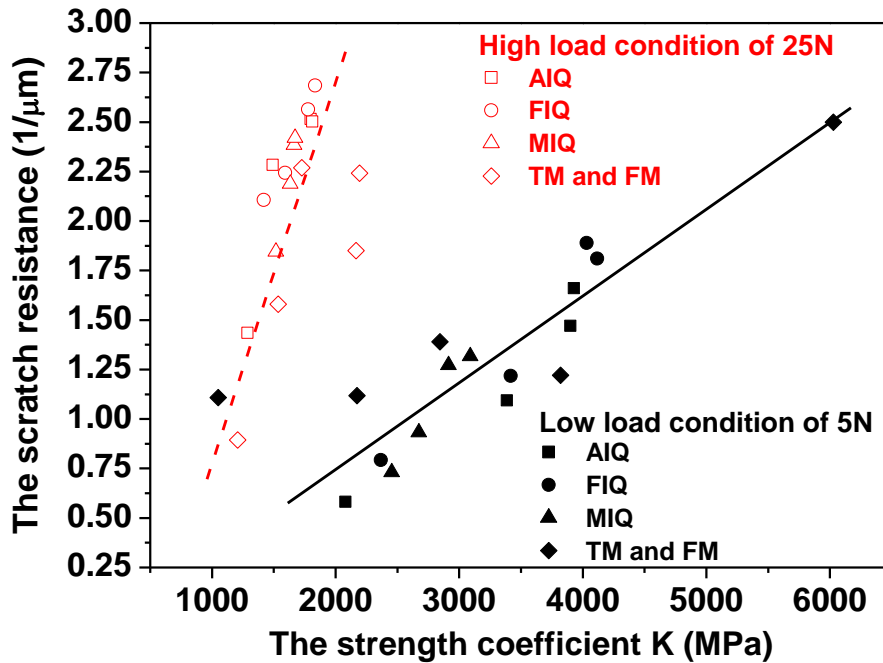


Fig. 8.10 The correlation of the scratch resistance and the strength coefficient K .

8.4.4 Correlation of the MPDI scratch test with the ASTM G65 abrasion test

Finally, the MPDI scratch test results are compared with those of the ASTM G65 test. Fig. 8.11 presents the correlation of ASTM G65 weight loss and the MPDI scratch depth under the low load of 5N for the three families of steel structures evaluated: the tempered martensite grades (FM & QT grade), the AIQ & FIQ grades and the MIQ grade. It can be observed that for all families linear dependences exist and that the data fields more or less overlap, but collectively do not form a very well defined master curve yet.

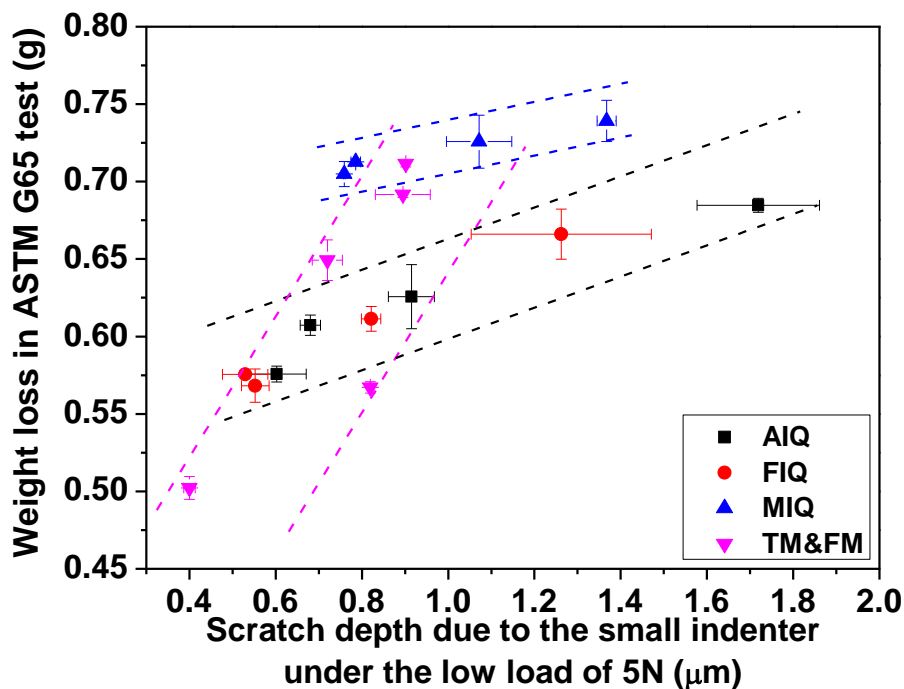


Fig. 8.11 The correlation of the weight loss and scratch depth under the low load condition of 5N. Dashed lines indicate the estimated boundaries of the linear scatter bands for the three microstructural families distinguished (TM&FM, AIQ&FIQ and MIQ).

8.5 Conclusions

The results of an experimental investigation into the dependence of the scratch and abrasion behaviour as a function of the tempering temperature for lean C-Mn construction steel are presented and the results are compared to similar data for the same steel heat treated to yield different ferrite-martensite dual phase microstructures. It is shown that the scratch and abrasion resistance of tempered martensite strongly depend on both the tempering temperature and the loading conditions applied. Under low load conditions, the scratch resistance decreases with increasing the tempering temperature, which is in line with the decrease of hardness. However, under high load conditions, the scratch resistance firstly increases with increasing the tempering temperature (i.e. the decrease of hardness) and then starts to drop. For such working conditions, an optimal

tempering temperature exists in which a higher scratch resistance is obtained despite a lower initial hardness. Regardless of the loading condition, the DP steels can sometimes yield a better combination of scratch/ abrasion resistance and hardness and hence can be considered as better alternatives for low-hardness high-abrasion resistant steels.

References

- [1] L. He, C.J. Zhang, An investigation of the role of secondary carbide in martensitic steel during three-body abrasion wear, *Wear* 176 (1994) 103-109.
- [2] Z. Lu, Q. Rao, Z. Jin, Investigation of the corrosion-abrasion wear behavior of 6% chromium martensitic cast steel, *J. Mater. Process. Technol.* 95 (1999) 180-184.
- [3] S.G. Sapate, A. Selokar, N. Garg, Experimental investigation of hardfaced martensitic steel under slurry abrasion conditions, *Mater. Des.* 31 (2010) 4001-4006.
- [4] E. Rabinowicz, *Friction and Wear of Materials*, Wiley-Interscience, New York, 1965.
- [5] A.D. Sarkar, *Wear of Metals*, Pergamon Press, Oxford, 1976.
- [6] M.W. Tong, P.K.C. Venkatsurya, W.H. Zhou, R.D.K. Misra, B. Guo, K.G. Zhang, W. Fan, Structure-mechanical property relationship in a high strength microalloyed steel with low yield ratio: The effect of tempering temperature, *Mater. Sci. Eng., A* 609 (2014) 209-216.
- [7] P.F. Stratton, Optimising nano-carbide precipitation in tool steels, *Mater. Sci. Eng., A* 448-451 (2007) 809-812.
- [8] M.H. Kim, K.Y. Rhee, Y.N. Paik, J.S. Hong, Y.S. Ham, Experimental investigation on the mechanical behavior of high-frequency induction-hardened mild carbon, SPS5 steel, *Mater. Sci. Eng., A* 485 (2008) 31-38.
- [9] L.Q. Xu, N.F. Kennon, A study of the abrasive wear of carbon-steels, *Wear* 148 (1991) 101-112.
- [10] M.A. Moore, The relationship between the abrasive wear resistance, hardness and microstructure of ferritic materials, *Wear* 28 (1974) 59-68.
- [11] A.M. El-Rakayby, B. Mills, The role of primary carbides in the wear of high speed steels, *Wear* 112 (1986) 327-340.
- [12] J.H. Ouyang, Y.T. Pei, X.D. Li, T.C. Lei, Effect of tempering temperature on microstructure and sliding wear property of laser quenched 4Cr13 steel, *Wear* 177 (1994) 203-208.

- [13] J.H. Lee, J.C. Oh, J.W. Park, H.C. Lee, S. Lee, Effects of tempering temperature on wear resistance and surface roughness of a high speed steel roll, *ISIJ Int.* 41 (2001) 859-865.
- [14] L. Bourithis, G.D. Papadimitriou, Synthesizing a class "M" high speed steel on the surface of a plain steel using the plasma transferred arc (PTA) alloying technique: Microstructure and wear properties, *Mater. Sci. Eng., A* 361 (2003) 165-172.
- [15] Y. Wang, L. Tingquan, Wear behavior of steel 1080 with different microstructures during dry sliding, *Wear* 194 (1996) 44-53.
- [16] D. Rai, B. Singh, J. Singh, Characterisation of wear behaviour of different microstructures in Ni–Cr–Mo–V steel, *Wear* 263 (2007) 821-829.
- [17] W.J. Salesky, G. Thomas, Medium carbon steel alloy design for wear applications, *Wear* 75 (1982) 21-40.
- [18] Y.P. Ma, Research on three-body abrasion of martensitic steels with an impact tester, Master Thesis, Xian Jiaotong University, 1990.
- [19] X. Xu, W. Xu, F.H. Ederveen, S. van der Zwaag, Design of low hardness abrasion resistant steels, *Wear* 301 (2013) 89-93.
- [20] K. Singh, R.K. Khatirkar, S.G. Sapate, Microstructure evolution and abrasive wear behavior of D2 steel, *Wear* 328-329 (2015) 206-216.
- [21] S.G. Sapate, A.D. Chopde, P.M. Nimbalkar, D.K. Chandrakar, Effect of microstructure on slurry abrasion response of En-31 steel, *Mater. Des.* 29 (2008) 613-621.
- [22] R.K. Khatirkar, P. Yadav, S.G. Sapate, Structural and wear characterization of heat treated En24 steel, *ISIJ Int.* 52 (2012) 1370-1376.
- [23] H. Fu, Q. Xiao, H. Fu, Heat treatment of multi-element low alloy wear-resistant steel, *Mater. Sci. Eng., A* 396 (2005) 206-212.
- [24] Y. Wang, T. Lei, J. Liu, Tribo-metallographic behavior of high carbon steels in dry sliding II. Microstructure and wear, *Wear* 231 (1999) 12-19.
- [25] K.H.Z. Gahr, *Microstructure and Wear of Materials*, Elsevier Science Ltd., Amsterdam, 1987.
- [26] J.S. Sun, Abrasion characteristics of some carbide containing alloys, in: *Wear of Materials: International Conference on Wear of Materials*, Reston, USA, 1983, pp. 79-86.
- [27] A.K. Jha, B.K. Prasad, O.P. Modi, S. Das, A.H. Yegneswaran, Correlating microstructural features and mechanical properties with abrasion resistance of a high strength low alloy steel, *Wear* 254 (2003) 120-128.
- [28] X. Xu, S. van der Zwaag, W. Xu, A novel multi-pass dual-indenter scratch test to unravel abrasion damage formation in construction steels, *Wear* 322-323 (2015) 51-60.

- [29] S. Zamberger, L. Whitmore, S. Krisam, T. Wojcik, E. Kozeschnik, Experimental and computational study of cementite precipitation in tempered martensite, *Modell. Simul. Mater. Sci. Eng.* 23 (2015).
- [30] S.K. Dhua, S.K. Sen, Effect of direct quenching on the microstructure and mechanical properties of the lean-chemistry HSLA-100 steel plates, *Mater. Sci. Eng., A* 528 (2011) 6356-6365.
- [31] H. Zhang, X. Cheng, B. Bai, H. Fang, The tempering behavior of granular structure in a Mn-series low carbon steel, *Mater. Sci. Eng., A* 528 (2011) 920-924.
- [32] C. Servant, G. Cizeron, Investigation into the structural evolutions of a low alloy steel during tempering, *Mater. Sci. Eng., A* 117 (1989) 175-189.
- [33] H. Bhadeshia, R. Honeycombe, *Steels: Microstructure and Properties*; Elsevier, Butterworth-Heinemann, 2006.
- [34] N. Prasad, S.D. Kulkarni, Relation between microstructure and abrasive wear of plain carbon steels, *Wear* 63 (1980) 329-338.
- [35] Y. Shang-lei, L. Xue-qin, Z. Zeng-da, L. Song-nian, Investigation of surfacing electrode with high hardness based on lath martensite, *Mater. Sci. Eng., A* 438-440 (2006) 281-284.
- [36] P. J. Mutton, J.D. Watson, Some effects of microstructure on the abrasion resistance of metals, *Wear* 48 (1978) 385 - 398.
- [37] L. Fang, Q.D. Zhou, Y.J. Li, An explanation of the relation between wear and material hardness in three-body abrasion, *Wear* 151 (1991) 313-321.
- [38] K.H.Z. Gahr, D.V. Doane, Optimizing fracture toughness and abrasion resistance in white cast irons, *Metall. Trans. A*, 11 (1980) 613-620.
- [39] S. Das, B.K. Prasad, A.K. Jha, O.P. Modi, A.H. Yegneswaran, Three-body abrasive wear of 0.98% carbon steel, *Wear* 162-164 (1993) 802-810.
- [40] D.A. Rigney, W.A. Glaeser, The significance of near surface microstructure in the wear process, *Wear* 46 (1978) 241-250.
- [41] M. Lindroos, K. Valtonen, A. Kemppainen, A. Laukkanen, K. Holmberg, V.T. Kuokkala, Wear behavior and work hardening of high strength steels in high stress abrasion, *Wear* 322-323 (2015) 32-40.
- [42] M.A. Moore, R.M. Douthwaite, Plastic deformation below worn surfaces, *Metall. Trans. A* 7 (1976) 1833-1839.
- [43] A.T. Alpas, H. Hu, J. Zhang, Plastic deformation and damage accumulation below the worn surfaces, *Wear* 162-164, Part A (1993) 188-195.
- [44] A. Ball, On the importance of work hardening in the design of wear-resistant materials, *Wear* 91 (1983) 201-207.

- [45] X. Xu, S. van der Zwaag, W. Xu, Prediction of the abrasion resistance of construction steels on the basis of the subsurface deformation layer in a multi-pass dual-indenter scratch test, *Wear* 338–339 (2015) 47-53.
- [46] Z. Jiang, Z. Guan, J. Lian, Effects of microstructural variables on the deformation behaviour of dual-phase steel, *Mater. Sci. Eng., A* 190 (1995) 55-64.
- [47] M.R. Akbarpour, A. Ekrami, Effect of ferrite volume fraction on work hardening behavior of high bainite dual phase (DP) steels, *Mater. Sci. Eng., A* 477 (2008) 306-310.
- [48] P. Movahed, S. Kolahgar, S.P.H. Marashi, M. Pouranvari, N. Parvin, The effect of intercritical heat treatment temperature on the tensile properties and work hardening behavior of ferrite-martensite dual phase steel sheets, *Mater. Sci. Eng., A* 518 (2009) 1-6.
- [49] A. Zare, A. Ekrami, Effect of martensite volume fraction on work hardening behavior of triple phase (TP) steels, *Mater. Sci. Eng., A* 528 (2011) 4422-4426.
- [50] Y. Mazaheri, A. Kermanpur, A. Najafizadeh, A novel route for development of ultrahigh strength dual phase steels, *Mater. Sci. Eng., A* 619 (2014) 1-11.
- [51] J.H. Hollomon, Tensile deformation, *Trans. AIME*, 162 (1945) 268-290.

Summary

Generally, in the steel industry the material hardness is taken as the main indicator for the abrasion resistance and hence all low alloyed construction and engineering steels are classified accordingly. However, many investigations have shown clearly that a high hardness cannot guarantee a high abrasion resistance. Furthermore it has become clear that it is difficult to build a general and quantitative description of the abrasion resistance as a function of other mechanical properties given the fact that the abrasion resistance is not an intrinsic property but the response of multi-parameter tribo-system and that the microstructures will develop during the abrasion process. Ultimately the hardness or the other mechanical properties including the abrasion resistance are eventually determined by the microstructural features. Therefore, in the view of a sustainable development, it is essential to directly link the abrasion resistance to the dominant microstructural features. This thesis aims to study the correlation between abrasion resistance and microstructural factors in order to develop low-hardness high-abrasion resistant steels for demanding industrial applications. For this purpose, a novel multi-pass dual-indenter (MPDI) scratch test method was designed to mimic real continuous abrasion processes and to reach a proper understanding of the effect of microstructural parameters on the abrasion resistance and associated damage mechanisms for different loading conditions.

The state of the art of abrasion resistant steels and the key scientific challenges underlying this thesis work are introduced in Chapter 1. The complex and very distinctive process of abrasion and the evolution of microstructures during abrasion process are the principle obstacles to build a general and quantitative mode for abrasion

resistance as a function of mechanical properties, which in essence are all determined by the microstructure. In Chapter 2, a qualitative hypothesis of desirable microstructures for low-hardness abrasion resistance is proposed, but the optimal microstructures for abrasion resistant steels cannot yet be quantified. Dedicated experiments are required in order to obtain a more detailed insight into the correlation between microstructure and abrasion resistance.

In Chapter 3, my novel multi-pass dual-indenter (MPDI) scratch method is described in detail. The new test does not use a single indenter and a single pass over a pristine surface as in conventional scratch tests, but combines a large indenter and small indenter. The sliding with the large indenter is designed to produce a local pre-deformed surface layer with a work hardening equivalent to the surface layer present during a real life abrasion process. The small indenter sliding over the pre-scratched surface is used to mimic the single particle behaviour in a real life steady-state abrasion process involving a work hardened surface state and to reveal the corresponding damage mechanisms. The scratch resistance is defined as the depth of the scratch produced by the small indenter with respect to the bottom of the wear track produced by the large indenter. An interesting yet explainable dependence of the depth of the final (sharp indenter produced) scratch on the load applied during pre-scratching with the large blunt indenter is presented.

A series of the MPDI scratching experiments on five construction steel grades with different work hardening capabilities is reported in Chapter 4. Interstitial-Free ferritic steel (IF steel), Fully Martensitic steel (FM steel), Dual Phase steel (DP steel), Quench Partitioning steel (Q&P steel) and TWining Induced Plasticity steel (TWIP steel) were used to explore the scratch behaviour. The abrasion/scratch resistance of a material is found to be strongly dependent on the strain and damage accumulation in the surface and subsurface layer. The accumulation of strain in (sub) surface layer during the process may result in either strain hardening or weakening (damage/material removal) of the surface layer, depending on the pre-scratch load applied with respect to the strain hardenability and failure strain of the material. Full martensitic steels with a high initial hardness are good options for mild abrasion conditions, while DP, Q&P and TWIP steel grades with a significant work hardening capability display superior wear resistances under higher loads, notwithstanding their relative low initial hardness. The conventional

single pass scratch mode is shown to just reflect the hardness test behaviour, but cannot properly reflect real life abrasion and will mislead the understanding of abrasion resistance. The current MPDI scratch methodology may provide a proper tool to rapidly screen the abrasion resistance of various steel grades, and to determine whether the material would be able to sustain the intended abrasive loading conditions.

In Chapter 5, the MPDI test method is applied to correlate with the ASTM G65 abrasion test results. The MPDI test reflects the two stages (run-in stage and steady state) of the abrasion process and reveals the corresponding damage mechanisms of materials studied for various loading conditions. The abrasion and scratch resistance were found to be controlled by the properties of the work hardening layer formed beneath the abraded surface. Once the correlation of scratch depth and the corresponding subsurface layer thickness is established, the subsurface layer thickness can be taken as a parameter to judge whether the material is applied in its working hardening or damage regime. The method can provide guidelines to select the proper material for a given application or to tune the performance of a given material. When applying the correct evaluation parameters defined by the thickness of the subsurface layer, the new scratch test MPDI methodology reproduces the material response to the ASTM G65 abrasion test rather well and provides a reproducible and quantitative method to screen the abrasion resistance of new construction steels. The MPDI scratch test can also quantify the abrasion resistance of material for working conditions beyond those of the standardized G65 test.

In Chapter 6, a systematic experimental investigation was conducted to study the effect of the martensite volume fraction on the scratch and abrasion resistance of a fixed composition single lean C-Mn construction steel heat treated to various ferrite-martensite dual phase (DP) microstructures. Tests were performed using the multi-pass dual-indenter (MPDI) scratch test as well as the ASTM G65 test. It is found that the scratch resistance depends on not only the volume fractions of each phase, but also the applied loading conditions creating the work hardened surface as formed during steady state abrasion. Under low load conditions representing a mild condition, the scratch depth decreases with increasing martensite fraction, in line with the increasing hardness. For this condition, the best scratch resistance and best abrasion resistance was obtained for a fully martensitic structure. However, for high load conditions representing an

aggressive abrasive condition, the scratch depth initially decreases with increasing martensite fraction up to a critical value (optimal fraction), beyond which the scratch depth starts to rise again. This optimal martensite fraction displaying the best scratch resistance despite a lower hardness was obtained for a DP grade with a martensite fraction of around 80%. The scratch behaviour was correlated to the tensile behaviour and the corresponding work hardening characteristics, applying a two-stage tensile strain hardening model. The result suggests that the tensile strain hardening, i.e. strain hardening exponent n and the strength coefficient K in the Hollomon equation ($\sigma = K\epsilon^n$), at the different stages well reflects the scratch resistance and resulting failure mechanisms under different pre-load conditions. In addition, the standard ASTM G65 test was found to correlate well MPDI scratch response for mild multi-pass pre-scratching conditions.

Chapter 7 presents a systematic experimental investigation concerning the effect of ferrite-martensite morphology on the scratch and abrasion resistance of ferrite-martensite dual phase (DP) steels using a multi-pass dual-indenter (MPDI) scratch test applying different load combinations and ASTM G65 abrasion test. A single low alloyed steel was subjected to different heat treatments to generate dual phase microstructures with different ferrite-martensite morphologies, i.e. fine granular martensite islands (AIQ grade), coarse granular martensite islands (FIQ grade) and quasi-homogeneous fine fibrous martensite islands (MIQ grade). Under low load conditions, the FIQ grade with coarse granular martensite islands possesses the highest scratch resistance, while the MIQ grade with a homogeneous fine fibrous martensite displays the lowest scratch resistance for a given martensite fraction. Under high scratch load conditions, all DP morphologies show comparable scratch performance levels, despite of the different initial indentation hardness values. It is found that altering the morphology of microstructure by tailoring the heat treatment is an attractive option to obtain low hardness materials without sacrificing the scratch/abrasion resistance. DP steels with fine granular martensite islands are the best microstructure for low-hardness abrasion resistant steel for mild abrasion conditions, while in an aggressive work condition the DP steels with fine (granular or fibrous) martensite structures are to be preferred. As in Chapter 6, the scratch resistance of all steels is linked to the strength coefficient K in the Hollomon equation ($\sigma = K\epsilon^n$) in this Chapter. It is shown that the

evolution of strength coefficient K in the two-stage tensile strain hardening model corresponds well with that of scratch resistance regardless of the morphology. As in Chapter 6 the results of the MPDI scratch test under mild conditions are in good agreement with those for the ASTM G65 multi-body abrasion test.

In Chapter 8 the scratch behaviour of tempered martensitic microstructures produced at various tempering temperatures was compared to those of the same steel produced to DP microstructures. The MPDI scratch test and ASTM G65 test experiments were carried out to systematically study the scratch and abrasive wear behaviour as a function of the tempered martensitic microstructure. The results show that the scratch and abrasion resistance of tempered martensite is strongly dependent on both the tempering temperature and the loading condition applied. Under low load conditions representing a mild abrasive condition, the scratch depth increases with increasing tempering temperature, in line with the consistent decrease of the hardness. However, under high load conditions representing a severe abrasive condition, the scratch depth initially decreases with increasing the tempering temperature (the decrease of hardness) up to a critical value beyond which the scratch depth starts to rise. In such working condition, an optimal tempering temperature for martensite steel exists in which a higher scratch resistance is obtained despite a lower initial hardness. Furthermore, a comparison was made between the behaviour of all DP steels (presented in Chapter 6 and 7) and the tempered martensitic steels. It is found that regardless of loading condition, the DP grades can properly yield a better combination of scratch/abrasion resistance and hardness and hence can be considered as better alternatives for low-hardness high-abrasion resistant steels than martensitic grades tempered to higher temperatures.

In conclusion, this thesis presents a novel multi-pass dual indenter (MPDI) scratch methodology. The scratch method successfully reproduces the real life abrasion behaviour and ranks the scratch/abrasion resistance not only for mild conditions (the ASTM G65 test condition), but also in a more aggressive abrasive condition. The scratch and abrasion resistance depends on both the microstructure (sub surface layer formed due to scratching and abrasion) and the working condition employed. The test shows that the design of abrasion resistant steels should not be oriented towards the initial hardness only, but also to the microstructural features most appropriate for the steady state working conditions. DP grades with an optimised volume fraction and morphology

yield a better combination of scratch/ abrasion resistance and the hardness and can be considered as a good alternative for low-hardness high-abrasion resistant steel in industrial application.

Samenvatting

In de staalindustrie wordt gewoonlijk de hardheid gezien als de belangrijkste indicator voor de te verwachten weerstand tegen abrasieve slijtage en alle constructiestaalsoorten worden dienovereenkomstig geclassificeerd. Diverse onderzoeken hebben echter aangetoond dat een hoge hardheid nog geen garantie is voor een hoge slijtvastheid. Het is ook duidelijk geworden dat het niet makkelijk is algemeen geldige en kwantitatieve richtlijnen te geven voor de slijtvastheid op basis van andere mechanische kentallen. Dit is gedeeltelijk het gevolg van het feit dat slijtvastheid geen materiaaleigenschap is maar een ‘systeemrespons’, welke bovendien nog verandert naarmate de slijtage voortschrijdt. Uiteindelijk worden de hardheid en de andere mechanische eigenschappen bepaald door de microstructuur. Het is daarom het doel van dit proefschrift om een relatie te leggen tussen het abrasieve slijtgedrag en de microstructurele parameters, om zo richting te geven aan de ontwikkeling van nieuwe staalsoorten met een lagere hardheid maar met behoud van een hoge slijtvastheid. Hiertoe is een ‘multi-pass dual indenter’ (MPDI) test ontwikkeld die het echte slijtgedrag redelijk goed in kaart brengt en op basis waarvan een goed en kwantitatief inzicht in de relevante processen onder diverse belastingcondities verkregen kan worden.

Een beknopt overzicht van de huidige inzichten met betrekking tot slijtvaste staalsoorten en de resterende wetenschappelijke uitdagingen worden gepresenteerd in Hoofdstuk 1. De diversiteit aan complexe processen tijdens abrasieve slijtage en de veranderingen van de microstructuur tijdens het slijtageproces zijn de belangrijkste obstakels voor het ontwikkelen van een algemeen geldig en kwantitatief slijtagemodel.

In Hoofdstuk 2 wordt op basis van een literatuurstudie een kwalitatieve hypothese voor de optimale microstructuur voor een slijtvastheid bij lage hardheid geformuleerd, maar deze hypothese kan nog niet kwantitatief gemaakt worden. Hiertoe zijn nieuwe experimenten nodig van waaruit een duidelijke correlatie tussen microstructuur en slijtvastheid vastgesteld kan worden.

In Hoofdstuk 3 presenteer ik mijn nieuwe ‘multi-pass dual-indenter (MPDI)’ methode. Deze nieuwe test maakt geen gebruik van een enkele krasnaald (‘indenter’) en een enkele krasbeweging zoals de bestaande kras-testen, maar maakt gebruik van een grote en een kleine krasnaald welke beiden in het zelfde krasspoor gebruikt worden. De initiële meervoudige passage van de grove stompere krasnaald over het oppervlak resulteert in een versterkte oppervlaktelaag zoals die ook tijdens abrasieve belastingen optreedt. De kleine scherpe krasnaald dient vervolgens om het gedrag van losse deeltjes tijdens abrasieve bewerkingen te simuleren en om abrasieve schade in het slijtspoor van de grote krasnaald te bewerkstelligen. Er is een interessante (maar verklaarbare) relatie tussen de diepte van de kras met de scherpe krasnaald en de loodrechte belasting op de grove krasnaald.

In Hoofdstuk 4 komen de resultaten van MPDI experimenten aan vijf constructiestaalsoorten met een verschillend verstevingsgedrag aan de orde. Interstitieel-vrij ferritisch (IF) staal, een twee-fasen (DP) staal, een martensitisch (FM) staal, een getemperd (Q&P) staal en een TWIP staal zijn onderzocht op hun krasvastheid. De slijtvastheid blijkt in sterke mate af te hangen van de opbouw van plastische vervorming in de oppervlaktelaag. Afhankelijk van de belasting op de grove naald kan het effect positief of negatief uitwerken. Bij lage belasting is het martensitische staal het meest slijtvast maar bij hogere belastingen zijn, ondanks hun lagere hardheid, DP, Q&P en TWIP staalsoorten te prefereren. De conventionele enkelvoudige krastest reflecteert enkel het verschil in hardheid maar geeft een onvolledig beeld van de slijtvastheid. De nieuwe MPDI test kan een geschikte test zijn om het slijtage gedrag van nieuwe staalsoorten snel in kaart te brengen en een eerste indruk te krijgen of het staalsoort geschikt is voor de beoogde toepassing.

In Hoofdstuk 5 worden de resultaten van de MDPI test gecorreleerd aan die van de ASTM G65 ‘multi-body’ slijtagetest. De MPDI test laat zowel het slijtagegedrag tijdens

de inloop- als de 'steady state' fase zien. De overgang tussen beide fasen wordt bepaald door het versterkingsgedrag. Als de correlatiefunctie eenmaal goed is vastgesteld kan de dikte van de oppervlaktelaag gebruikt worden om vast te stellen in welke toestand het product zich bevindt. Daarmee wordt de test ook geschikt voor het selecteren van staalsoorten voor specifieke belastingscondities. De MPDI test is ook geschikt om uitspraken te doen over het slijtagegedrag onder condities die in de ASTM G65 test niet bereikt kunnen worden.

Hoofdstuk 6 geeft de resultaten van een systematisch onderzoek naar het effect van het volumepercentage martensiet op het kras- en slijtagegedrag van een laag gelegeerd C-Mn constructiestaal dat via passende warmtebehandelingen een reeks van ferriet-martensiet microstructuren verkregen had. Het slijtagegedrag hangt niet alleen af van het volumepercentage martensiet, maar ook van de opgelegde belastingen. Bij lage krasbelastingen neemt de krasdiepte af met toenemend martensietpercentage om een minimum te bereiken bij een volledige martensietstructuur. Voor zwaardere belastingen is er een specifieke belasting op de stompe krasnaald waarbij een optimale krasvastheid verkregen wordt. Deze optimale slijtvastheid wordt bereikt voor een DP staalsoort met een martensiet-volume fractie rond 80%. Het krasgedrag werd verder vergeleken met het tweetraps versterkingsgedrag van deze staalsoorten in een reguliere trekproef. De resultaten lieten een mooie correlatie zien met de waarde van de K-factor in het Holloman model ($\sigma = K\varepsilon^n$). Wederom werd aangetoond dat bij lage belastingen de MPDI test de ASTM G65-ranking goed kan voorspellen.

Hoofdstuk 7 geeft de resultaten van een experimenteel onderzoek naar het effect van de ferriet-martensiet morfologie op het kras- en slijtagegedrag van DP staalsoorten. Het staal van Hoofdstuk 6 werd onderworpen aan verschillende warmtebehandelingen om een reeks van DP microstructuren te krijgen. De volgende microstructuren werden verkregen: kleine martensiet eilanden in een ferriet matrix (AIQ soort); grove granulaire martensiet eilanden in een ferriet matrix (FIQ soort) en een quasi-homogene vezelachtige martensietstructuur (MIQ soort). Bij lage belastingen gaf de FIQ kwaliteit het beste gedrag en de MIQ het slechtste. Bij hoge belastingen gaven alle kwaliteiten een soortgelijk gedrag dat beter werd bij hogere martensiet fracties. Het onderzoek liet zien dat het mogelijk is door een gerichte warmtebehandeling het slijtagegedrag te verbeteren. Wederom werd een goede correlatie met de K factor in de Hollomon

vergelijking verkregen. Bij lage belastingen werd de relatieve slijtvastheid in de ASTM G65 test goed voorspeld door de MPDI test.

In Hoofdstuk 8 wordt het slijtagegedrag van ontlaten martensitische microstructuren vergeleken met dat van het zelfde staal maar dan in de DP toestand. De resultaten laten zien dat de slijtvastheid sterk afhangt van de ontlaattoemperatuur en de opgelegde belastingen bij het maken van de versterkte oppervlaktelaag. Bij lage belastingen neemt de krasdiepte toe met toenemende ontlaattoemperaturen, d.w.z. met afnemende hardheid. Bij hogere belastingen kan een optimale slijtvastheid verkregen worden bij een conditie die niet de hoogste hardheid heeft. Tot slot wordt een vergelijking gemaakt tussen de slijtvastheid van de ontlaten martensietstructuur en die van de DP staalkwaliteiten uit hoofdstuk 6 en 7. Onafhankelijk van de belasting bleek er altijd een DP kwaliteit te zijn die een betere slijtvastheid te zien gaf dan een ontlaten martensietstructuur.

Samenvattend: dit proefschrift presenteert een nieuwe ‘multi-pass dual-indenter (MPDI)’ slijtagetest. Met de nieuwe testmethode kan het slijtagegedrag onder echte toepassingen goed in kaart gebracht worden. Het kras- en slijtagegedrag hangt af van de microstructuur (en daarmee van de gesteldheid van de oppervlaktelaag tijdens abrasieve belasting) en de lokale belastingen. De testen laten zien dat industriële ontwikkelprogramma's voor slijtvaste staalsoorten zich niet uitsluitend moeten richten op het verkrijgen van een staalsoort met een maximale hardheid maar zich bovenal moeten richten op een microstructuur die het beste past bij de beoogde applicatie. DP staalkwaliteiten met de juiste microstructuur en volumefractie martensiet lijken een veelbelovende optie te zijn voor nieuwe staalsoorten ten behoeve van industriële abrasieve toepassingen.

Acknowledgements

The four-year journey of PhD life leaves me HAPPY and painful memories. With ups and downs, all the past days flash in my mind as I recall and are still as fresh as yesterday. During my travelling, there are quite a lot of bright people I met and many things I experienced, which make this journey more joyful and colourful. I would have been impossible to have this moment without the supervision, assistance, support and accompany of many individuals. Hence, I would like to thank here all who contributed to this journey either directly or indirectly.

First of all, I would like to express my sincere gratitude to my supervisor, Prof. Sybrand van der Zwaag, for offering me the opportunity to pursue my Ph.D. degree and for his excellent guidance, inspiring, care, patience, continuous support in my research and real life. He always gives me enthusiastic discussion and encourages me on my way down. I thank him very much for providing me with an excellent atmosphere of enough freedom and trust, and for his high efficiency of revising my manuscripts. Another special thanks to him is for impressive words that “finding the right position is vital as you are seeing a picture. Either being too close (losing the whole) or being too far (missing the details) cannot capture the real information”, which is beneficial to me and will be valuable throughout my life. I could not have imagined having a better promoter for my Ph.D. study. Thank you very much Sybrand!

Another very important person to whom I am especially grateful is my daily supervisor, Dr. Wei Xu. Perhaps life is a coincidence. I highly appreciate this coincidence due to him, to give me the chance to start the PhD journey. I thank him for enormous efforts to guide my research for the first year and help me to develop my background in metallurgy and tribology. I very much appreciate that during the four years he help me in shaping my knowledge, and gave me the strength, encouragement and motivation to face the challenge. I would also like to thank him for his great help in improving my written English, especially correcting the manuscript in details. I have learnt a lot from

him. Besides the academic life, I really enjoy your nice cooking and beers. I still remember I got terrible drunk only three times in Delft, but gave you two times! It will be a good memory, and hopefully continue to do so in China. Thanks a lot Wei!

I would like to express my sincere gratitude to the financial support from the China Scholarship Council with co-financing by OCAS, ArcelorMittal. I am very grateful to Dr. Lode Duprez (OCAS, ArcelorMittal) for stimulating discussions and to OCAS management for making experiment test facility available. Prof. Erik Schlangen (CiTG) is greatly acknowledged for his support and assistance for the nano-indentation measurement and discussion. I also thank Mr. Sander van Asperen (3ME) for metallographical sample preparations, Mr. Richard Huizenga (3ME) for XRD test, and Frans Oostrum and Lijing Xue for SEM test. I would also like to thank Mr. Fre Ederveen for interesting discussion and continuous help during my PhD study.

I would like to take this opportunity to thank Dr. Lie Zhao (3ME) for his help in homogenization experiments and interesting discussions. I am very grateful to Prof. Mingxin Huang (The University of Hong Kong) for providing some of the test materials. I am also very grateful to Prof. Jiahu Ouyang (Harbin Institute of Technology) and Prof. Shouwen Yao (Beijing Institute of Technology) for interesting scientific talking, and inviting me to visit his group. Special thanks go to the supervisor of my master thesis, Prof. Hanwei Liu and Prof. Minhao Zhu (Southwest Jiaotong University), who brought me into the research field of material science and tribology. I am great grateful to Prof. Guojiang Wan and Prof. Zheng Li for their hospitality during my visiting.

I would like to express my sincere gratitude to Dr. Lode Duprez (OCAS, ArcelorMittal, Belgium), Prof. Patrick De Baets (Universiteit Gent, Belgium), Prof. Cees van Rhee (TU Delft), Prof. Guido C.A.M. Janssen (TU Delft), Prof. Ian Richardson (TU Delft), Prof. Pim Groen (TU Delft) for being the members of the doctoral committee.

I feel so lucky to be a member of the most international group NovAM in which there are so many lovely people around me and one could learn a lot besides science. I really enjoy the four-year time with my nice group (ex-) members, whom I would like to thank. I am very grateful to Shanta for her continuous support and assistance in the past four years. Special thanks to Dr. Hao Chen (ex-officemate) who is at Tsinghua University for his stimulating scientific discussion, continuous suggestion, encouragement and assistance during the course of my PhD life. I am also grateful to

Mr. Zenan Yang (ex-officemate) for both daily scientific and non-scientific discussion, help during my PhD study and hospitality during my visiting at Beijing. My officemates, Dr. Marek Prajer, Hussein Farahani, Hao Yu, are also acknowledge for such a nice work environment. Thank Xiaomin, Jie, Jianwei, Qi, Qingbao, Jesus, Casper, Theo, Santiago, Maruti, Ugo, Ranjita, Michiel, Richardo, Nijesh, Huiyu, Mina, Johan, Zeljka, Hamideh, Daniella, Martino, Arijana, Jimmy, Hongli, Nan, Wouter (P), Wouter (V), Jasper, Mladen, Marianella, Jibrán, Pim, Antonio, Jeroen, Srikanth, Christian, Le, Jasper, Nora, Maarten, Kevin, Frederik, Renee, Yupeng, Haixing, Shasha... and all other former Novam members for the interesting discussion during coffee and lunches, help and cakes. I express my sincere gratitude to all my non-academic friends accompanying my PhD life, Yannian, Cong, Zhenpei, Dan, Bin, Mingxin, Haoyu, Lizuo, Yujie, Chao, Yue for this every weekend party in Prof. Telderslaan at the early-stage in Delft, Wenbo, Xinchao, Weiling, Huajie, Lei, Liaojun, Jiangjun, Xi, Yueting, Jing, Yang, Guowen... for help, social activities, beer, food in the past four years. The time we enjoyed together will benefit me for my rest of life.

Special thanks to Shuanghou Deng, Xiaojia Zhao, Qingqing Ye, Ye Zhang, Zi Wang. Thanks a lot for the fun, the help, the dinner, studying together. After all, life and friendship do not stop with a PhD. Your friendship will be a significant part of my life forever.

I would like to thank my parents, elder brother for their love, encouragement and support, without them I would not have made it so far. “*ba*” and “*ma*”, which are the only words they know, 感谢你们的“锲而不舍”硬生生地把一个只知道以放牛作为毕生理想的放牛娃培养成一个天天与书本为伴的博士生；其中各种曲折和不易，非感谢二字所能表达。Last but certainly not least, a very special thanks to my girl, Zhe Sun, who accompany me throughout my PhD life, not only for your encouragement, support and care, but also for your trust and understanding. During these years, we have both gone through a lot and I would probably not be where I am today without you. A smile is the most charming part of a person forever. Please keep your smile every day!

Curriculum Vitae

Xiaojun Xu

Born on June 17, 1986

Jiujiang, Jiangxi province, China

Sept. 2004 – Jul. 2008

Bachelor of Science in Materials Science, in School of Materials Science and Engineering, Nanchang Hangkong University, Nanchang, China.

Sept. 2008 – Jul. 2011

Master of Science in Materials Science, in School of Materials Science and Engineering, Southwest Jiaotong University, Chengdu, China.

Oct. 2011 – Oct. 2015

Ph.D. Candidate in Novel Aerospace Materials group, Faculty of Aerospace Engineering, Delft University of Technology, Delft, The Netherlands

List of Publications

Journal

12. **X. Xu**, F.H. Ederveen, S. van der Zwaag, W. Xu, Statistical analysis of the relationship among the microstructures, mechanical properties and abrasion resistance in a family of low alloyed steels, to be submitted to *Wear*, 2015.
11. **X. Xu**, S. van der Zwaag, W. Xu, The scratch and abrasive wear behaviour of a tempered martensitic construction steel and its dual phase variants, *Wear*, under revision, 2015.
10. **X. Xu**, S. van der Zwaag, W. Xu, The effect of ferrite-martensite morphology on the scratch and abrasive wear behavior of a dual phase construction steel, *Wear* 348-349 (2016) 148-157.
9. **X. Xu**, S. van der Zwaag, W. Xu, The effect of martensite volume fraction on the scratch and abrasion resistance of a ferrite-martensite dual phase steel, *Wear* 348-349 (2016) 80-88.
8. **X. Xu**, S. van der Zwaag, W. Xu, Prediction of the abrasion resistance of construction steels on the basis of the subsurface deformation layer in a multi-pass dual-indenter scratch test, *Wear* 338-339 (2015) 47-53.
7. **X. Xu**, S. van der Zwaag, W. Xu, A novel multi-pass dual-indenter scratch test to unravel abrasion damage formation in construction steels, *Wear* 322-323 (2015) 51-60.
6. H. Chen, **X. Xu**, W. Xu, S. van der Zwaag, Predicting the austenite fraction after intercritical annealing in lean steels as a function of the initial microstructure, *Metallurgical and Materials Transactions A: Physical Metallurgy and Materials Science* 45 (2014) 1675-1679.

5. **X. Xu**, W. Xu, F.H. Ederveen, S. van der Zwaag, Design of low hardness abrasion resistant steels, *Wear* 301 (2013) 89-93.
4. **X. Xu**, W. Xu, S. van der Zwaag, A study on correlating microstructural features with abrasion resistance of a high strength low alloy steel, *International Journal Sustainable Construction & Design* 4 (2013) 2.
3. W. Xu, Q. Lu, **X. Xu**, S. van der Zwaag, The structure of a general materials genome approach to the design of new steel grades for specific properties, *Computer Methods in Materials Science* 13 (2013) 382-394.
2. H.W. Liu, **X.J. Xu**, M.H. Zhu, P.D. Ren, Z.R. Zhou, High temperature fretting wear behavior of WC25Co coatings prepared by D-gun spraying on TiAlZr titanium alloy, *Tribology International* 44 (2011) 1461-1470.
1. **X.J. Xu**, H.W. Liu, M.H. Zhu, S.Y. Qiu, Z.R. Zhou, Study on high temperature fretting wear of Ti-Al-Zr alloy, *Nuclear Power Engineering* 31 (2010) 42-47.

Conference presentations

9. **Xiaojun Xu**, Sybrand van der Zwaag, Wei Xu, The effect of ferrite-martensite morphology on scratch and abrasion behaviour of low alloyed DP steels, 42th Leeds-Lyon Symposium on Tribology, Lyon, France. (Oral presentation)
8. **Xiaojun Xu**, Sybrand van der Zwaag, Wei Xu, The effect of martensite volume fraction in a dual phase steel on the scratch behaviour in a multi-pass dual-indenter scratch test and its correlation with abrasion resistance, 20th International Conference on Wear of Materials, Toronto, Canada. (Oral presentation)
7. **Xiaojun Xu**, Sybrand van der Zwaag, Wei Xu, A novel multi-pass dual-indenter scratch test to unravel abrasion damage formation in construction steels, 41st Leeds-Lyon Symposium on Tribology 2014, Leeds, UK. (Oral presentation)
6. **Xiaojun Xu**, Sybrand van der Zwaag, Wei Xu, A study into the correlation between abrasion resistance and steel microstructures using single and multiple scratching, European Symposium on Friction, Wear and Wear protection 2014, Karlsruhe, Germany. (Oral presentation)
5. **Xiaojun Xu**, Sybrand van der Zwaag, Wei Xu, A novel multi-pass dual-indenter scratch test to unravel abrasion damage formation in construction steels, European Symposium on Friction, Wear and Wear protection 2014, Karlsruhe, Germany. (Poster)
4. **Xiaojun Xu**, Wei Xu, Sybrand van der Zwaag, Design of low hardness abrasion resistant steels, WOM 2013, Portland, US. (Oral presentation)
3. **Xiaojun Xu**, Wei Xu, Sybrand van der Zwaag, A study on correlating microstructural features with abrasion resistance of a high strength low alloy steel, SCAD 2013, Ghent, Belgium. (Oral presentation)
2. **Xiaojun Xu**, Wei Xu, Sybrand van der Zwaag, Designing abrasion resistant steels using reported correlations between abrasion resistance, mechanical properties and microstructure in advanced steels, MSE 2012, Darmstadt, Germany. (Oral presentation)

1. **Xiaojun Xu**, Wei Xu, Sybrand van der Zwaag, Computational design of high abrasion resistance - Low hardness multiple phase steels, National Student Conference in Metallic Materials 2012, Manchester, UK. (Oral presentation)